TECHNICAL MEMORANDUM
X-92

EFFECTS OF WING-CRANK, LEADING-EDGE CHORD EXTENSIONS AND HORIZONTAL-TAIL HEIGHT ON THE LONGITUDINAL STABILITY OF SWEPT-WING MODELS AT MACH NUMBERS FROM 0.6 TO 1.4

By Roy M. Wakefield

Ames Research Center
Moffett Field, Calif.

NATIONAL AERONAUTICS AND SPACE ADMINISTRATION
WASHINGTON

October 1959

NATIONAL AERONAUTICS AND SPACE ADMINISTRATION

TECHNICAL MEMORANDUM X-92

EFFECTS OF WING-CRANK, LEADING-EDGE CHORD EXTENSIONS AND HORIZONTAL-TAIL HEIGHT ON THE LONGITUDINAL STABILITY OF SWEPT-WING MODELS AT MACH NUMBERS FROM 0.6 TO 1.4*

By Roy M. Wakefield

SUMMARY

An investigation was made to determine the effects of plan-form modifications and horizontal-tail height on the transonic stability of wing-body and wing-body-tail models with a wing of 53.13° leading-edge sweepback. Wing plan-form modifications evaluated were a leading-edge chord extension combined with wing crank, a leading-edge chord extension alone, and the reduction of wing leading-edge sweepback. A comparison was made of the effects of the combined leading-edge chord extension and wing crank on the longitudinal stability of models with horizontal tails of various heights. The Mach number range was 0.6 to 1.4; the angle of attack ranged from -4° to 24°; and the nominal Reynolds number was 1.5 million.

The use of combined leading-edge chord extensions and wing crank provided a significant improvement in static longitudinal stability at subsonic and transonic speeds. The change in stability characteristics resulted from an alteration of the flow over the outboard areas of the wing. A similar degree of improvement did not result from the addition of a chord extension alone or from the reduction of the leading-edge sweepback to the average sweepback of the wing with the combined modifications.

The wing-body-tail models with the unmodified wing were stable with a horizontal tail located below or in the wing chord plane and were unstable with the horizontal tail at either of two locations above the wing chord plane. The wing-body-tail models employing the wing with the combined modifications were stable with all but the highest horizontal tail.

*Title, Unclassified

The models with the combined wing modifications, without or with a horizontal tail, had reduced maximum lift-drag ratios and increased minimum drag at transonic and supersonic speeds.

INTRODUCTION

In attempting to eliminate or alleviate the pitch-up tendency of thin, sweptback wings at subsonic and transonic speeds, the effects of wing modifications, such as leading-edge chord extensions, fences, slots, flaps, and wing crank, have been investigated. Many of the wing modifications have proven to be effective at subsonic speeds but less effective or ineffective at transonic speeds. (See ref. 1 for results at low subsonic speeds and refs. 2 to 7 for results at higher subsonic speeds and transonic speeds.)

An investigation was made to evaluate the effects of a combination of leading-edge chord extension with various amounts of wing crank applied to a wing-body model having a thin wing with 53.13° leading-edge sweepback. To provide a comparison with a wing of leading-edge sweepback equal to the average leading-edge sweepback of the cranked wing, data were also obtained for a wing-body model with 45° leading-edge sweepback, with and without a leading-edge chord extension. To evaluate the influence of the wing modifications on the characteristics of a wing-body-tail model, an investigation was made employing horizontal tails of various heights in combination with a 53.13° sweptback basic wing and one modified wing. The results of the investigation are presented and discussed herein.

NOTATION

b	wing span
C_D	drag coefficient, $\frac{\text{drag}}{qS_w}$
$C_{D_{min}}$	minimum-drag coefficient
C_L	lift coefficient, $\frac{\text{lift}}{qS_w}$
$\frac{dC_L}{d\alpha}$	lift-curve slope
$C_{m_{\bar{c}/4}}$	pitching-moment coefficient about quarter point of mean aerodynamic chord, $\frac{\text{pitching moment}}{qS_w\bar{c}}$

$\frac{dC_m}{dC_L}$	pitching-moment-curve slope
c	local chord
$\bar{c}$	mean aerodynamic chord
$\left(\frac{L}{D}\right)_{max}$	untrimmed maximum lift-drag ratio
l	length of body including portion removed to accommodate the model support sting
l_t	tail length, from $\bar{c}/4$ of the wing to $\bar{c}/4$ of the tail, measured in the extended wing-chord plane
M	free-stream Mach number
r	local radius of body
r_o	maximum radius of body
S_w	wing area, including area within body
S_t	horizontal-tail area, including area enclosed in body
x	longitudinal distance from nose of body
ΔC_D	drag coefficient less zero-lift drag coefficient
$\frac{\Delta C_D}{C_L^2}$	drag-rise factor
ΔC_{m_t}	pitching-moment contribution of horizontal tail in presence of wing and body, $C_{m_{\text{tail on}}} - C_{m_{\text{tail off}}}$ at constant α
α	angle of attack
λ	taper ratio, $\frac{\text{tip chord}}{\text{root chord}}$

MODELS AND APPARATUS

Models

Wings.- Six wing-body models were used - two with unmodified and four with modified wings. Plan views and details are given in figures 1 and 2. The two unmodified wings, of 45° and 53.13° leading-edge sweepback, had an aspect ratio of 3.00, a taper ratio of 0.4, and a linear taper in thickness ratio from root to tip (NACA 0005.8 root and NACA 0003 tip). The modified wings had an aspect ratio of 2.91, a taper ratio of 0.44 and were identical to the unmodified wing in tapered thickness ratio. Modifications to the wings were made by adding a 10-percent local chord extension, from the 0.6 wing semispan to the wing tip, and, for two of the wings, the leading-edge sweep of the outboard wing panels was reduced. The basic wing thickness variation was maintained for the modified outboard panels; thus a surface discontinuity existed at the juncture of the wing panels. All wings had 0° incidence, dihedral, and twist.

Leading-edge sweepback of the inboard and outboard wing panels and designations for the respective models are as follows:

Model designation	Leading-edge sweepback angle, deg	
	Inboard panel	Outboard panel
45	45	45
45-47	45	46.62
53	53.13	53.13
53-32	53.13	32.16
53-43	53.13	43.22
53-54	53.13	54.28

Body.- A Sears-Haack body was used with a fineness ratio of 12.48, based on the closed body length. The body was truncated at 78.8 percent of the closed length to accommodate the model support sting.

The wing-body-tail configurations utilized a slightly modified version of the previously described body and either the 53 or 53-32 wing plan forms. Dimensioned sketches are shown in figures 3 and 4. The body modification consists of a cylindrical extension inserted ahead of the tail to provide a reasonable tail length for all models. Wing-body models used to provide tail-off data included the body extension.

Horizontal tails.- The horizontal-tail surfaces had an aspect ratio of 3.99, taper ratio of 0.38, leading-edge sweepback of 8.53° and circular-arc airfoil sections of 3-percent maximum thickness at the unswept 30-percent chord line. Tail span was 0.514 wing span and tail lengths (distance between the quarter mean aerodynamic chord points of the wing and horizontal tail, measured in the wing-chord plane) were 0.262 and 0.272 wing semispan, respectively, for the 53 wing and the 53-32 wing models. Horizontal tails were 0.333, 0.167, and 0 wing semispan above and 0.167 wing semispan below the wing chord plane, measured from the extended wing chord plane to the horizontal-tail chord plane, and were designated as high, intermediate, mid, and low tail, respectively. All tails had 0° incidence, dihedral, and twist.

Apparatus

The models were sting supported in the wind tunnel on a flexure-pivot, internal-strain-gage balance of the type described in reference 8. Figure 5 is a photograph of the complete model with the 53-32 wing plan form and intermediate horizontal-tail configuration mounted in the Ames 2- by 2-foot transonic wind tunnel.

The Ames 2- by 2-foot transonic tunnel is a closed-circuit, variable-pressure tunnel with a ventilated test section in which the Mach number can be varied continuously to 1.4. A complete description of the tunnel and its air-flow characteristics are provided in reference 8.

TESTS

Tests were conducted to determine the static longitudinal aerodynamic characteristics of all configurations. Lift, drag, and pitching-moment data were obtained through an angle-of-attack range from approximately -4° to 24° in 1° increments at Mach numbers of 0.60, 0.80, 0.90, 0.94, 0.98, 1.02, 1.06, 1.10, 1.20, and 1.4. Limited visual flow studies of wing-body models were made at a Mach number of 0.94 utilizing sublimation patterns, tuft patterns, and schlieren photographs. A nominal Reynolds number of 1.5 million, based on the mean aerodynamic chord of the unmodified wings, was maintained except at higher Mach numbers and angles of attack where it was necessary to reduce the Reynolds number (up to 37 percent) to remain within safe operating limits of the equipment. Boundary-layer trip wires, 0.004 inch in diameter, were placed on all wing and tail surfaces at 25 percent of the chord.

CORRECTIONS

The angles of attack have been corrected for deflection of the balance and support system resulting from aerodynamic loads. The axial force was adjusted to a condition of free-stream static pressure acting at the base of the model.

Corrections to the data for stream angularity and wind-tunnel wall interference were not made. Air stream angularity was negligible. Consideration of subsonic wall interference (based on ref. 9) indicated relatively small values. Reference 10 indicated that for wing-body models of the size employed (approximately 0.53-percent blockage), the influence of the reflected waves on the model characteristics was small and was confined to the Mach number range from 1.00 to 1.15. For the wing-body-tail models, data irregularities between Mach numbers of 0.94 and 1.15, which vary systematically with horizontal-tail height and angle of attack at a constant Mach number, are presumed to result from reflected waves.

Apart from the errors resulting from neglecting the wall interference, random errors existed which determined the precision or repeatability of the data. The estimated random errors for a moderate angle of attack and Mach number are as follows:

$$\begin{aligned} M &= \pm 0.002 \\ \alpha &= \pm 0.10^{\circ} \\ C_L &= \pm 0.006 \\ C_D &= \pm 0.001 \\ C_m &= \pm 0.007 \end{aligned}$$

RESULTS

Lift, drag, and pitching-moment data were obtained for all models and are presented as follows:

Models	Variables	Figures
53 series wing and body	C_L with C_m, α, C_D	6,7
45 series wing and body	C_L with C_m, α, C_D	8,9
All wing and body	$dC_L/d\alpha$ and dC_m/dC_L at $C_L = 0$ $C_{D_{min}}$, $\Delta C_D/C_L{}^2$, and $(L/D)_{max}$ with M	10,11
53 wing-body-tail	C_L with C_m, α, C_D	12,13
53-32 wing-body-tail	C_L with C_m, α, C_D	14,15

Models	Variables	Figures
All wing-body-tail	$dC_L/d\alpha$ and dC_m/dC_L at $C_L = 0$	16,17
	$C_{D_{min}}$, $\Delta C_D/C_L^2$, and $(L/D)_{max}$ with M	
All wing-body-tail	ΔC_{m_t} with α	18

DISCUSSION

Wing-Body Models

Pitching-moment characteristics.- Shown in figure 6 are data for the 53-series models. The wing of the 53 model was unmodified whereas the wings of the 53-32 and 53-43 models were modified with leading-edge chord extensions and wing crank, and the wing of the 53-54 model was modified with a chord extension only. Improvements in longitudinal stability were realized with the combined wing modifications at high angles of attack, in comparison with the unmodified wing model. Although the reduction in stability, typical for swept wings at subsonic and transonic speeds, was less severe, there were undesirable jogs in the pitching-moment curves for the 53-32 and 53-43 models at several transonic Mach numbers.

In contrast to the improvement in subsonic and transonic stability by the combined wing modifications, the use of a leading-edge chord extension alone resulted in improved stability only at subsonic speeds. At Mach numbers less than 0.94, the instability of the 53-54 model occurred at a higher lift coefficient than for the 53 model. At Mach numbers of 0.98 and greater, the data for the 53-54 model and the 53 model were similar.

It is of interest to compare the pitching-moment characteristics of a wing with the combined modifications (53-32) and an uncranked wing, with and without a chord extension (45-47 and 45), having leading-edge sweepback nearly equal to the average sweepback of the modified wing. As shown by a comparison of the data for the 53-32 model (fig. 6) and the 45 and 45-47 models (fig. 8), the reduction in sweep of the complete panels was not as effective as the combined wing modifications. In contrast to the generally acceptable high-lift stability of the 53-32 model (fig. 6), the 45 and 45-47 models (fig. 8) had less desirable characteristics at subsonic and transonic speeds and marked reductions in stability at supersonic speeds.

Flow characteristics.- A limited flow visualization study, utilizing sublimation, tuft, and schlieren techniques, was made to determine the flow characteristics of the 53 and 53-32 wing plan forms. Presented in figure 19 are photographs of tuft and sublimation patterns and sketches

showing the principal features of the flow at M = 0.94 and α slightly above 9°. It is recognized that the data for the 53-32 model have a break at $\alpha \approx 8°$. However, the data variation is regular from this point of discontinuity to higher angles of attack and no abrupt flow changes were shown by the flow visualization study; therefore it is felt that the principal features of the flow pattern are typical of the 53-32 wing at this Mach number and angle-of-attack range. The sublimation and tuft patterns for the 53 model showed evidence of leading-edge flow separation and areas of flow separation at the tip. The schlieren photographs showed a strong shock wave extending from the body and passing across the wing rearward of most of the separated area at the wing tip. (These results are in general agreement with the flow studies of ref. 11.) In the tuft and sublimation pattern photographs for the 53-32 model, leading-edge separation was evidenced on the inboard wing panel and, on the outboard wing panel, an area of laminar flow was shown from the leading edge to the rear of the white triangular areas (the areas parallel to the outboard wing panel leading edge in the sublimation pattern photograph). Flow separation was indicated over the rearward wing area in the vicinity of the juncture of the inboard and outboard wing panels (apparently a spillage of separated air flow from the inboard wing panel). Schlieren photographs of the 53-32 model showed the previously mentioned strong shock to pass across the outboard wing panel just forward of the trailing edge or to miss the wing tip completely at transonic Mach numbers.

The improved stability of the modified wing may be attributed to the development of attached flow over the outboard lifting areas. Attached leading-edge flow resulted from the reduction in leading-edge sweepback, and shock-induced tip separation was avoided by placement of the outboard wing areas ahead of the strong shocks in the flow field.

Lift characteristics.- Lift characteristics of the 53 series models (figs. 6 and 10(a)) varied much less than pitching-moment characteristics with wing plan-form modifications. At Mach numbers of 0.6 and 0.8, maximum-lift coefficients were slightly decreased by the wing modifications. At transonic and supersonic speeds, the modified wing models had greater initial lift-curve-slope values, which increased as the outboard panel leading-edge sweepback was decreased. The 45 and 45-47 models had higher initial lift-curve slopes at transonic Mach numbers than the corresponding values for the 53-32 model (fig. 10).

Drag characteristics.- At subsonic speeds, the untrimmed minimum-drag coefficients of the 53 series models were approximately the same (fig. 11(a)). At transonic and supersonic speeds, minimum-drag coefficients increased and maximum lift-drag ratios decreased with reduction in outboard-panel sweepback. The 53-32 model had nearly equal values of minimum-drag coefficient, greater values of drag-rise factor, and lower values of maximum lift-drag ratio than the respective values for the 45 and 45-47 models.

Wing-Body-Tail Models

Pitching-moment characteristics.- There were some major effects of tail height on the pitching-moment characteristics for both the 53 or 53-32 wing models and also a marked effect of wing plan form for one particular tail height.

The low-tail models with either the 53 or 53-32 wing plan form had similar, generally stable pitching-moment characteristics. At 0.8 Mach number limited regions of instability were indicated for both models. The tail contributions increased with increasing angle of attack to the highest test angle of attack at most Mach numbers (fig. 18).

The mid-tail models with the 53 and 53-32 wing plan forms also had similar stable pitching-moment characteristics throughout the test Mach number range.

There was a marked difference in the pitching-moment characteristics of the unmodified-wing and modified-wing models with the intermediate tail. The 53 wing-body-tail model had extensive unstable regions at all subsonic and transonic Mach numbers in contrast with the limited instability of the 53-32 wing-body-tail model. With increasing supersonic Mach number, the 53 wing model became stable; however, the pitching-moment characteristics remained less uniform and hence were less desirable than the characteristics of the 53-32 wing model. At high angles of attack, values of ΔC_{m_t} were lower for the intermediate tail than for the models with the mid tail; the decrease in ΔC_{m_t} was considerably less for the model with the modified wing (fig. 18).

At all test Mach numbers, the high-tail models were severely unstable in the upper range of lift coefficients. The instability of both models, at corresponding Mach numbers, occurred in the same angle-of-attack range and was due to large reductions in the pitching-moment contributions of the high tail.

Summary of characteristics.- The 53 models with the low or mid tails had generally satisfactory stability and lift characteristics, lower transonic and supersonic minimum drag, and slightly higher maximum lift-drag ratios than the models with the 53-32 wing and the same tail configurations. Therefore, in applications where such low or mid tails would be permitted, an unmodified wing would be preferable. However, if a moderately high horizontal-tail location were required, the modified wing would provide a statically stable configuration.

CONCLUDING REMARKS

The addition of a leading-edge chord extension and wing crank modifications to a thin wing of 53.13° leading-edge sweepback provided an improvement in tail-off, high lift stability at Mach numbers from 0.6 to 1.4, whereas the use of a chord extension alone resulted in improved stability only at subsonic speeds. The reduction of leading-edge sweepback of a wing, to a value nearly equal to the average leading-edge sweepback of a wing with the combined modifications, did not duplicate the improvement in transonic and supersonic tail-off pitching moments shown by the combined modifications.

The effect of the wing modifications on the lift and drag characteristics was less pronounced than the effect on the pitching-moment characteristics. With the combined wing modifications, transonic initial lift-curve slopes and minimum-drag coefficients were increased. Increased lift at moderate angles with no significant difference in drag characteristics was shown for the models with reduced leading-edge sweepback, in comparison with the models with the combined wing modifications.

With the addition of wing crank and a leading-edge chord extension, attached flow was established at the leading edge of the outboard wing panels and tip separation was reduced.

The longitudinal-stability characteristics of the wing-body-tail models varied with horizontal-tail height and, for one particular tail height, with wing plan form. With a horizontal tail located below or in the wing chord plane, models with the wing plan form unmodified or with the combined modifications were generally stable. With a horizontal tail of intermediate height, the unmodified-wing-model was unstable and the modified-wing model was, for the most part, stable. With the highest horizontal tail, models with either wing plan form were severely unstable. Reduction or loss of stability of the wing-body-tail models at high angles of attack was due to decreasing tail contributions to stability with increasing horizontal-tail height.

Ames Research Center
National Aeronautics and Space Administration
Moffett Field, Calif., May 28, 1959

REFERENCES

1. Furlong, Chester G., and McHugh, James G.: A Summary and Analysis of the Low-Speed Longitudinal Characteristics of Swept Wings at High Reynolds Number. NACA RM L52D16, 1952.

2. Goodson, Kenneth W., and Few, Albert G., Jr.: Effect of Leading-Edge Chord-Extensions on Subsonic and Transonic Aerodynamic Characteristics of Three Models Having 45° Sweptback Wings of Aspect Ratio 4. NACA RM L52K21, 1953.

3. West, F. E., Jr., and Henderson, James H.: Relationship of Flow Over a 45° Sweptback Wing With and Without Leading-Edge Chord Extensions to Longitudinal Stability Characteristics at Mach Numbers from 0.60 to 1.03. NACA RM L53H18b, 1953.

4. Hieser, Gerald: An Investigation at Transonic Speeds of the Effects of Fences, Drooped Nose, and Vortex Generators on the Aerodynamic Characteristics of a Wing-Fuselage Combination Having a 6-Percent-Thick, 45° Sweptback Wing. NACA RM L53B04, 1953.

5. Goodson, Kenneth W., and Becht, Robert E.: Wind-Tunnel Investigation at High Subsonic Speeds of the Stability Characteristics of a Complete Model Having Sweptback-, M-, W-, and Cranked-Wing Plan Forms and Several Horizontal-Tail Locations. NACA RM L54C29, 1954.

6. Whitcomb, Richard T., and Kelly, Thomas C.: A Study of the Flow Over a 45° Sweptback Wing-Fuselage Combination at Transonic Mach Numbers. NACA RM L52D01, 1952.

7. Stephenson, Jack D., Bandettini, Angelo, and Selan, Ralph: Longitudinal Stability Characteristics at Mach Numbers up to 0.92 of a Wing-Body-Tail Combination Having a Wing with 45° of Sweepback and a Tail in Various Vertical Positions. NACA RM A54K09, 1955.

8. Spiegel, Joseph M., and Lawrence, Leslie F.: A Description of the Ames 2- by 2-Foot Transonic Wind Tunnel and Preliminary Evaluation of Wall Interference. NACA RM A55I21, 1956.

9. Baldwin, Barrett S., Jr., Turner, John B., and Knechtel, Earl D.: Wall Interference in Wind Tunnels with Slotted and Porous Boundaries at Subsonic Speeds. NACA TN 3176, 1954. (Supersedes NACA RM A53E29)

10. Stivers, Louis S., Jr., and Lippmann, Garth W.: Effects of Fixing Boundary-Layer Transition for an Unswept-Wing Model and an Evaluation of Porous Tunnel-Wall Interference for Mach Numbers from 0.60 to 1.40. NACA TN 4228, 1958.

11. Hall, I. M., and Rogers, E. W. E.: The Flow Pattern on a Tapered Swept-Back Wing at Mach Numbers Between 0.6 and 1.6. British A.R.C. 19,691, Nov. 26, 1957.

Body:

$$\frac{r}{r_o} = \left[1 - \left(1 - \frac{2x}{l}\right)^2\right]^{\frac{3}{4}}$$

$r_o = 0.794$

$l = 19.833$

Note: All dimensions are in inches except as noted.

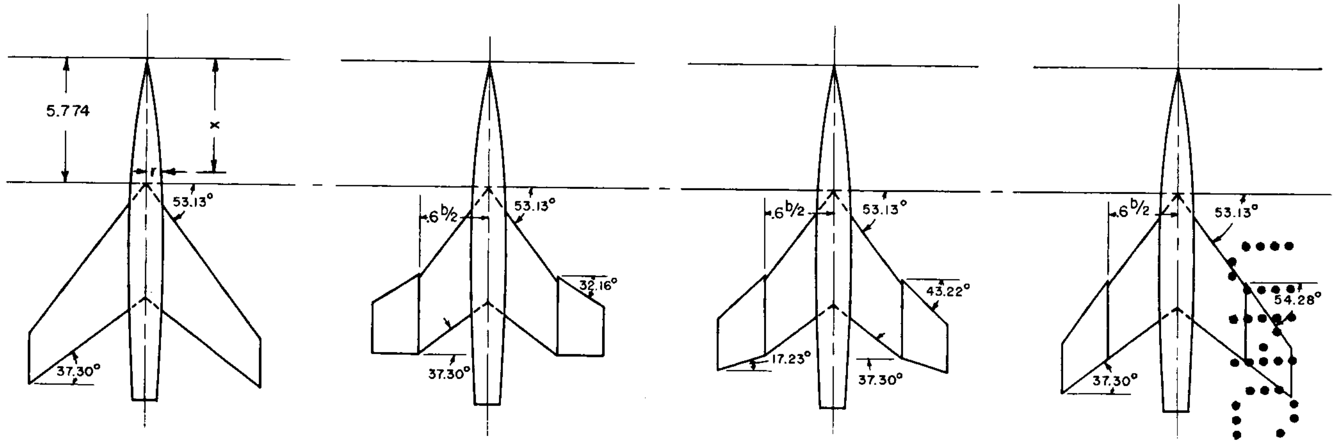

Model	53	53-32	53-43	53-54
Aspect Ratio	3.00	2.91	2.91	2.91
Wing Span	10.800	10.800	10.800	10.800
Wing Area	38.889	40.039	40.039	40.039
Mean Aerodynamic Chord	3.820	3.877	3.877	3.877

Model 53:

	Inboard Panel		Outboard Panel	
	Root	.6 b/2	.6 b/2	Tip
Chord	5.143	3.292	3.292	2.057
NACA Airfoil Section	0005.8	0004.75	0004.75	0003

Model 53-32:

	Inboard Panel		Outboard Panel	
	Root	.6 b/2	.6 b/2	Tip
Chord	5.143	3.292	3.621	2.263
NACA Airfoil Section	0005.8	0004.75	0004.75	0003

Model 53-43:

	Inboard Panel		Outboard Panel	
	Root	.6 b/2	.6 b/2	Tip
Chord	5.143	3.292	3.621	2.263
NACA Airfoil Section	0005.8	0004.75	0004.75	0003

Model 53-54:

	Inboard Panel		Outboard Panel	
	Root	.6 b/2	.6 b/2	Tip
Chord	5.143	3.292	3.621	2.263
NACA Airfoil Section	0005.8	0004.75	0004.75	0003

Figure 1.- Plan views and geometric details of wing-body models having an inboard-wing-panel leading-edge sweepback of 53.13°.

UNCLASSIFIED

Body:

$$\frac{r}{r_o} = \left[1-\left(1-\frac{2x}{l}\right)^2\right]^{\frac{3}{4}}$$

$r_o = 0.794$

$l = 19.833$

Note: All dimensions are in inches except as noted.

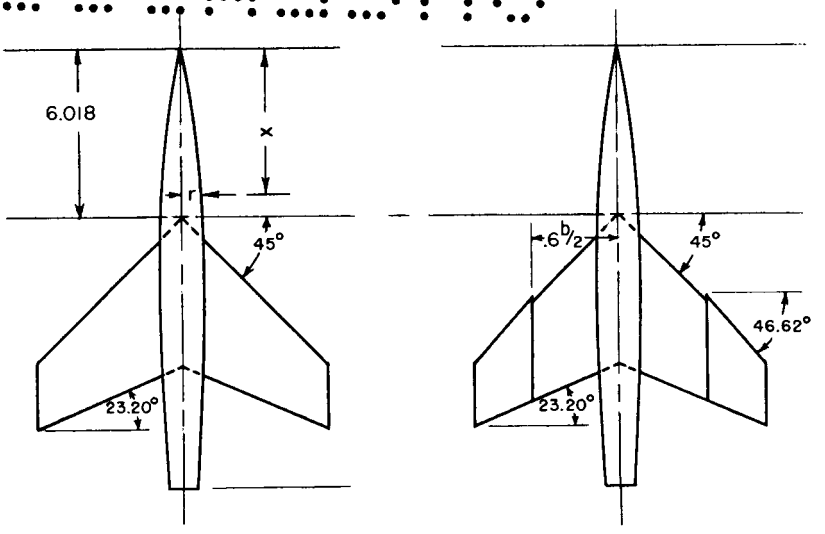

	45	45-47
Model		
Aspect Ratio	3.00	2.91
Wing Span	10.800	10.800
Wing Area	38.889	40.039
Mean Aerodynamic Chord	3.820	3.877

	Inboard Panel		Outboard Panel	
	Root	.6 b/2	.6 b/2	Tip
Chord	5.143	3.292	3.292	2.057
NACA Airfoil Section	0005.8	0004.75	0004.75	0003

	Inboard Panel		Outboard Panel	
	Root	.6 b/2	.6 b/2	Tip
Chord	5.143	3.292	3.621	2.263
NACA Airfoil Section	0005.8	0004.75	0004.75	0003

Figure 2.- Plan views and geometric details of wing-body models having an inboard-wing-panel leading-edge sweepback of 45°.

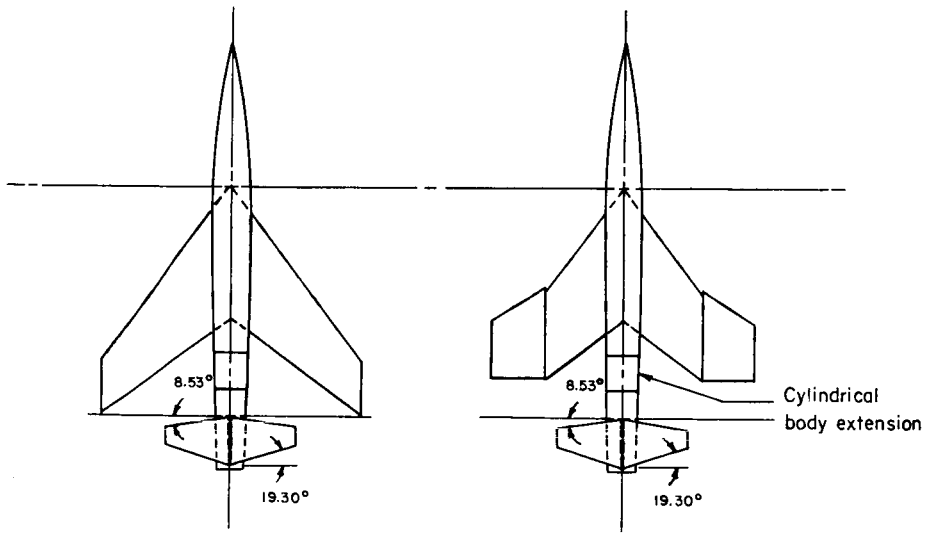

	53+Tail	53-32+Tail
Tail aspect ratio	3.994	3.994
Tail taper ratio	0.334	0.334
Tail span	5.560	5.560
Tail area	7.740	7.740
Tail airfoil section	Cir. arc of 3% max. thickness at 30% chord	Cir. arc of 3% max. thickness at 30% chord

Figure 3.- Plan views and geometric details of wing-body-tail models.

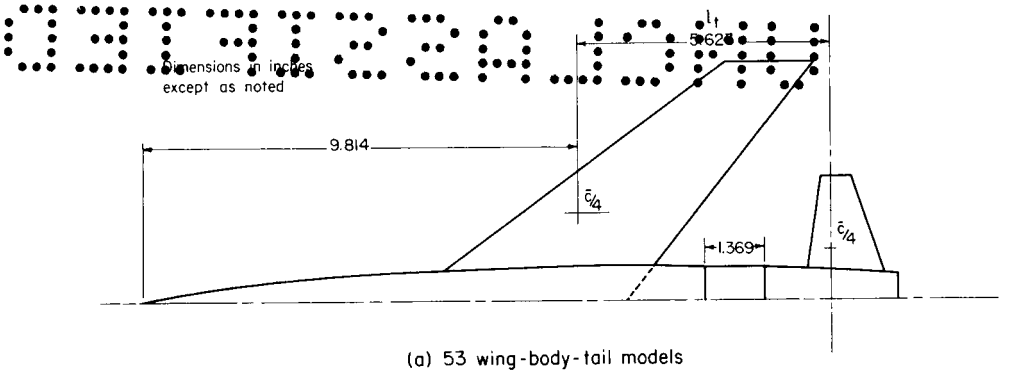

(a) 53 wing-body-tail models

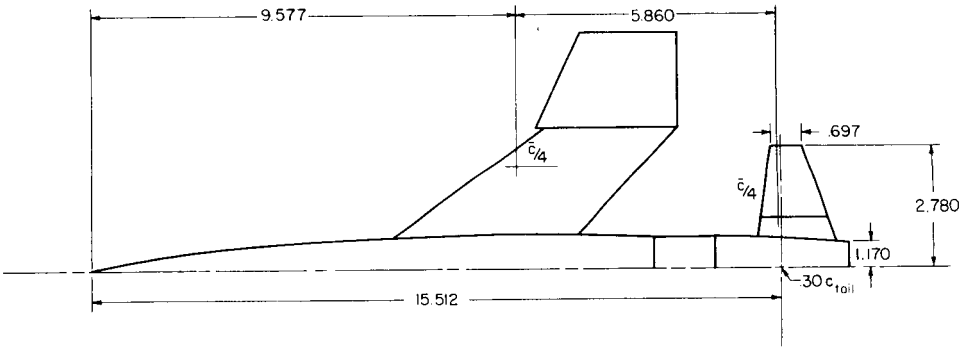

(b) 53.32 wing-body-tail models

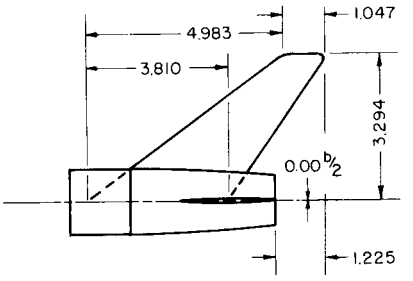

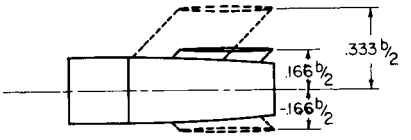

(c) Tails used with 53 and 53.-32
Wing - body - tail models

Figure 4.- Details of wing-body-tail models and tail configurations.

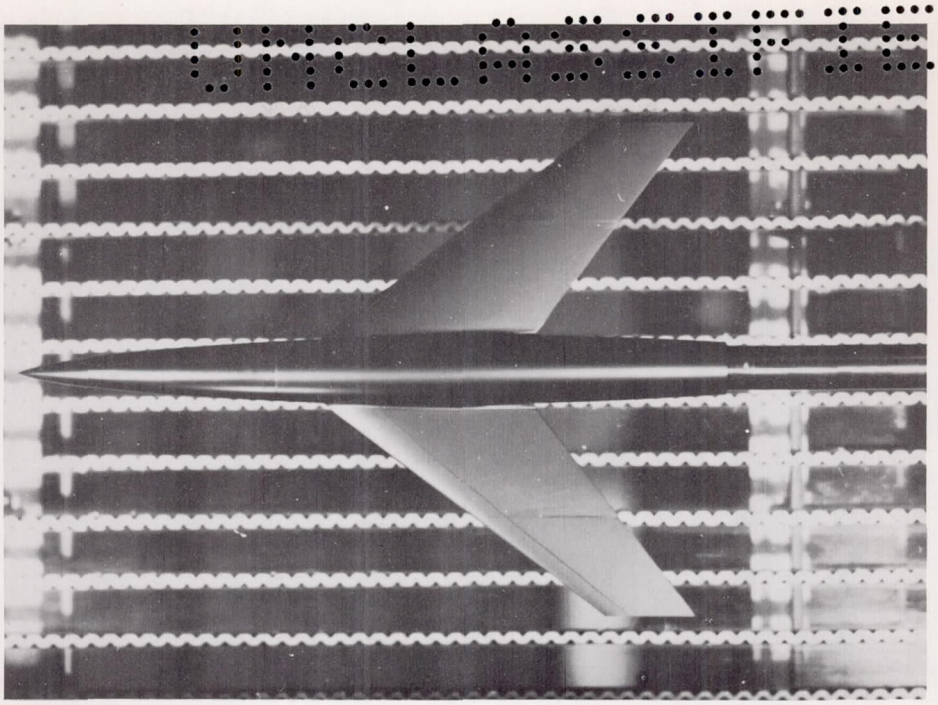

Figure 5.- Typical model installation in the Ames 2- by 2-foot transonic wind tunnel.

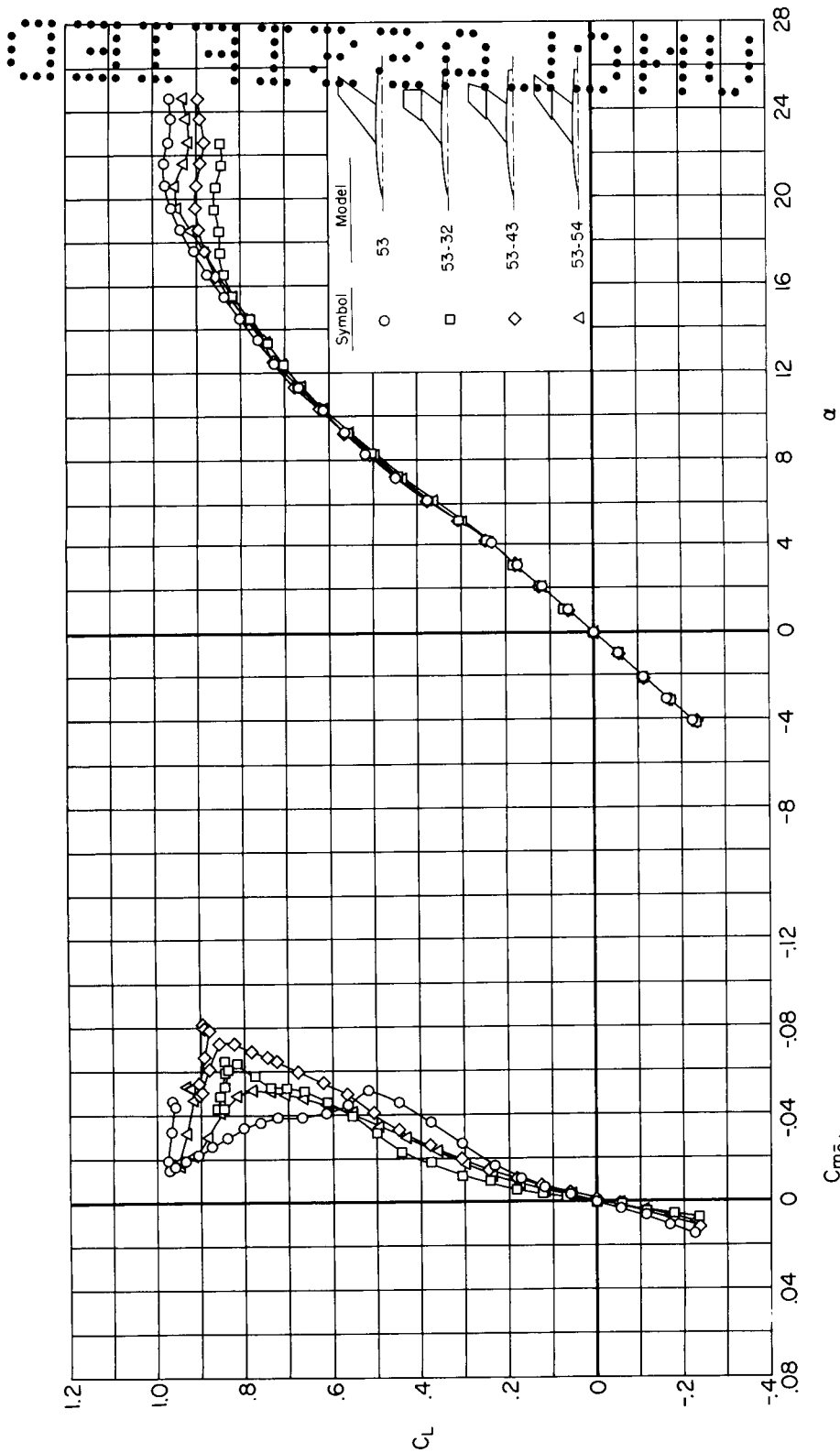

(a) M = 0.60

Figure 6.- Variation of lift coefficient with pitching-moment coefficient and angle of attack for the 53 series models.

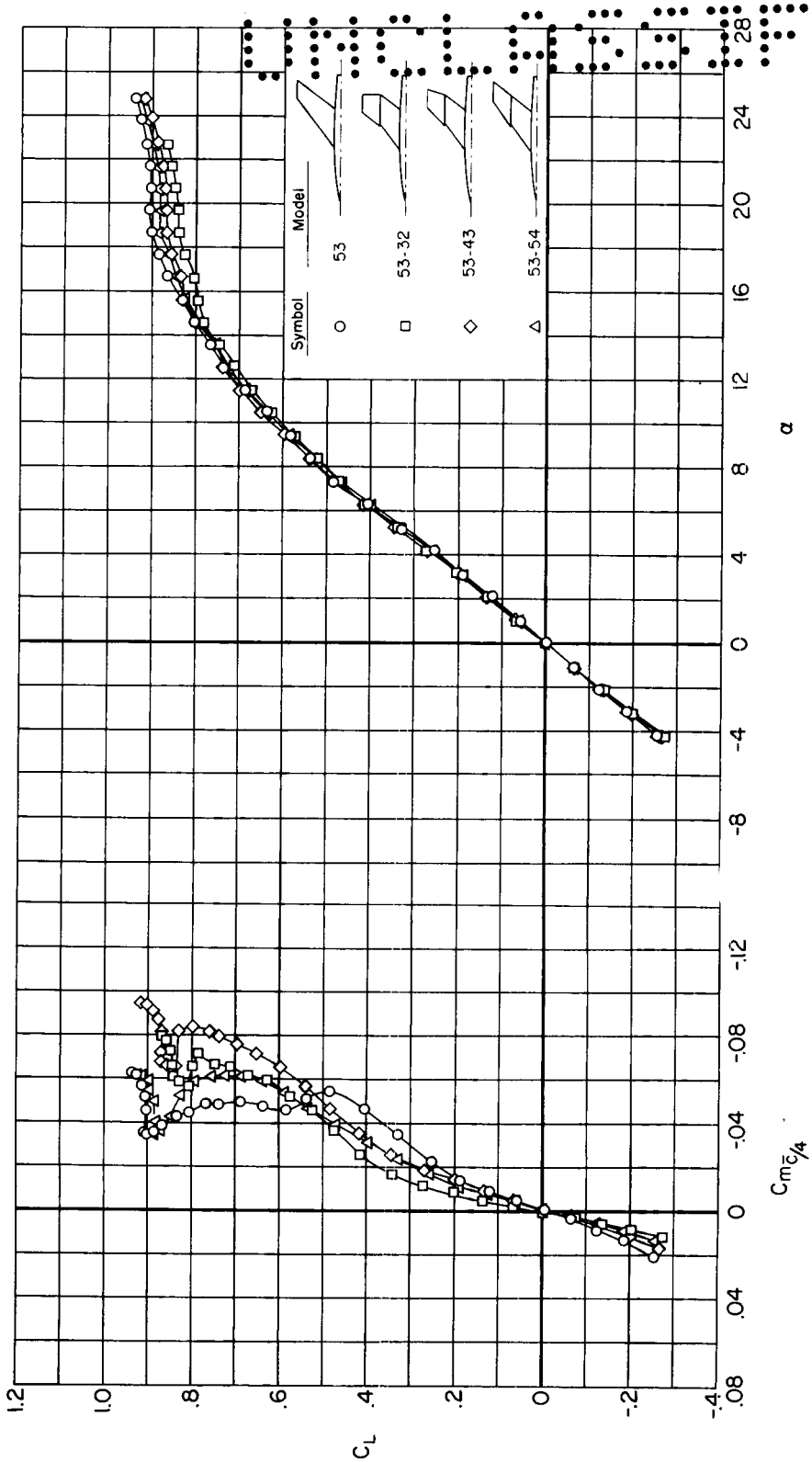

(b) M = 0.80

Figure 6.- Continued.

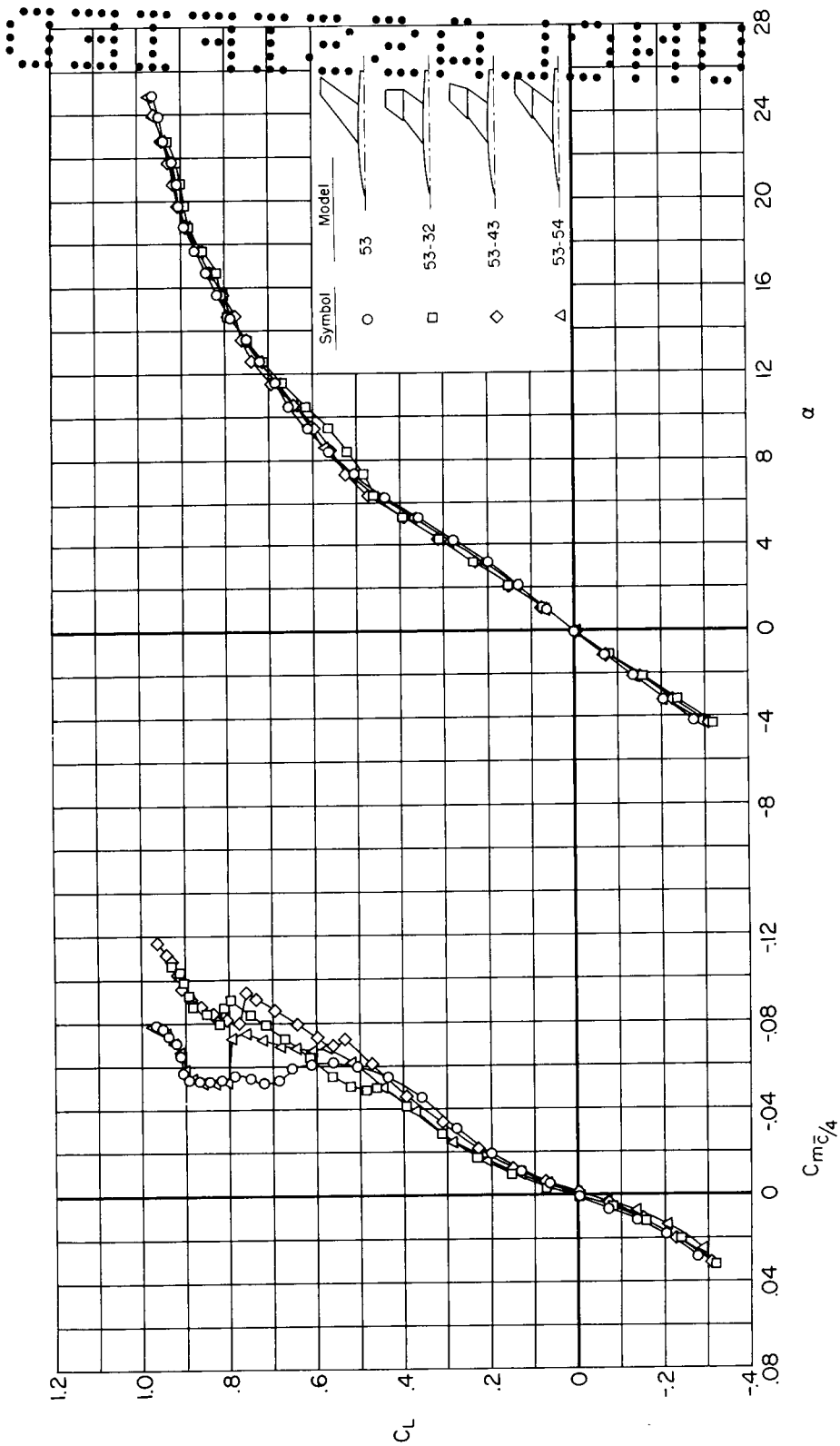

(c) M = 0.90

Figure 6.- Continued.

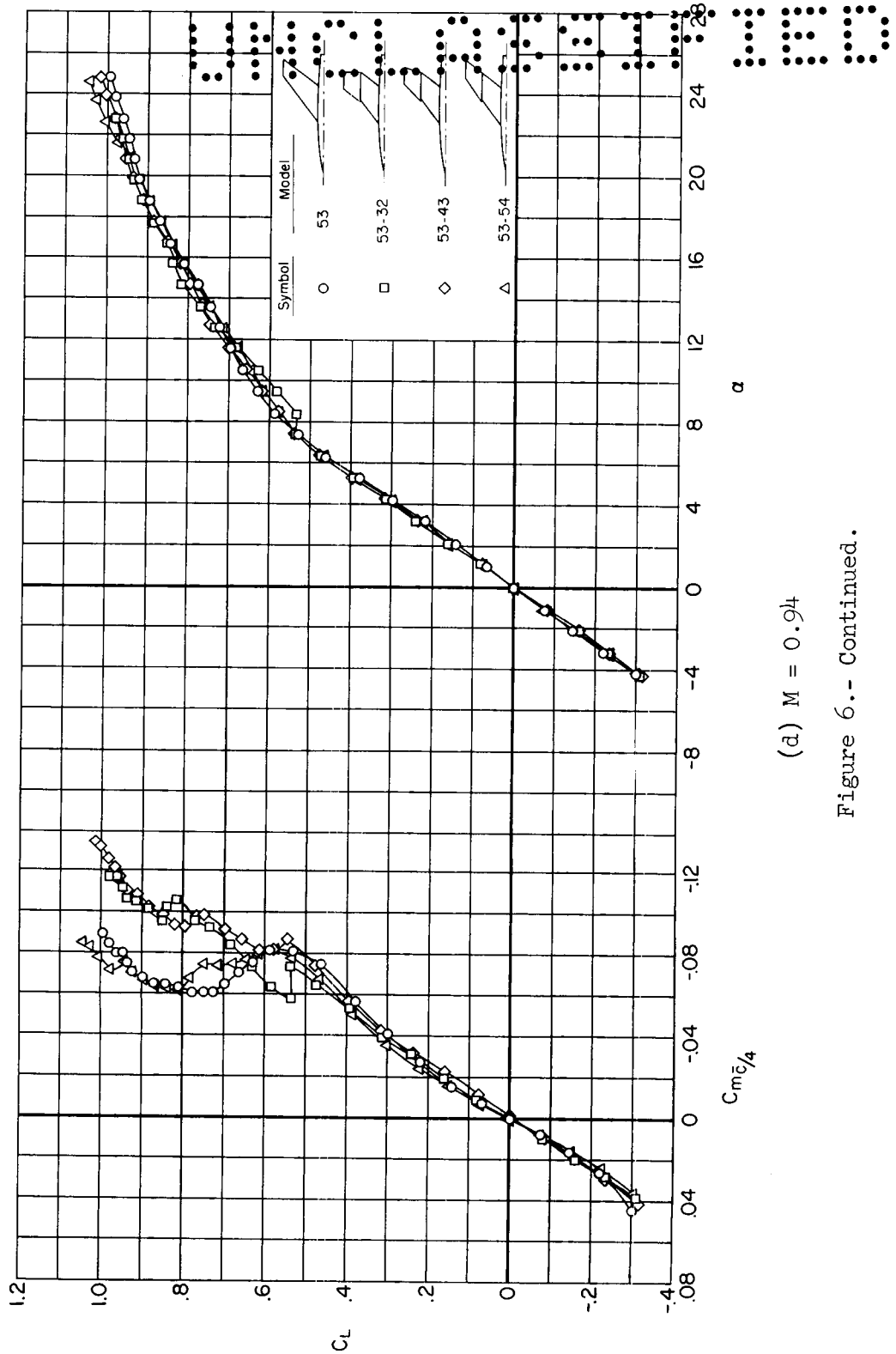

(d) M = 0.94

Figure 6.- Continued.

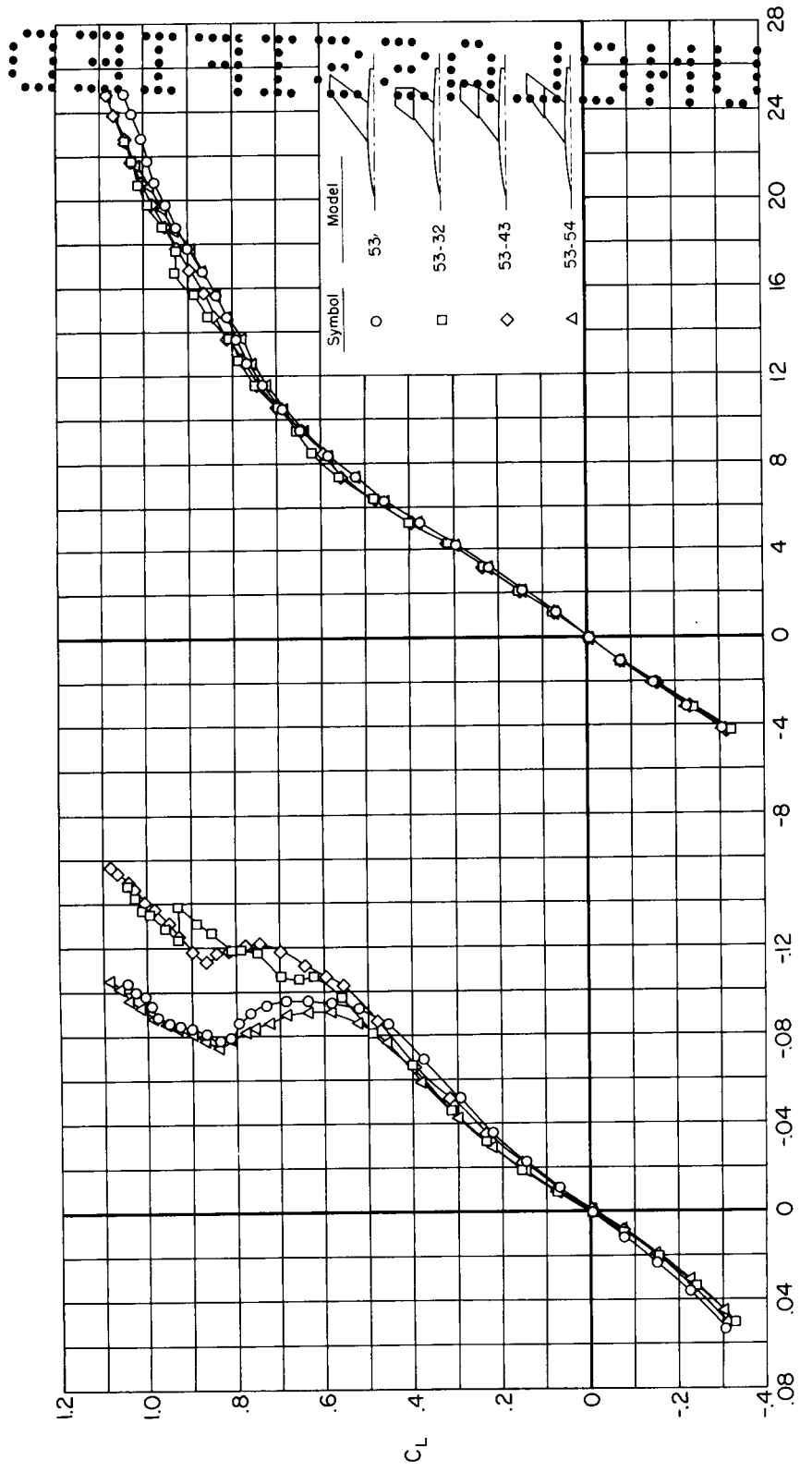

(e) M = 0.98

Figure 6.- Continued.

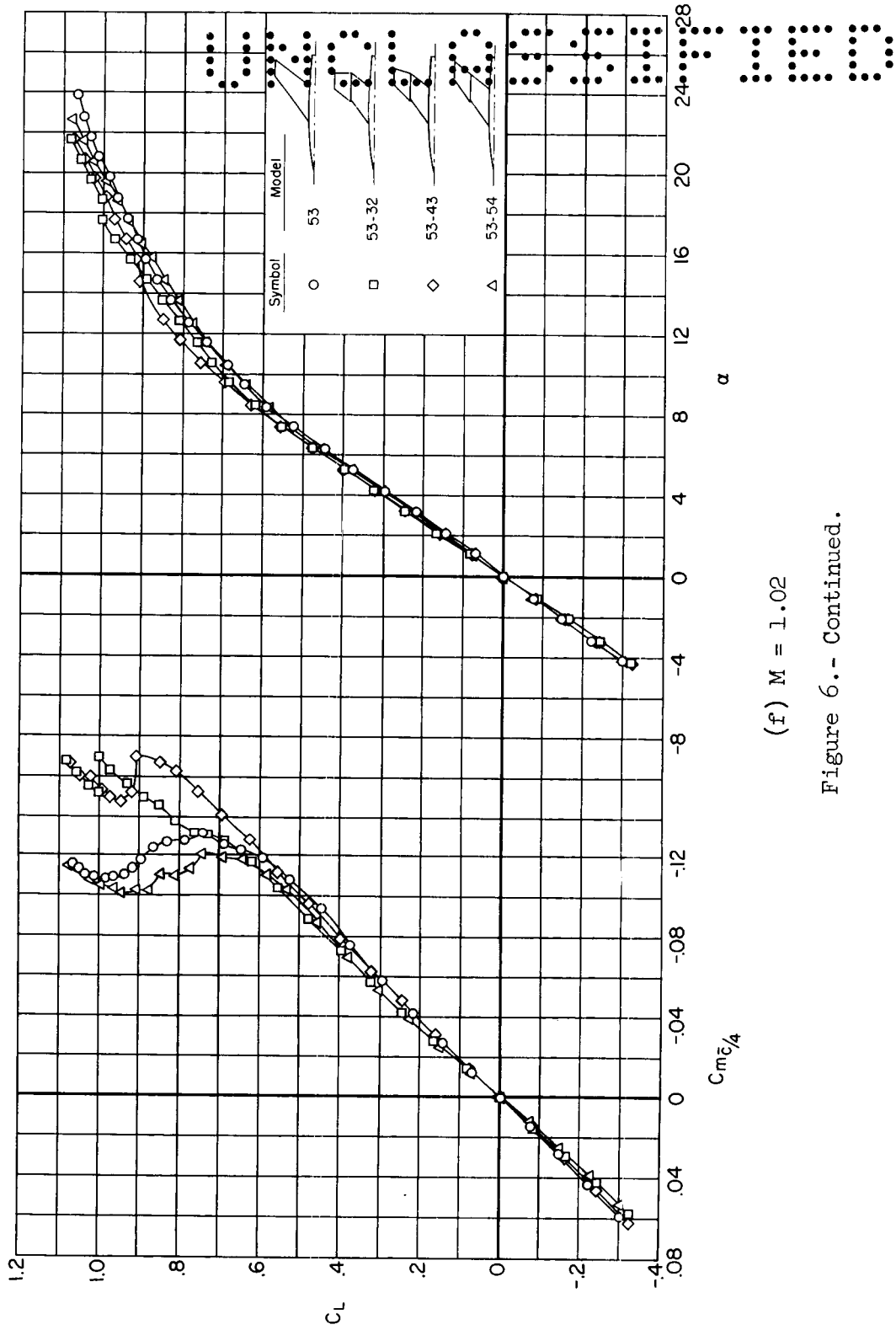

(f) M = 1.02

Figure 6.- Continued.

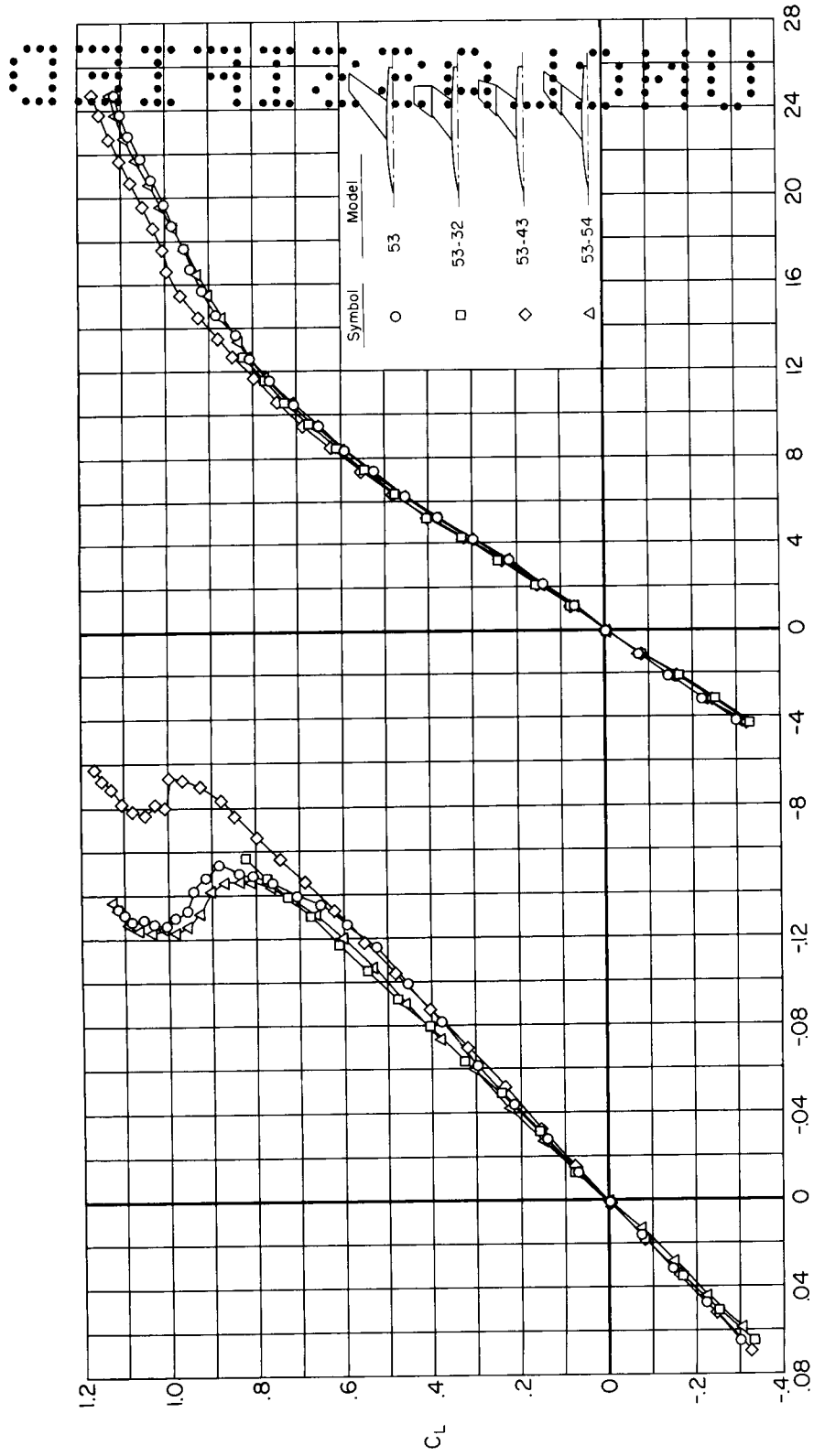

(g) M = 1.06

Figure 6.- Continued.

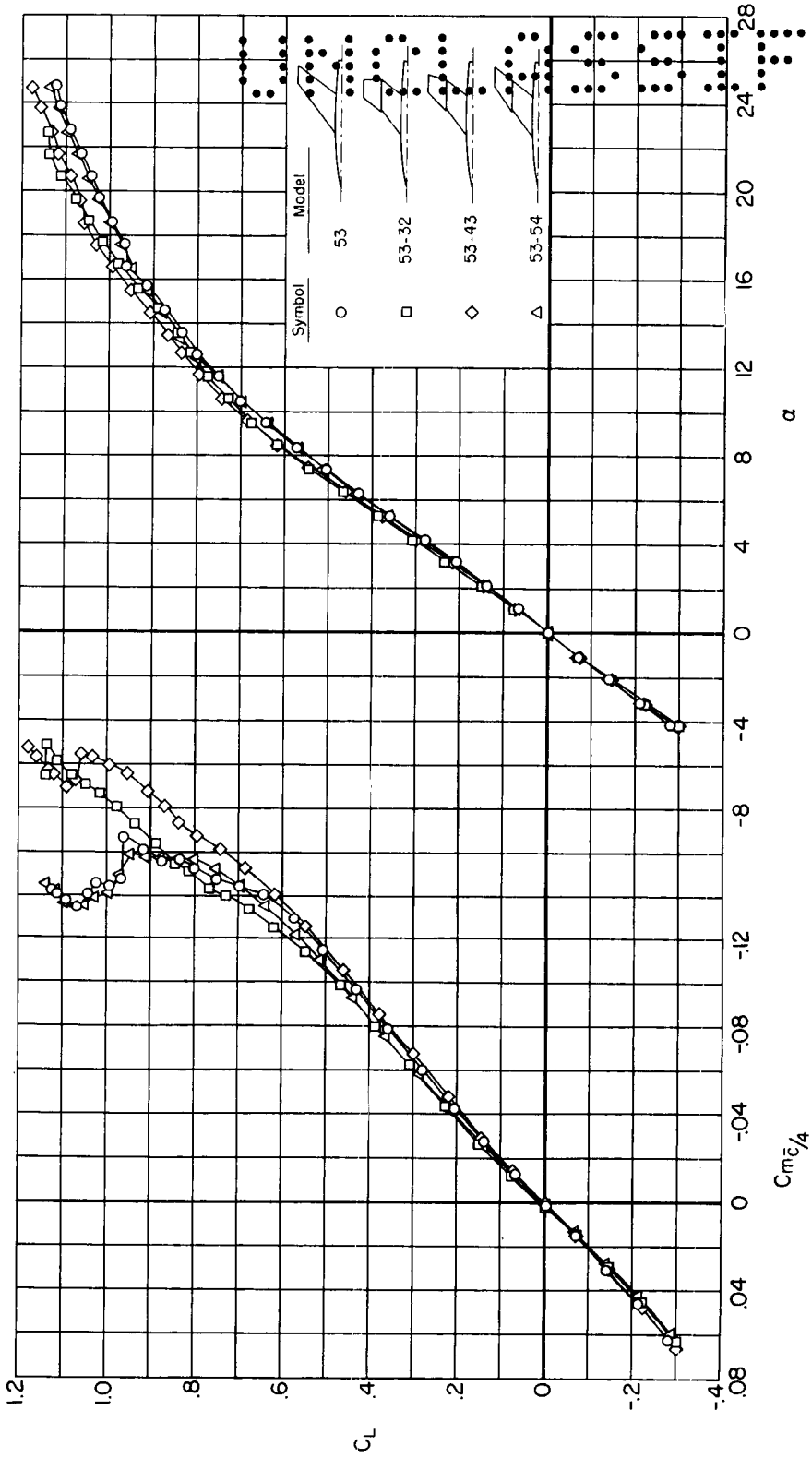

(h) M = 1.10

Figure 6.- Continued.

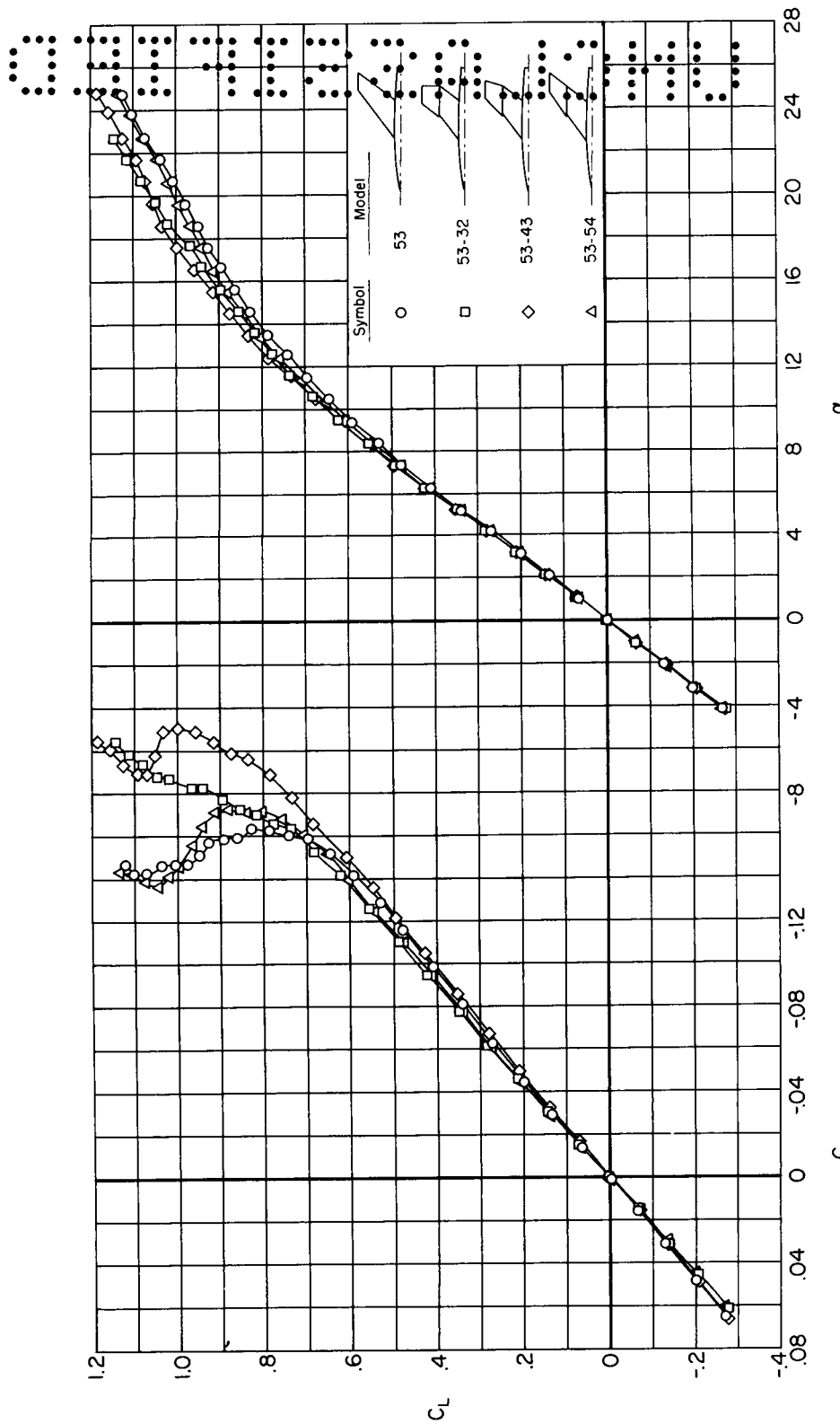

(i) M = 1.20

Figure 6.- Continued.

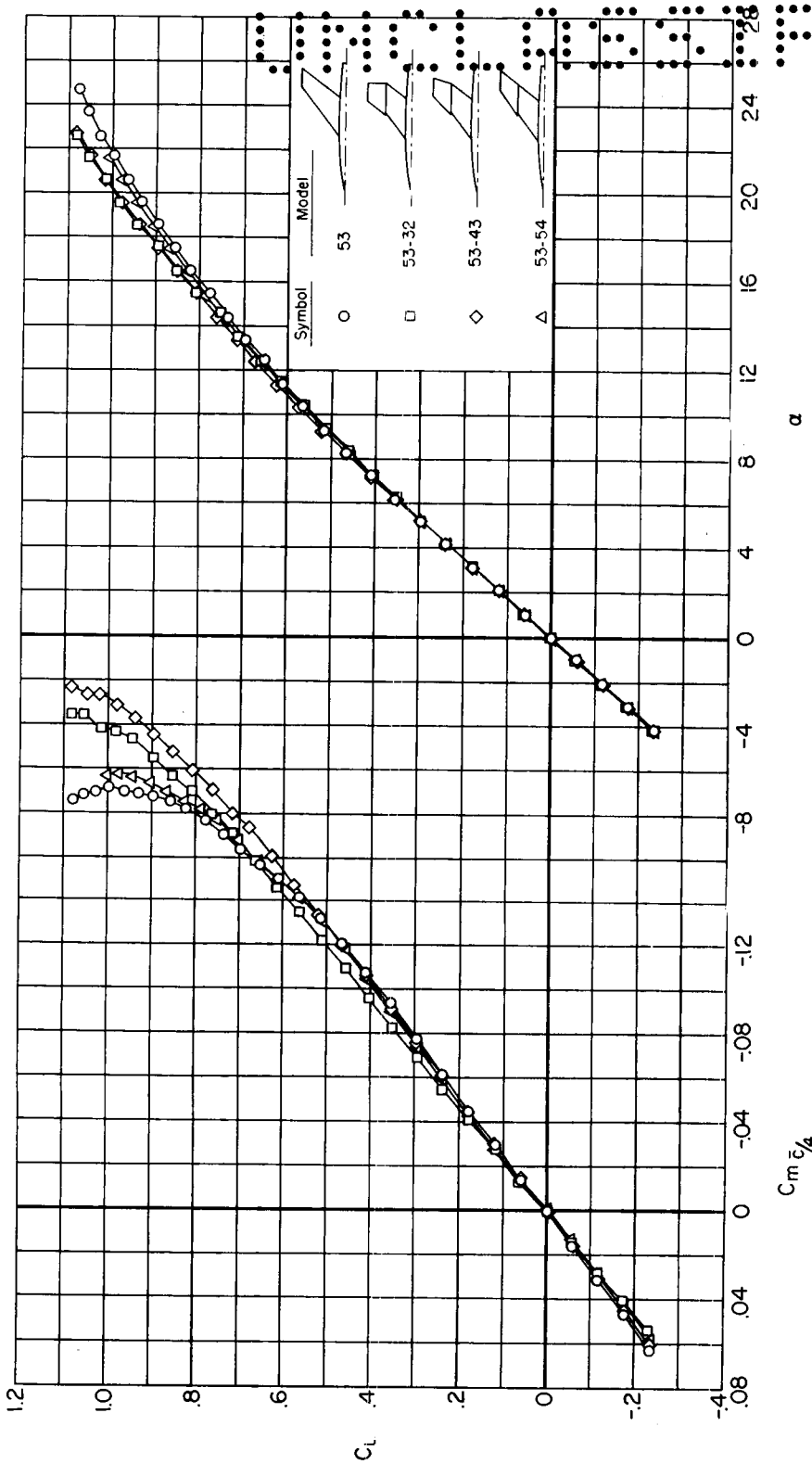

(j) M = 1.40

Figure 6.- Concluded.

A-187

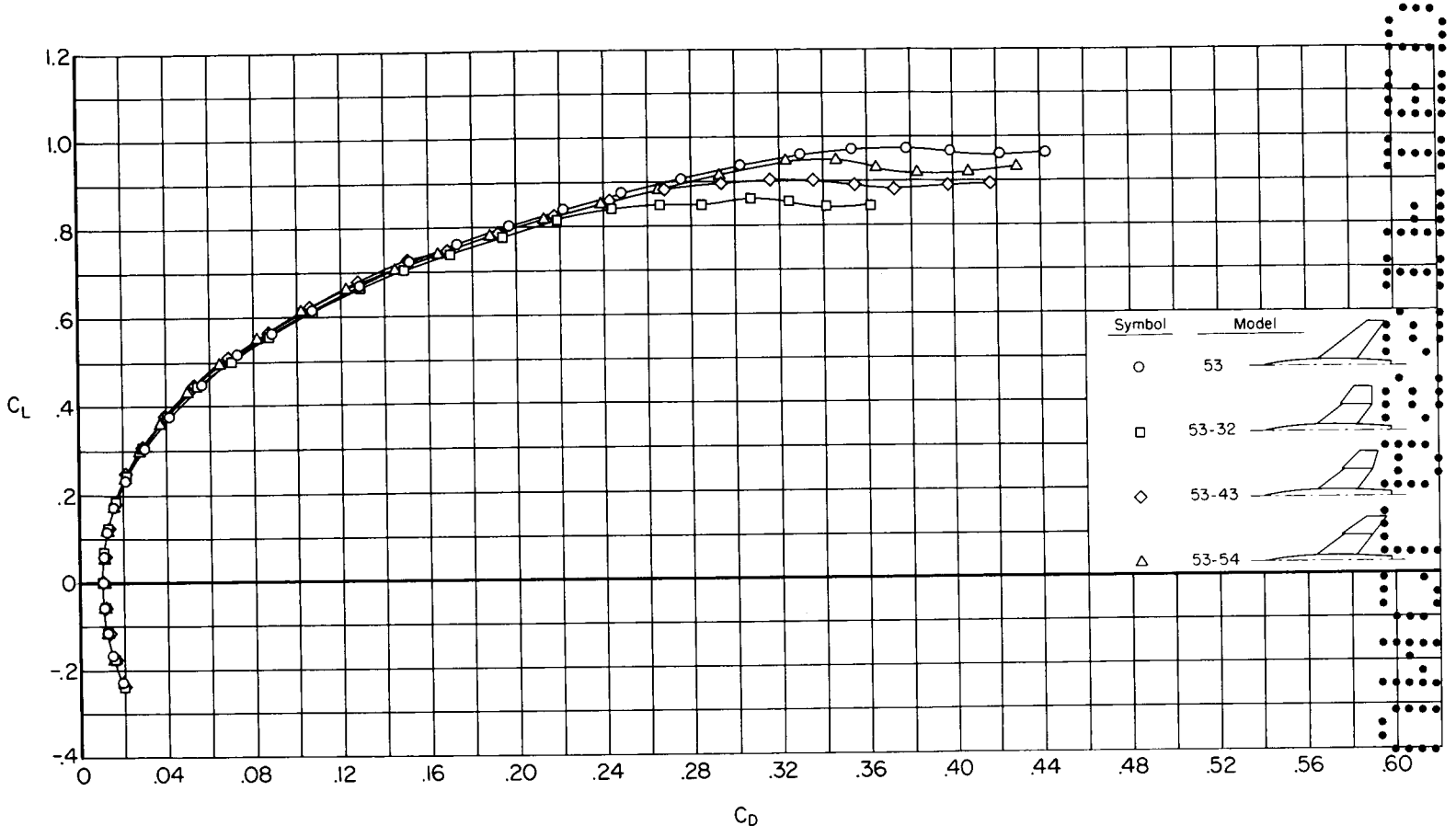

(a) M = 0.60

Figure 7.- Variation of lift coefficient with drag coefficient for the 53 series models.

CONFIDENTIAL

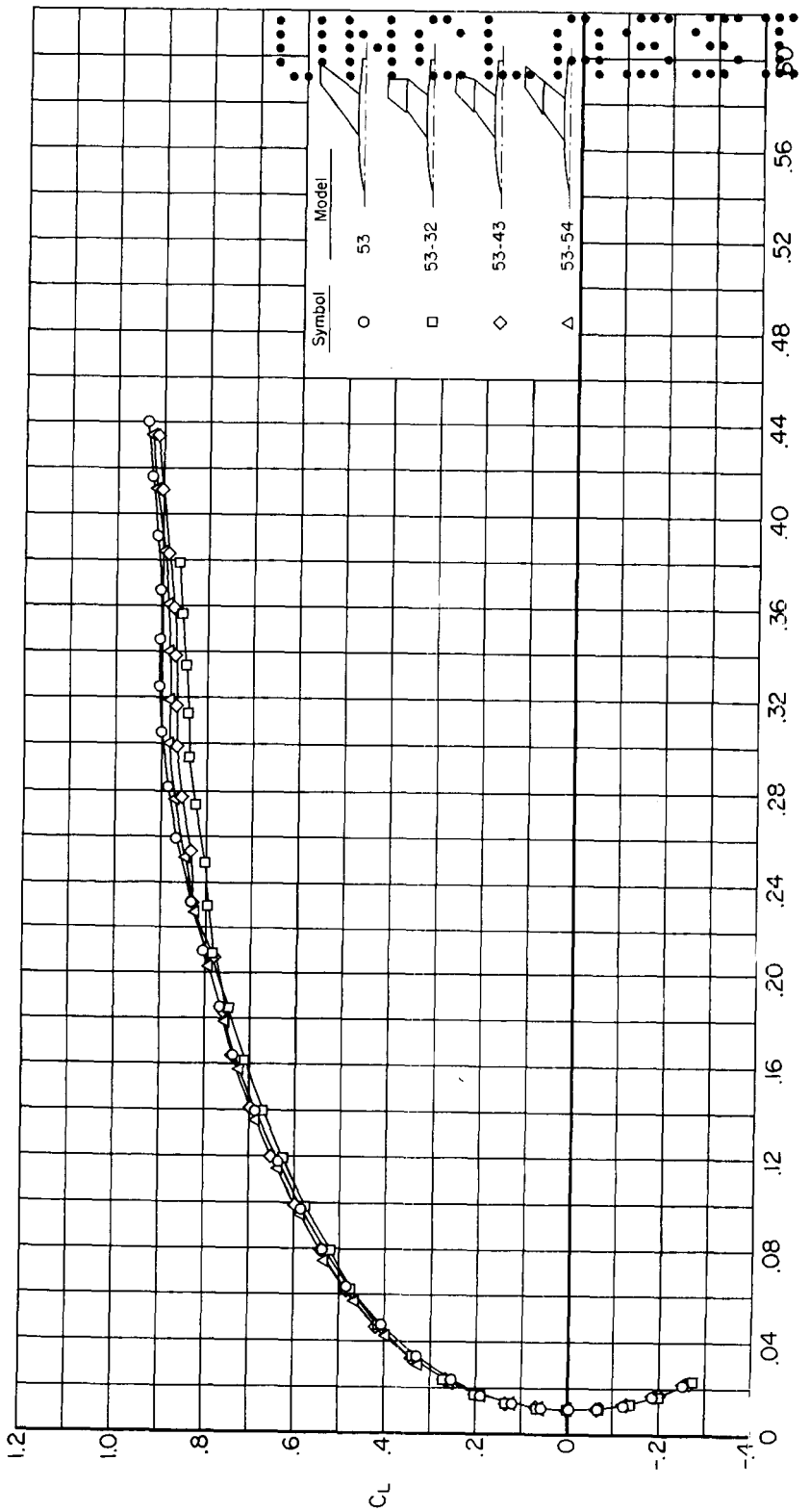

(b) M = 0.80

Figure 7.- Continued.

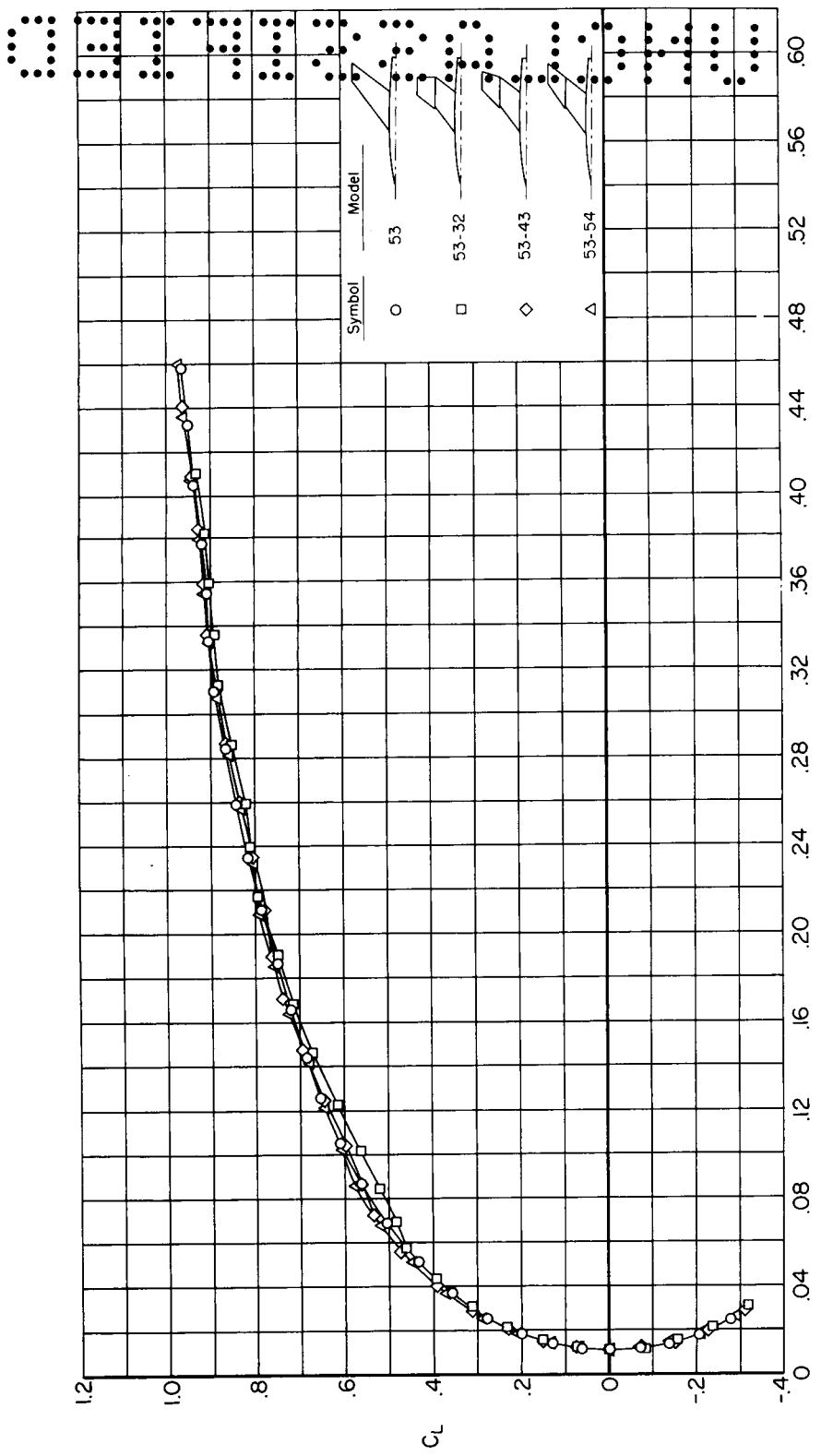

(c) M = 0.90

Figure 7.- Continued.

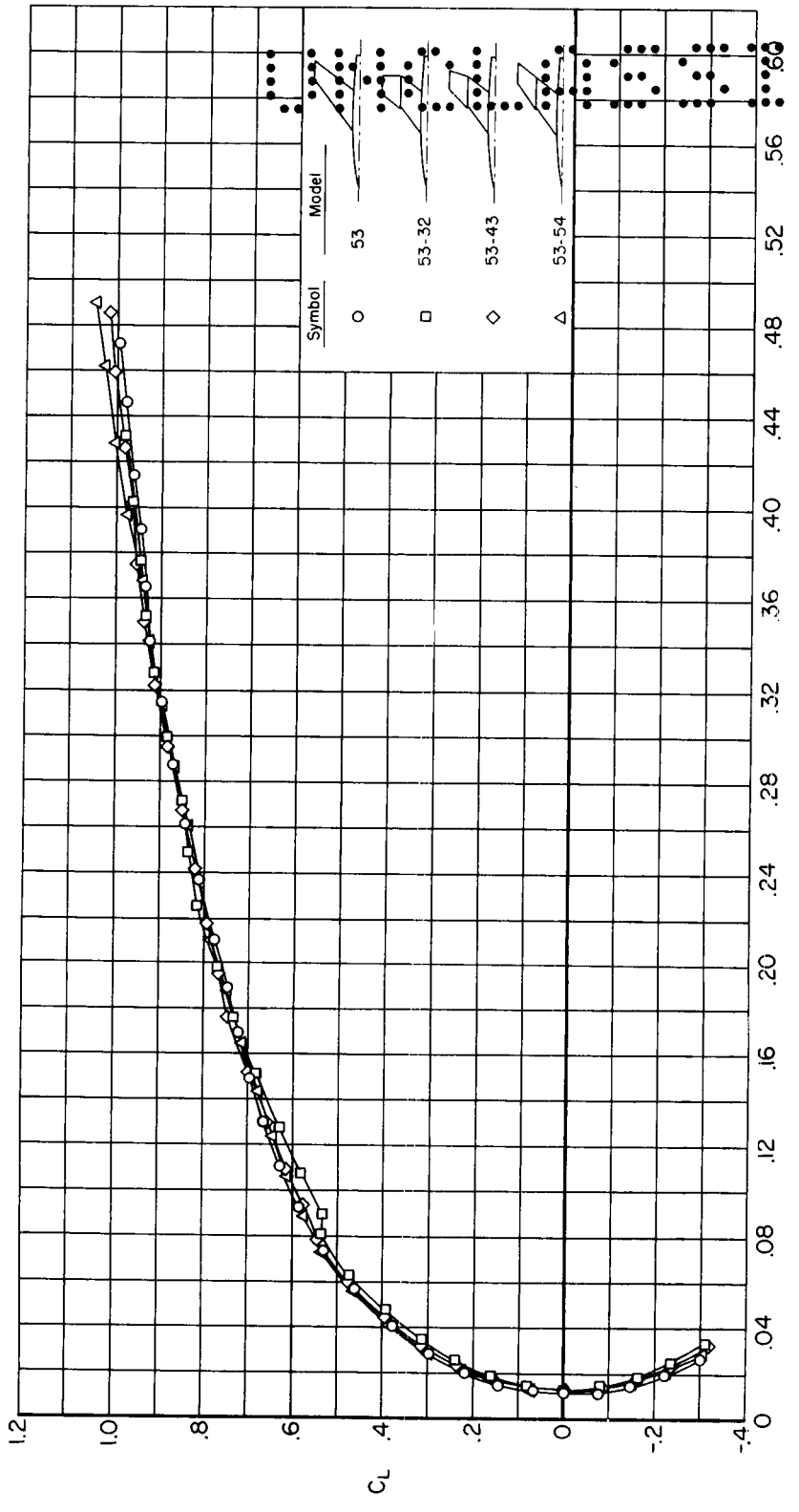

(d) M = 0.94

Figure 7.- Continued.

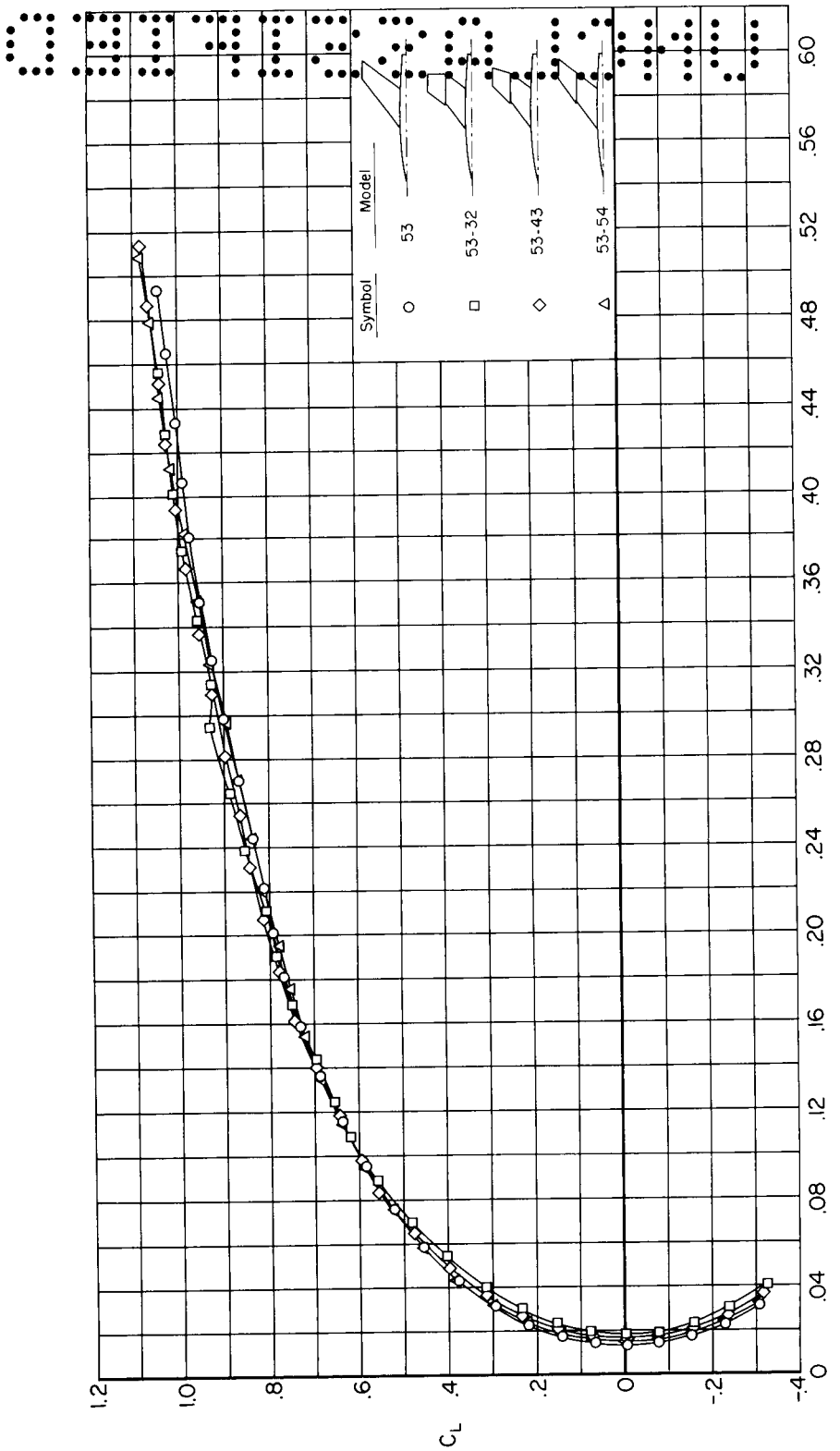

(e) M = 0.98

Figure 7.- Continued.

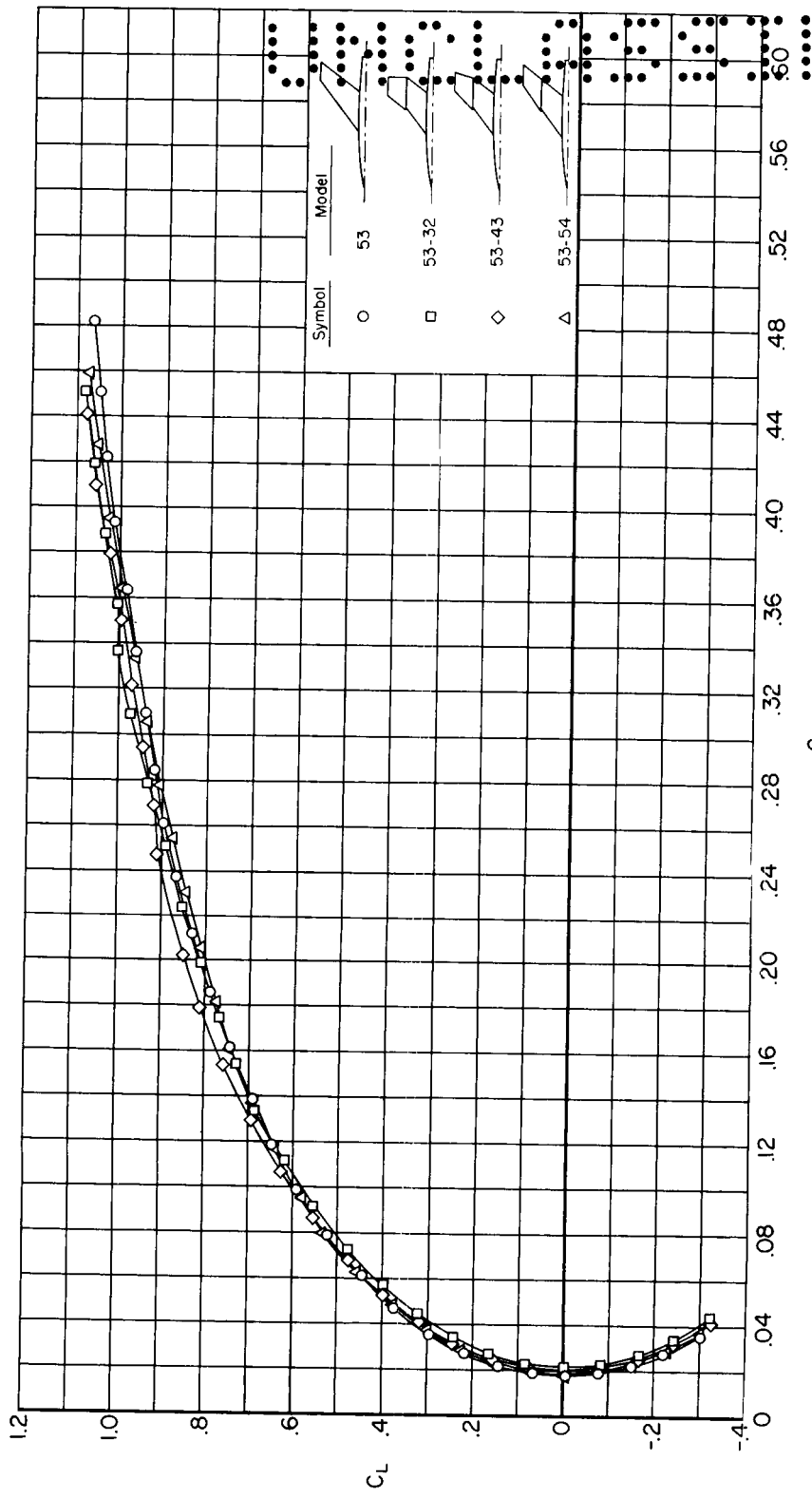

(f) M = 1.02

Figure 7.- Continued.

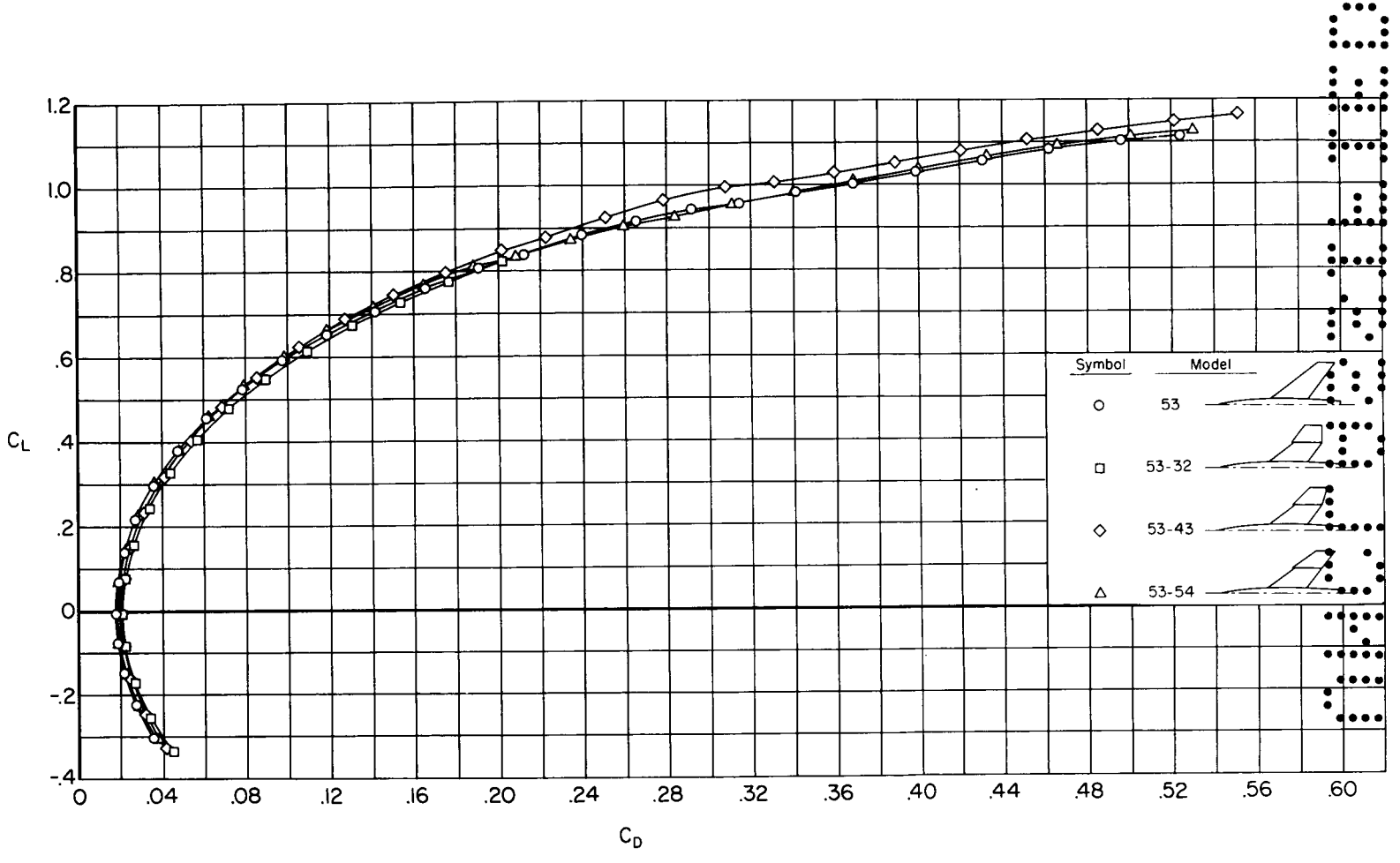

(g) M = 1.06

Figure 7.- Continued.

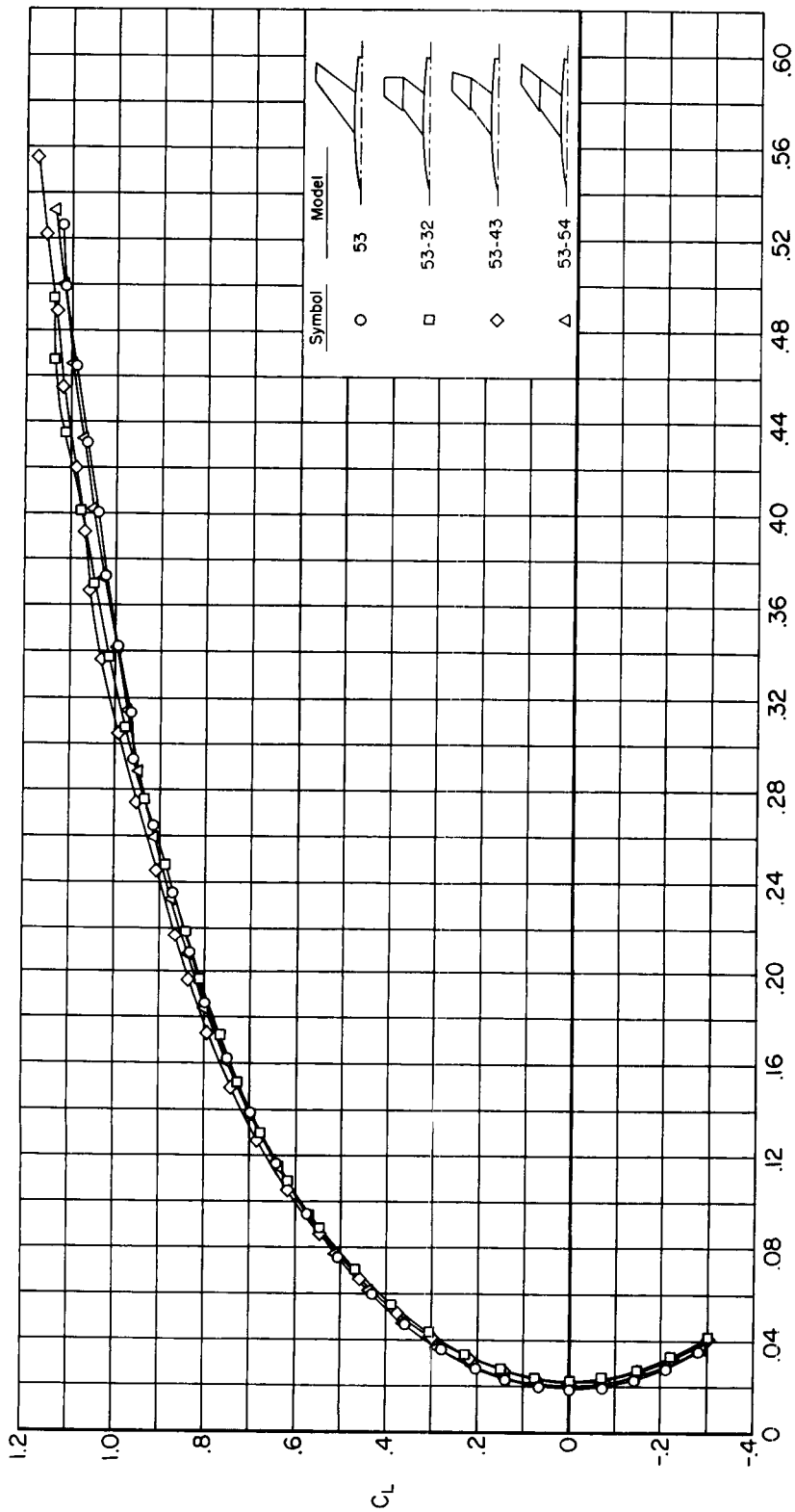

(h) M = 1.10

Figure 7.- Continued.

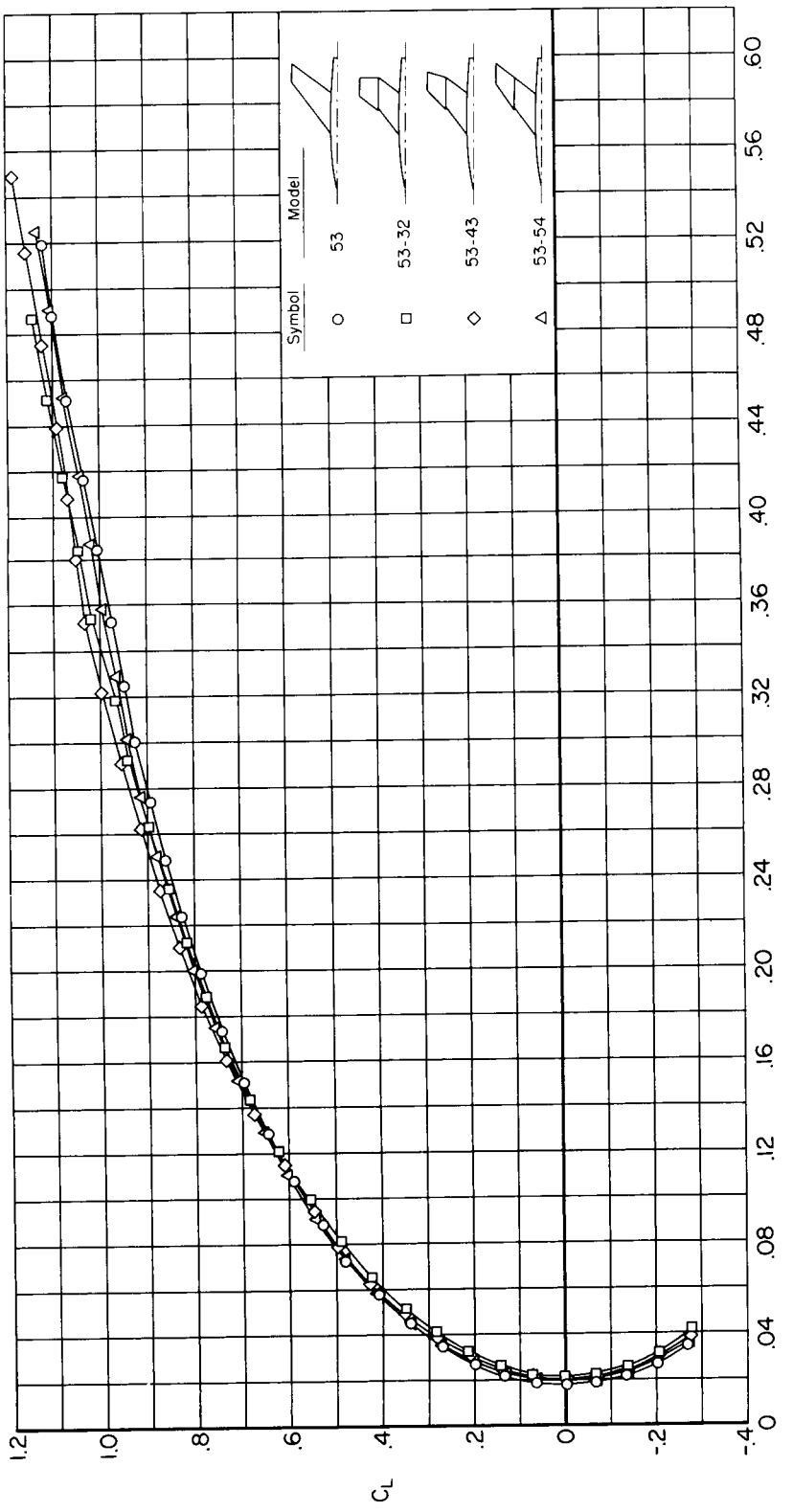

(i) M = 1.20

Figure 7.- Continued.

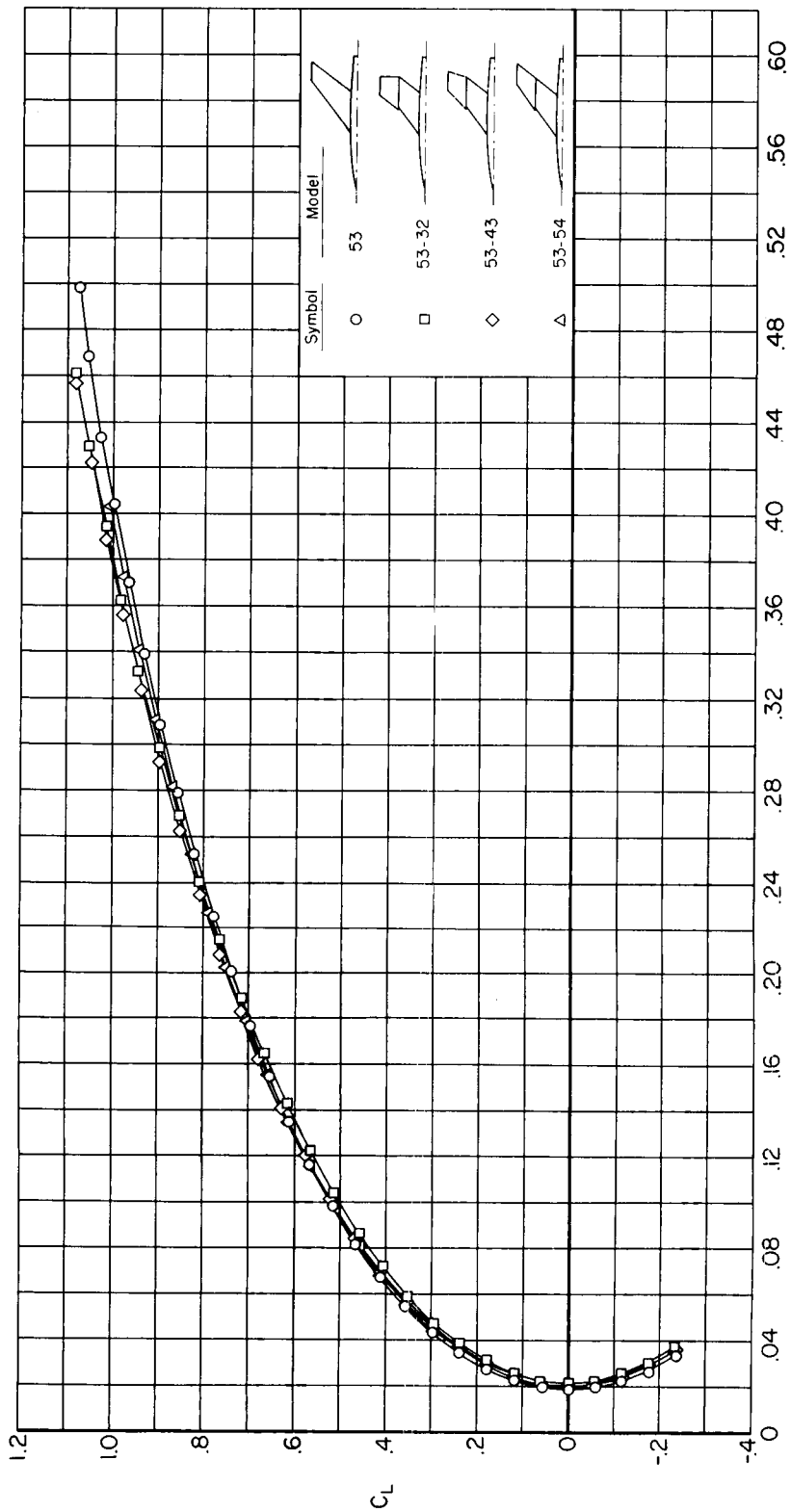

(j) M = 1.40

Figure 7.- Concluded.

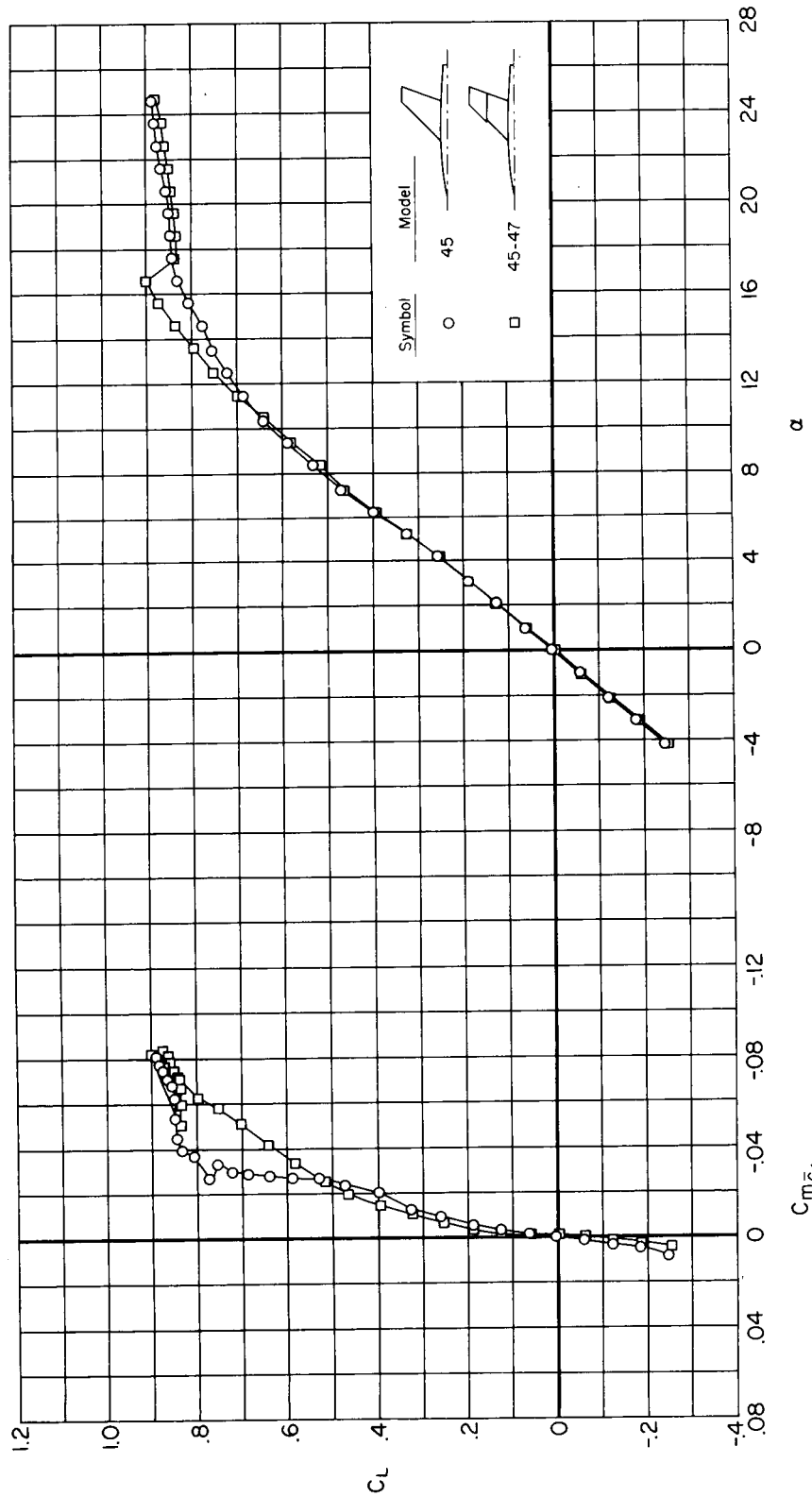

(a) M = 0.60

Figure 8.- Variation of lift coefficient with pitching-moment coefficient and angle of attack for the 45 series models.

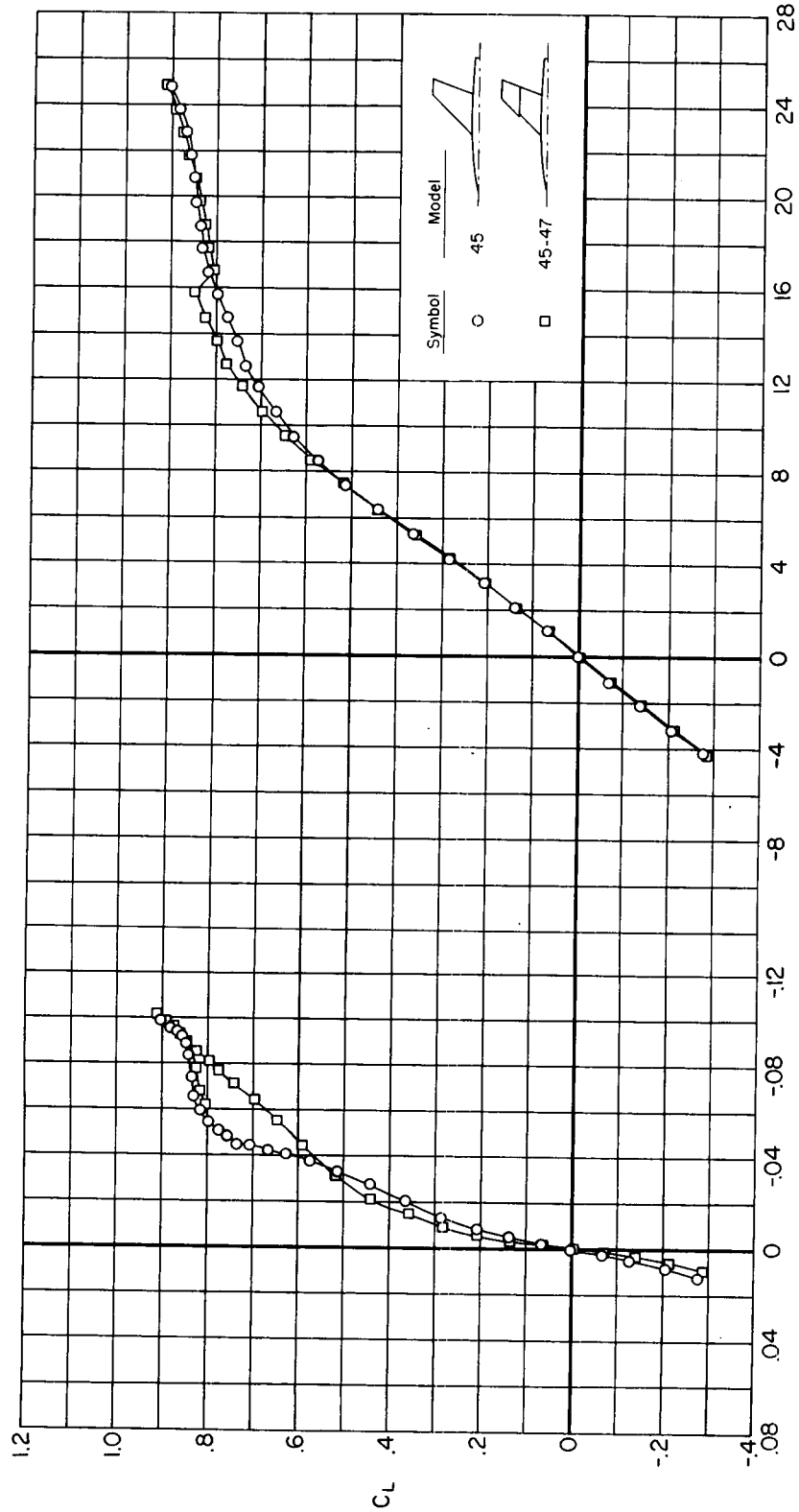

(b) M = 0.80

Figure 8.- Continued.

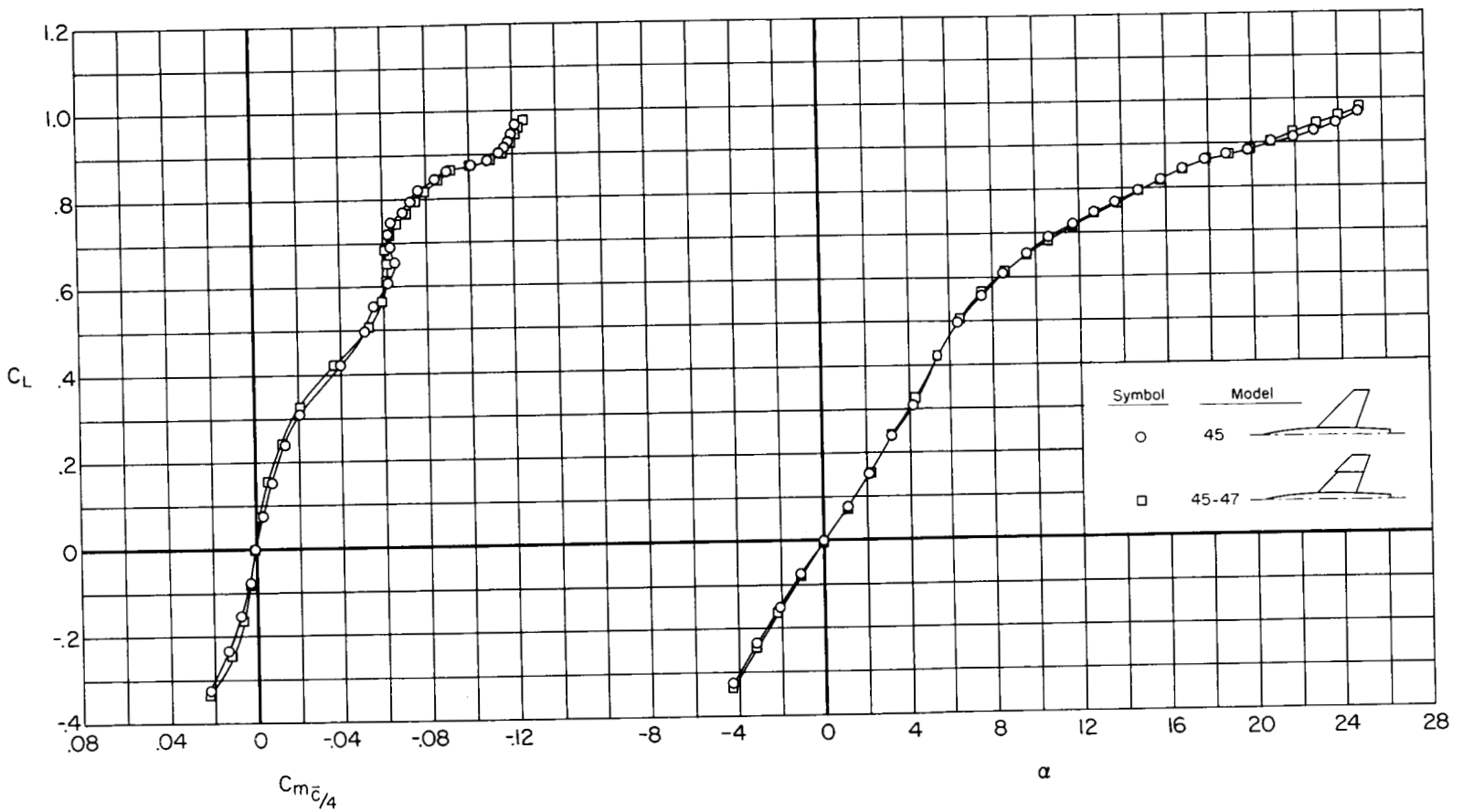

(c) M = 0.90

Figure 8.- Continued.

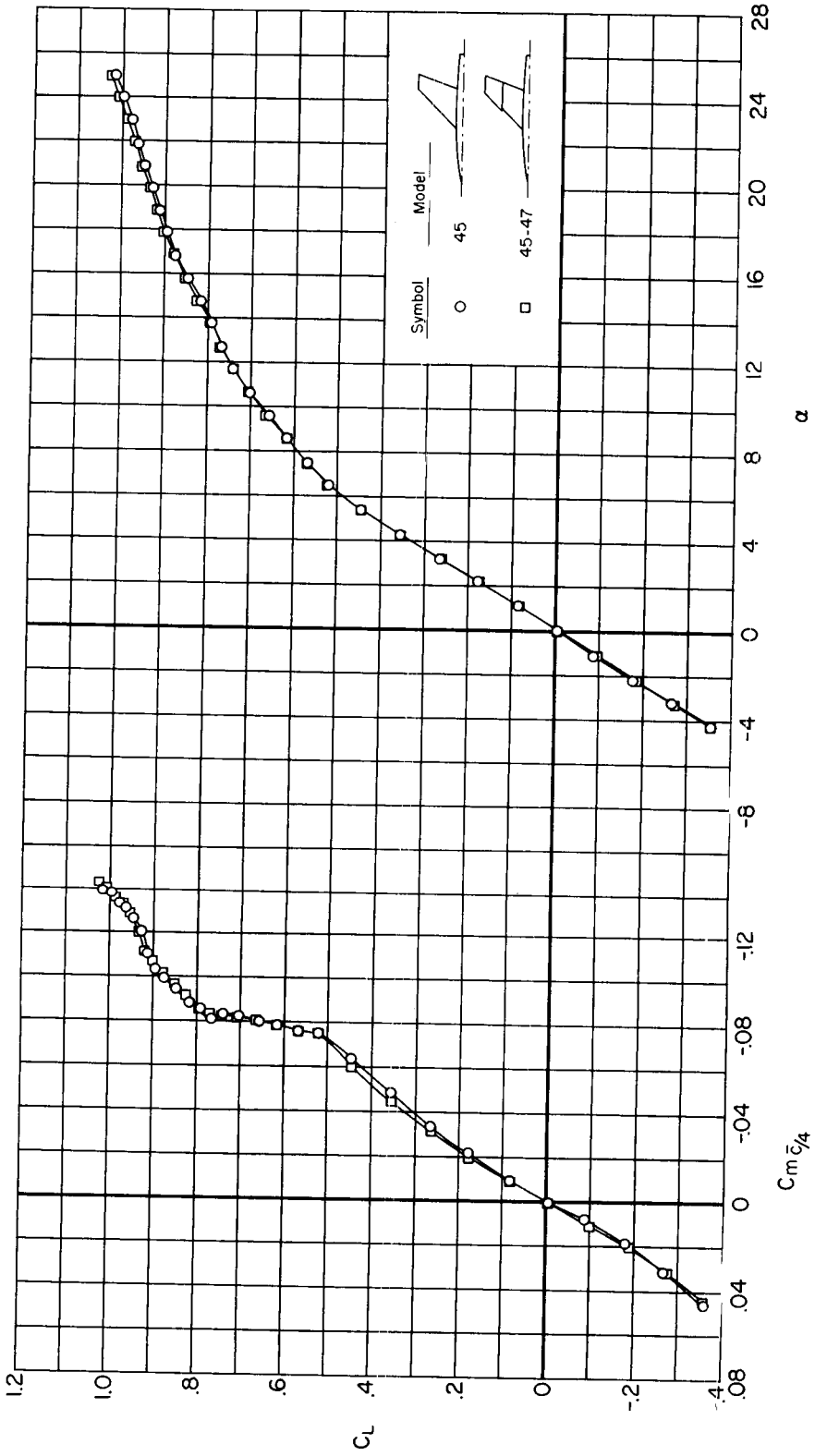

(d) M = 0.94

Figure 8.- Continued.

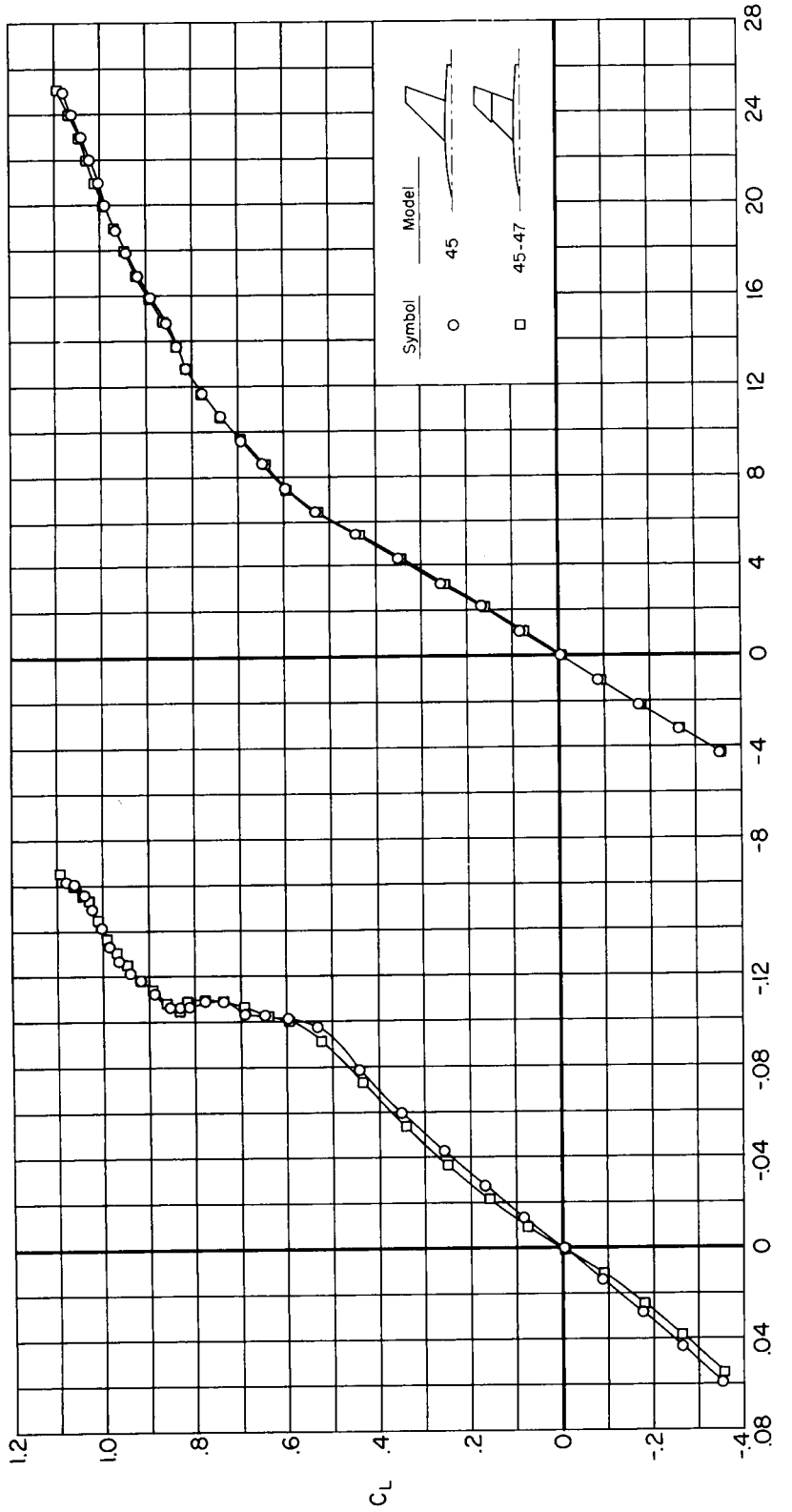

(e) M = 0.98

Figure 8.- Continued.

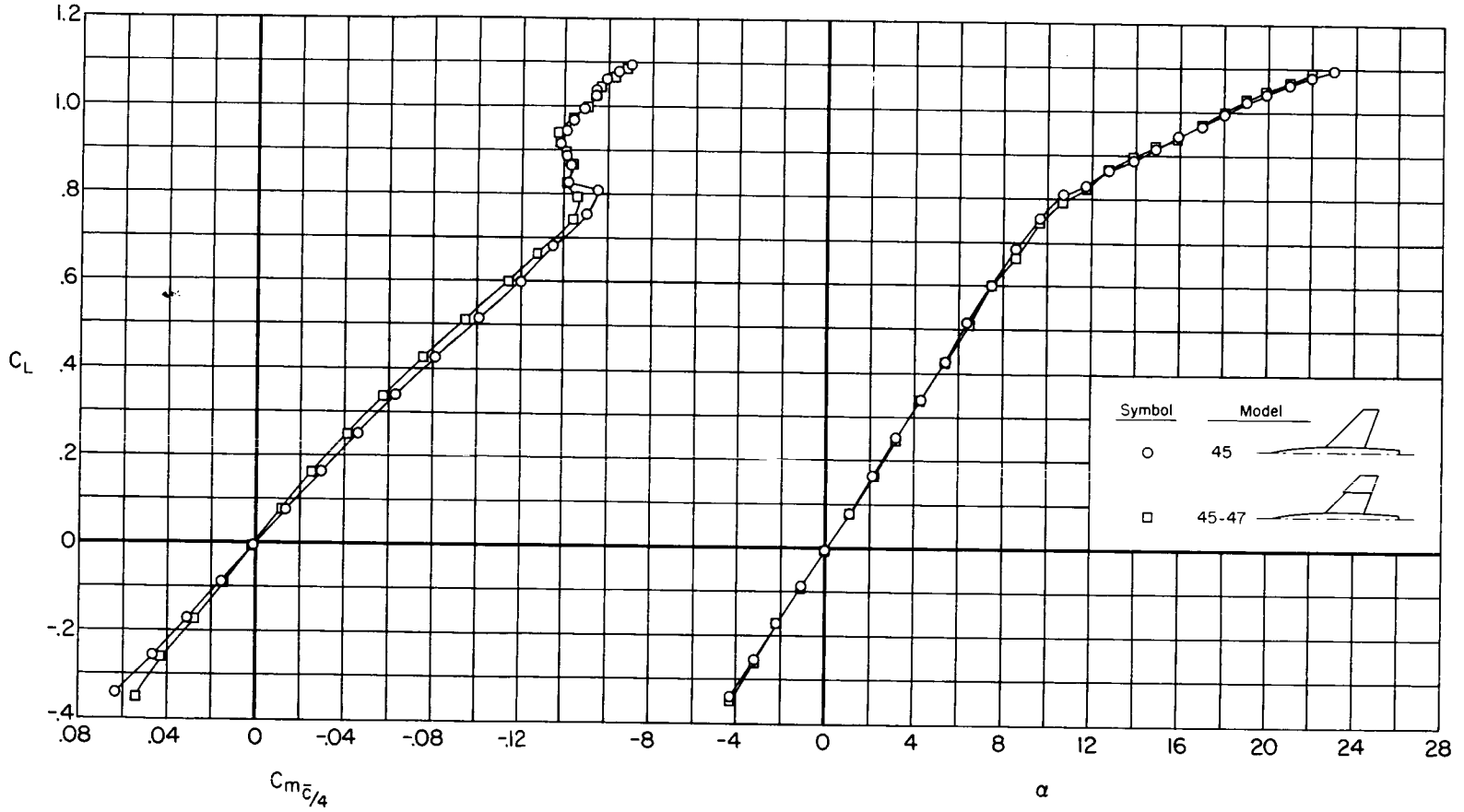

(f) M = 1.02

Figure 8.- Continued.

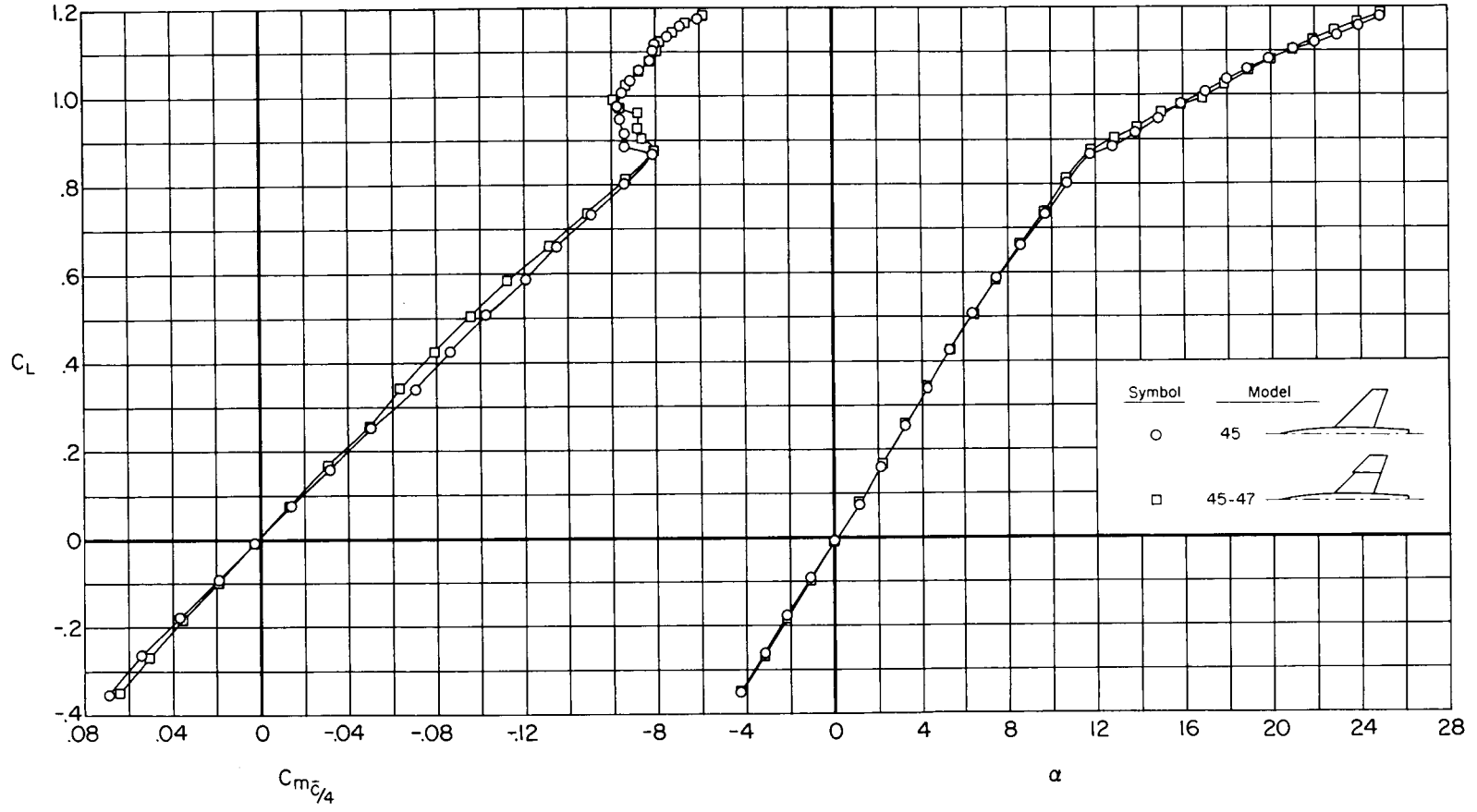

(g) M = 1.06

Figure 8.- Continued.

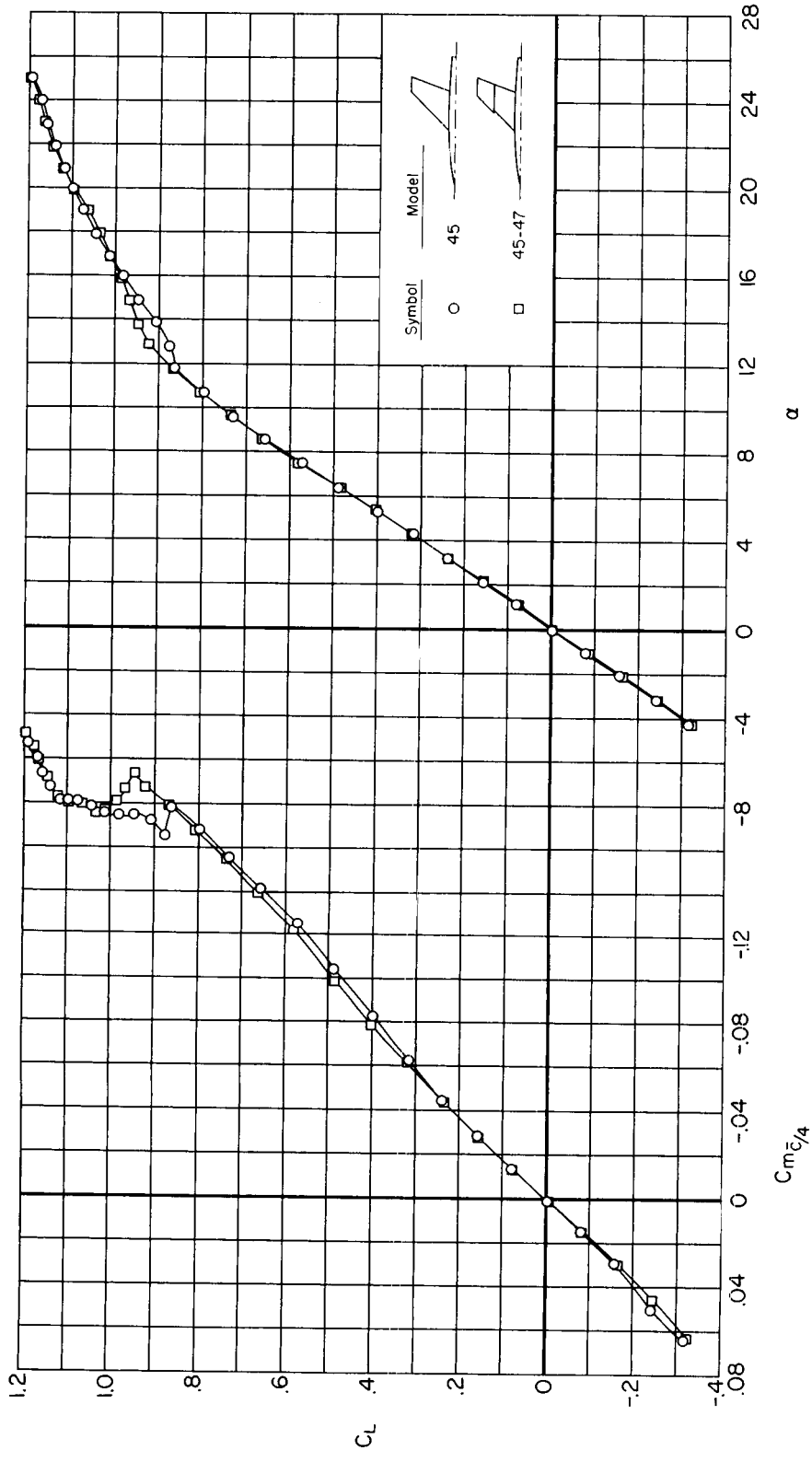

(h) M = 1.10

Figure 8.- Continued.

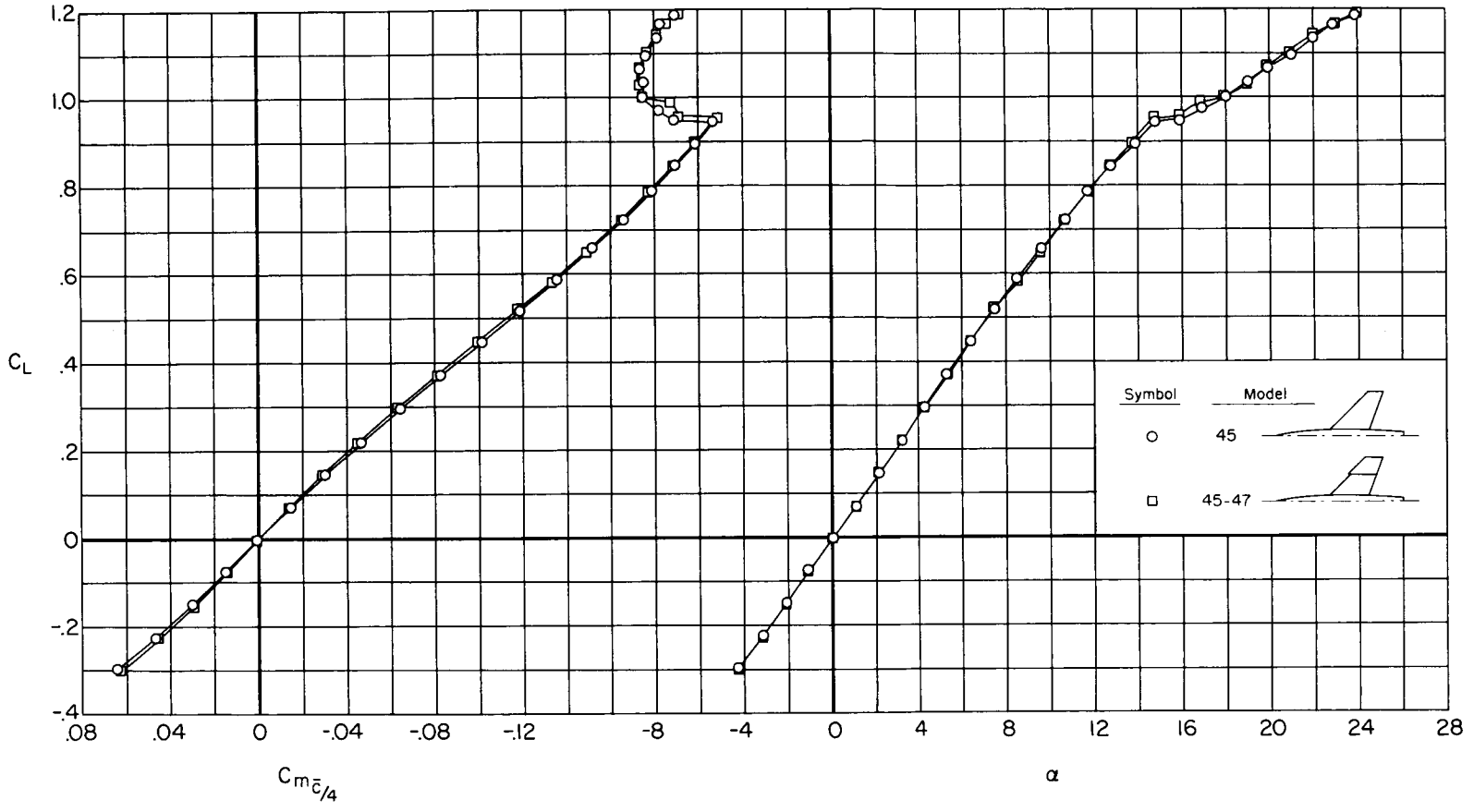

(i) M = 1.20

Figure 8.- Continued.

CONFIDENTIAL

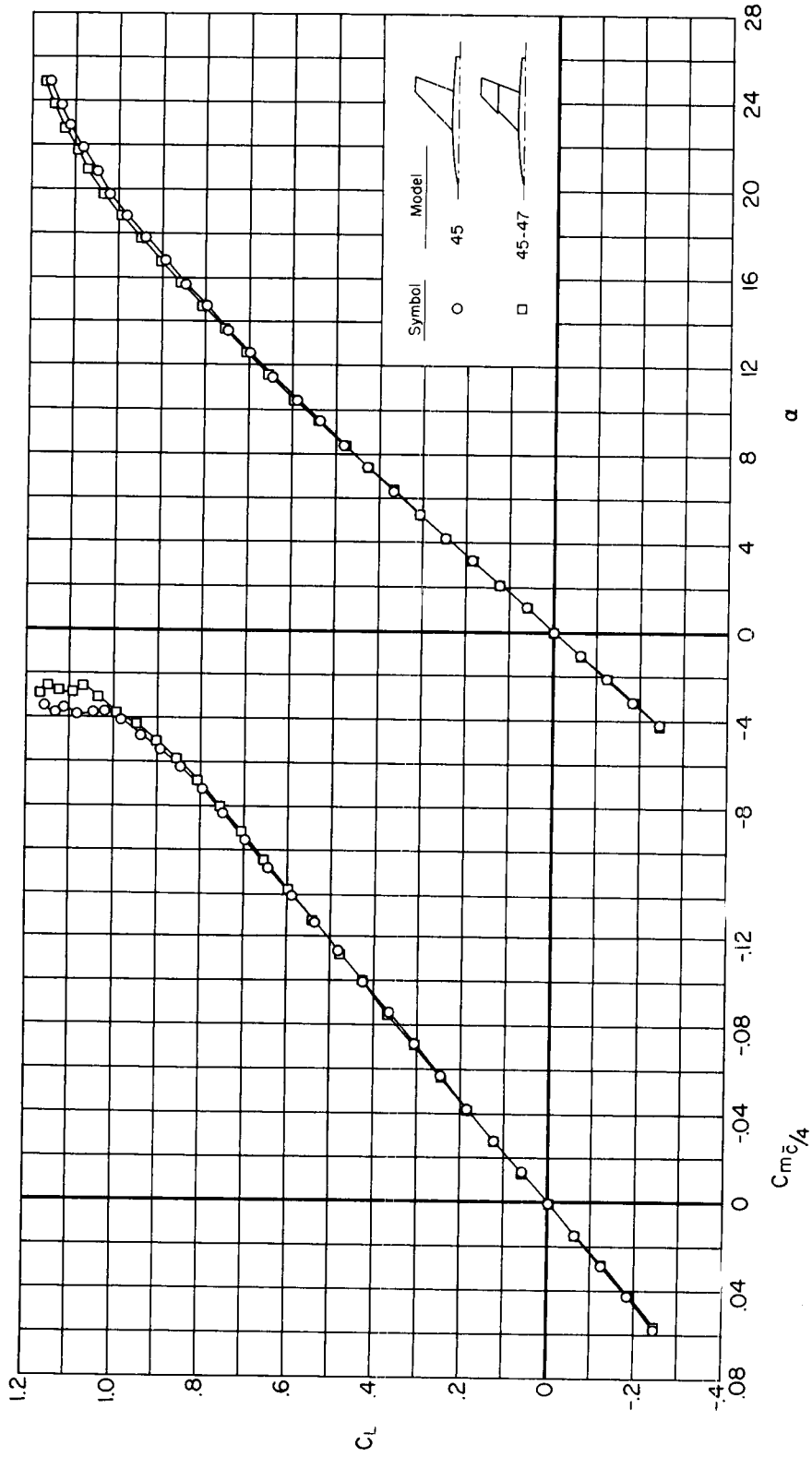

(j) M = 1.40

Figure 8.- Concluded.

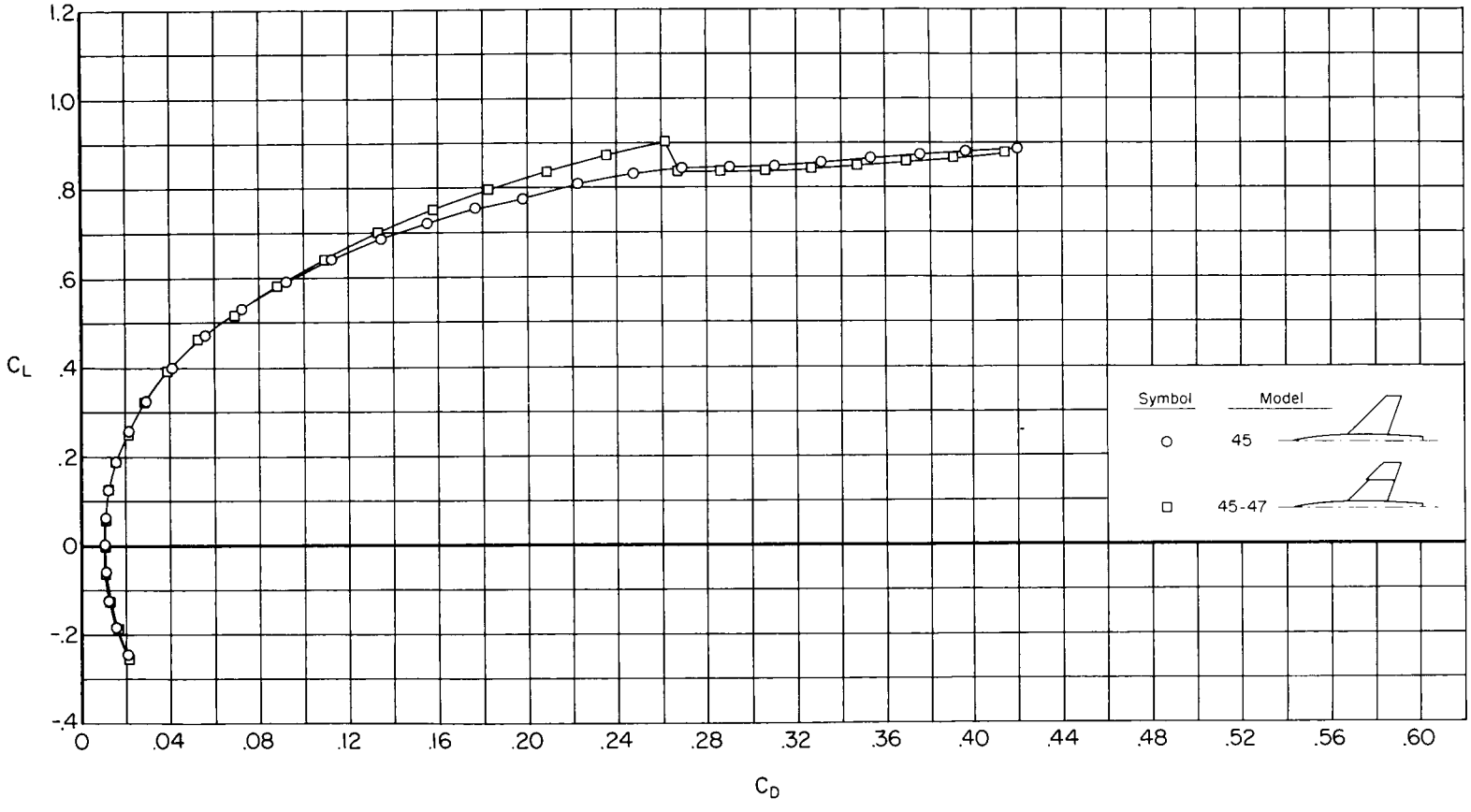

(a) M = 0.60

Figure 9.- Variation of lift coefficient with drag coefficient for the 45 series models.

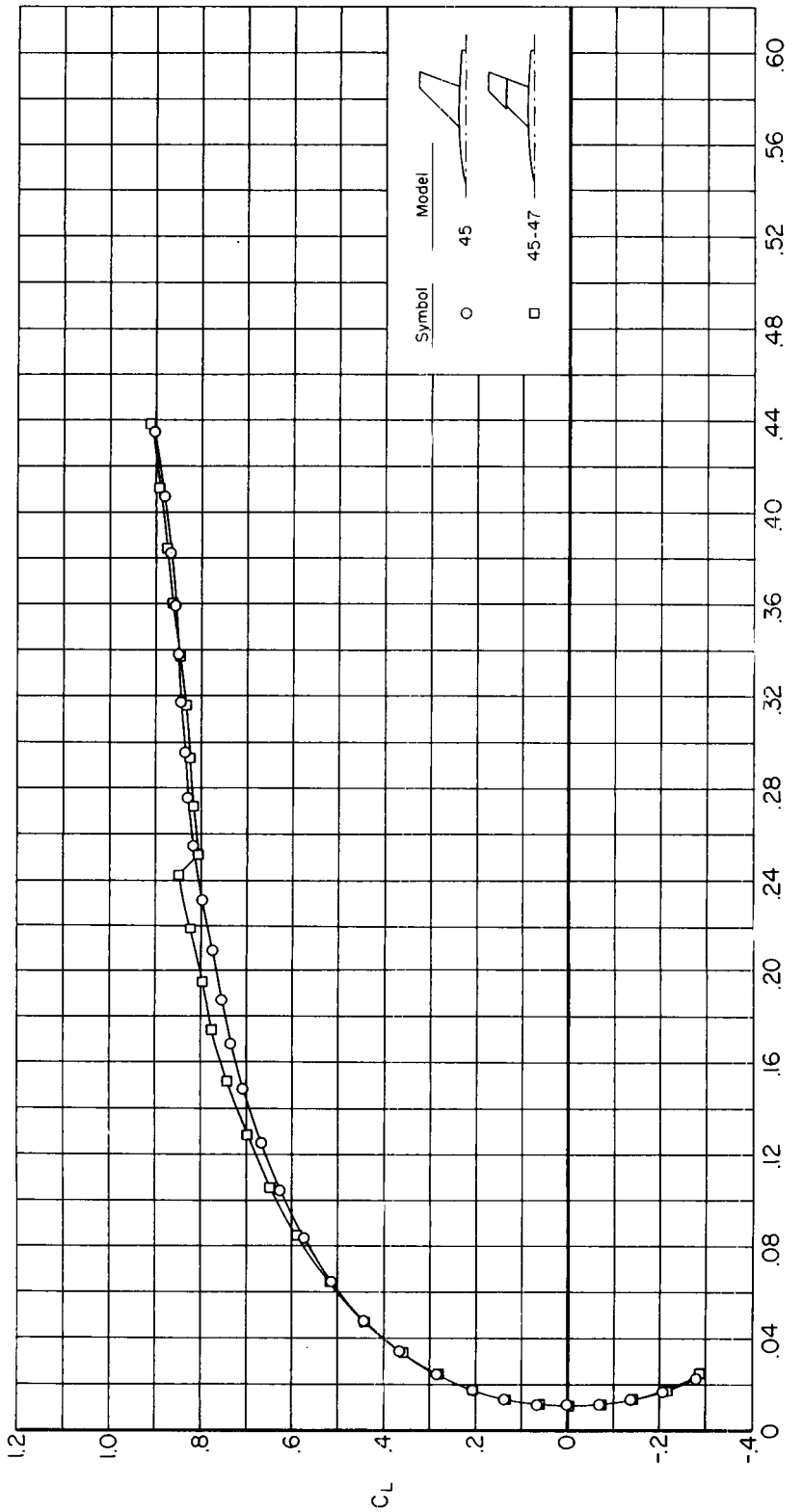

(b) M = 0.80

Figure 9.- Continued.

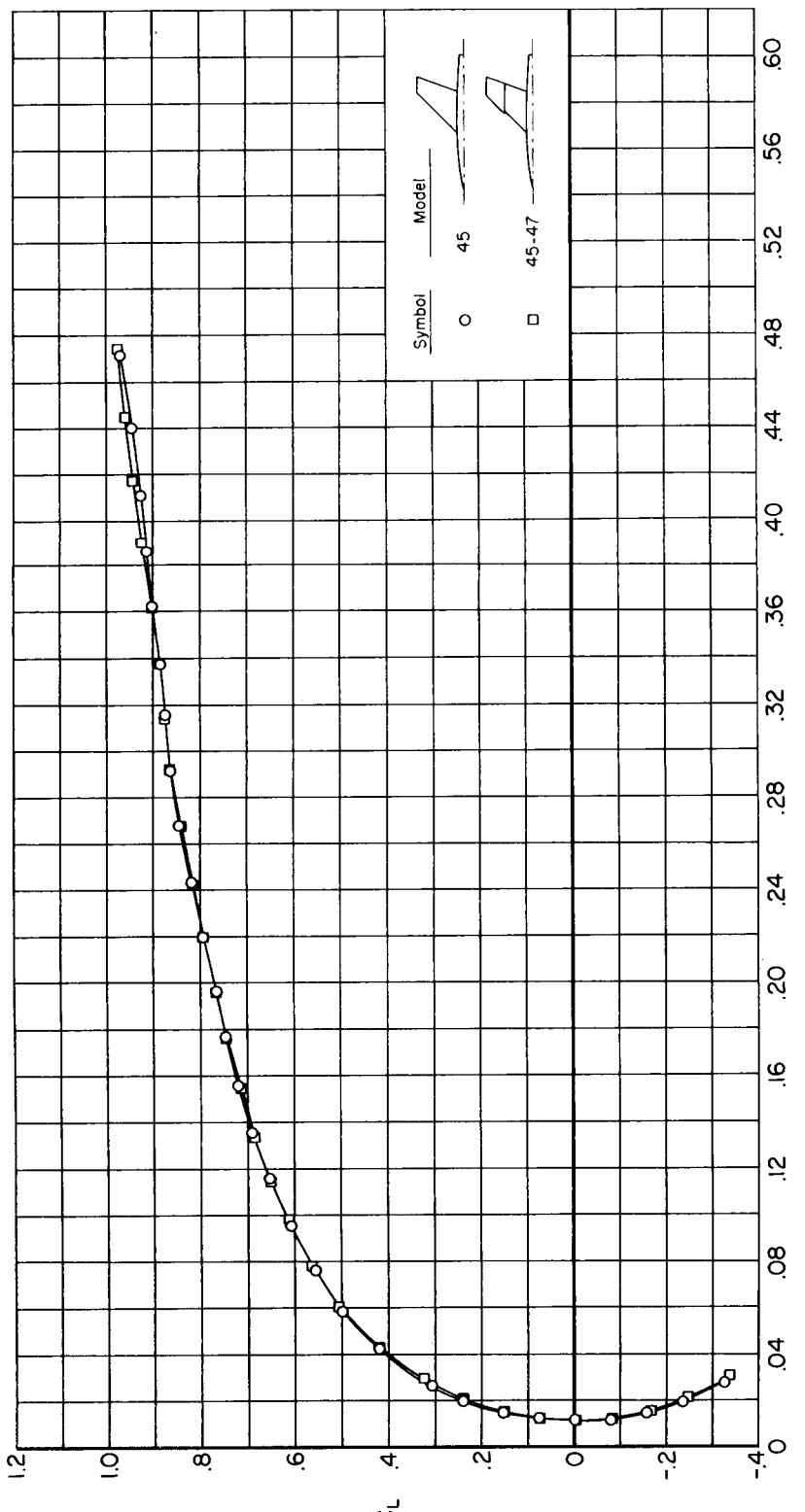

(c) M = 0.90

Figure 9.- Continued.

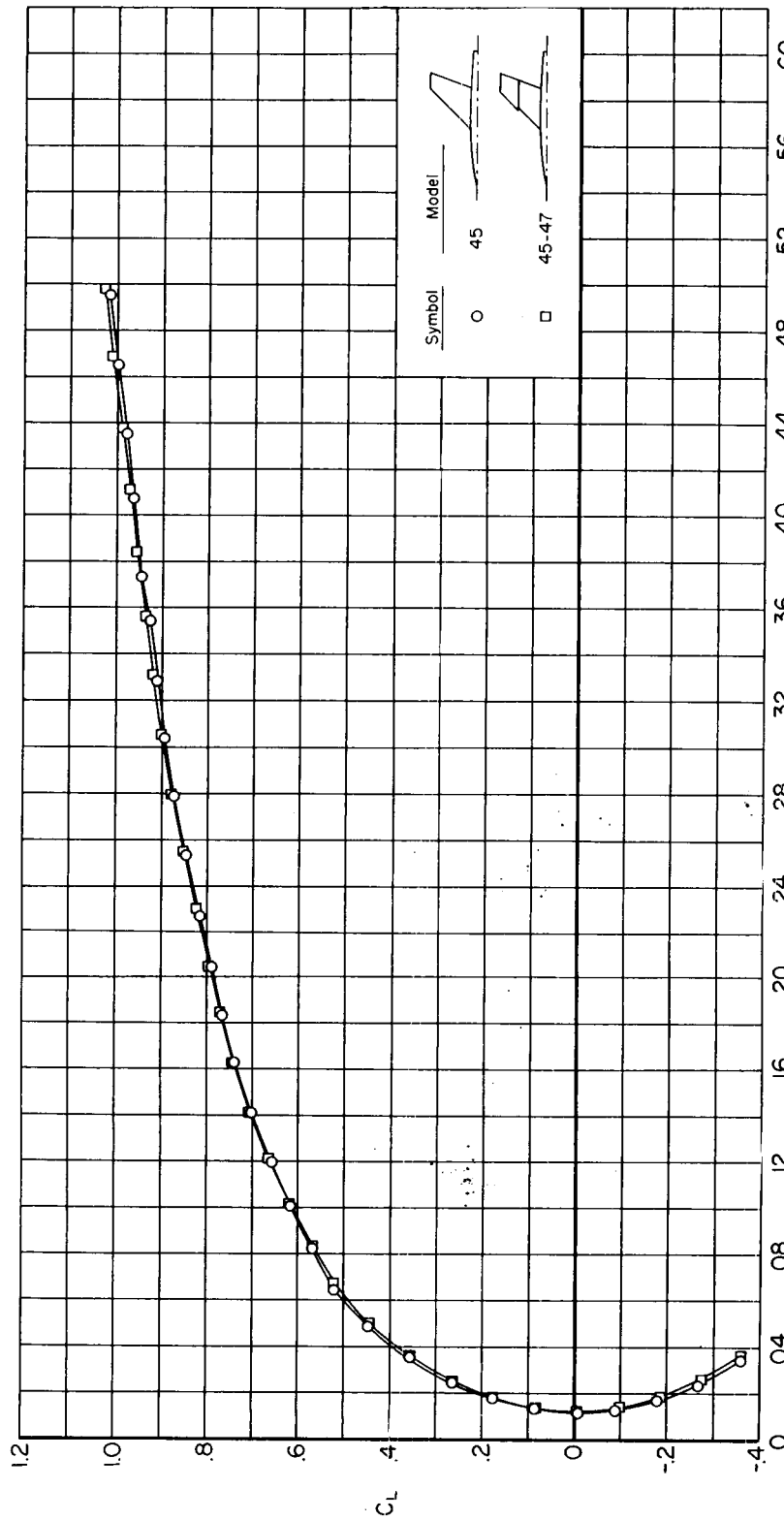

(d) M = 0.94

Figure 9.- Continued.

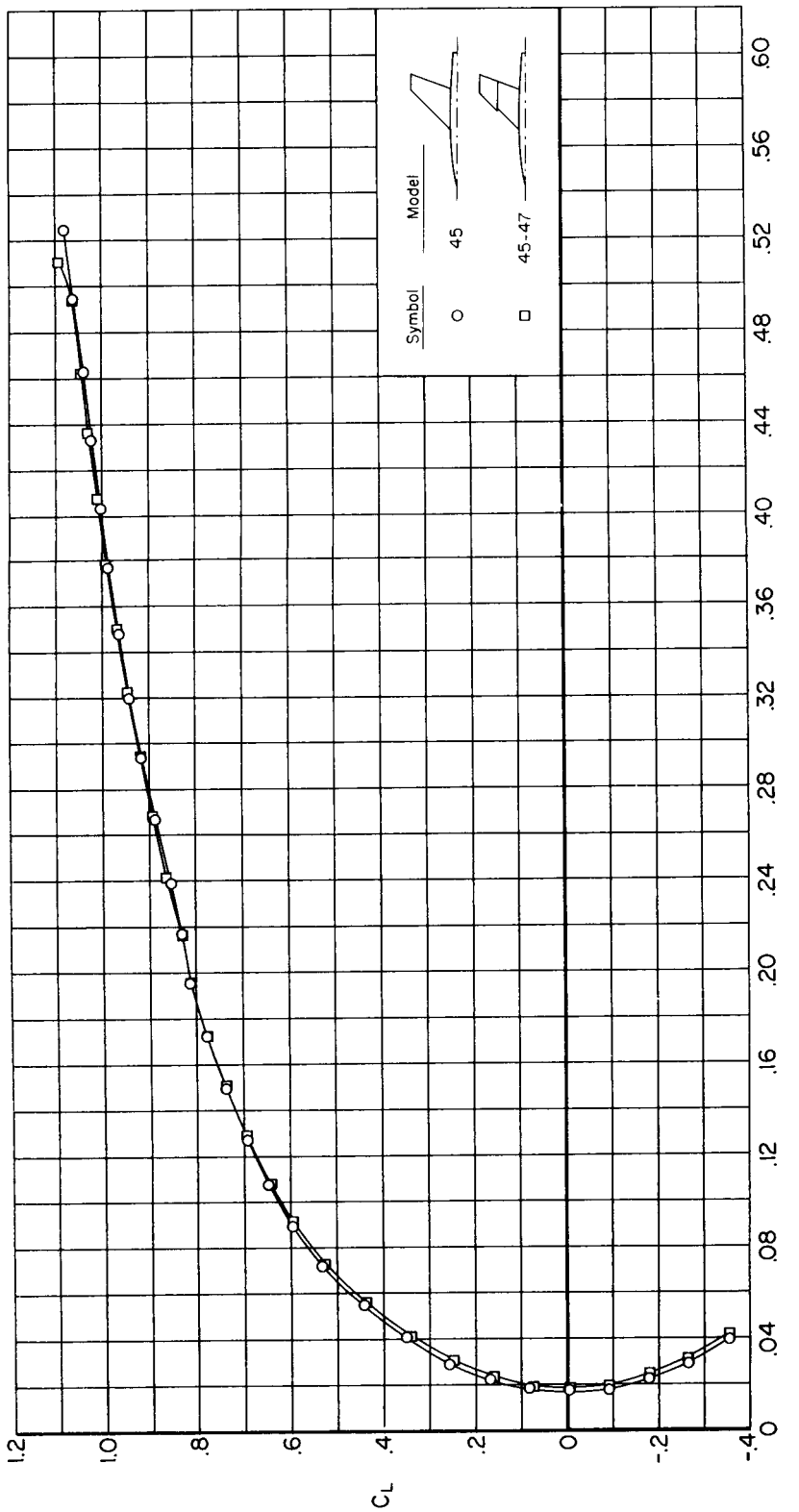

(e) M = 0.98

Figure 9.- Continued.

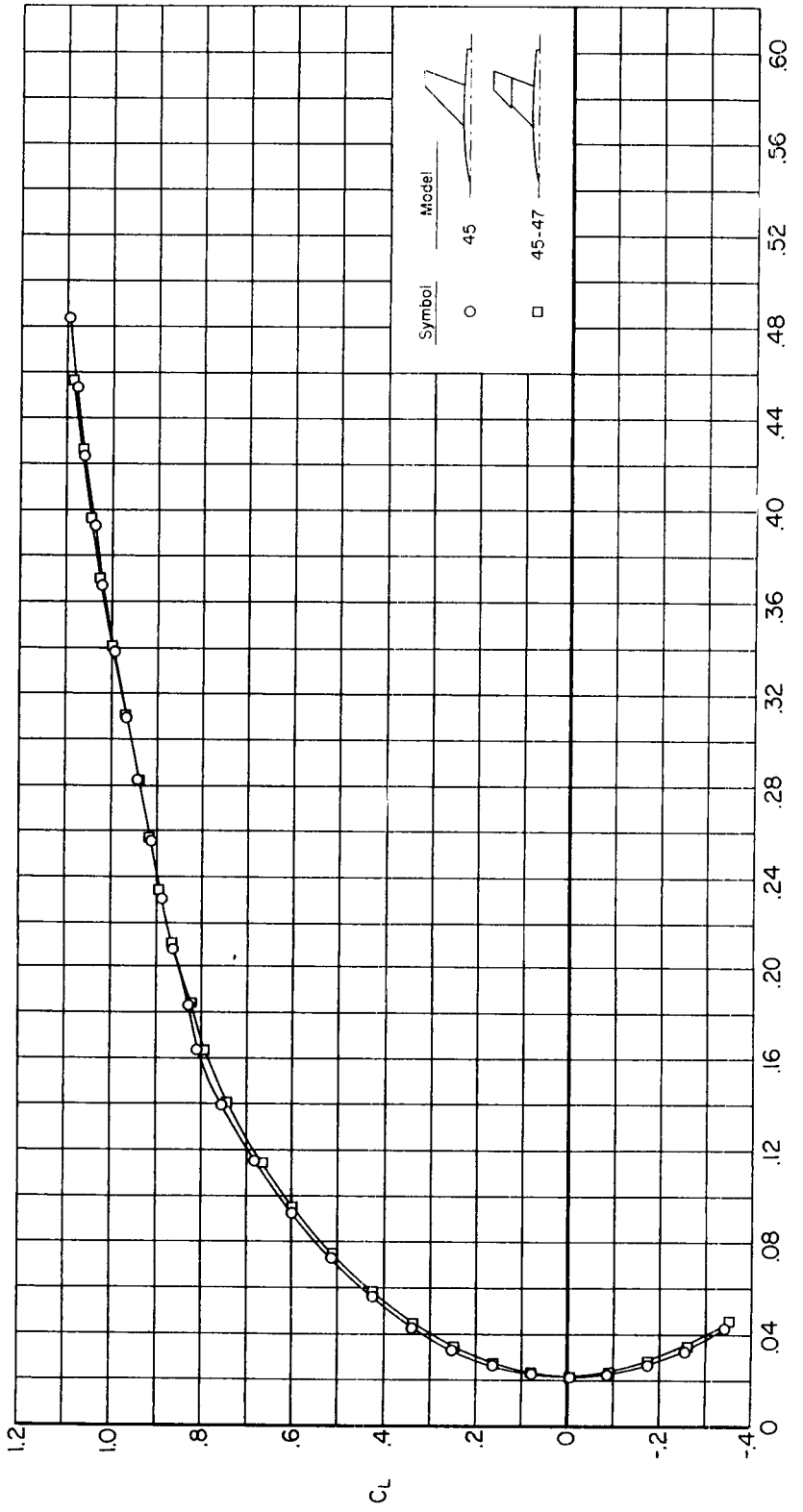

(f) M = 1.02

Figure 9.- Continued.

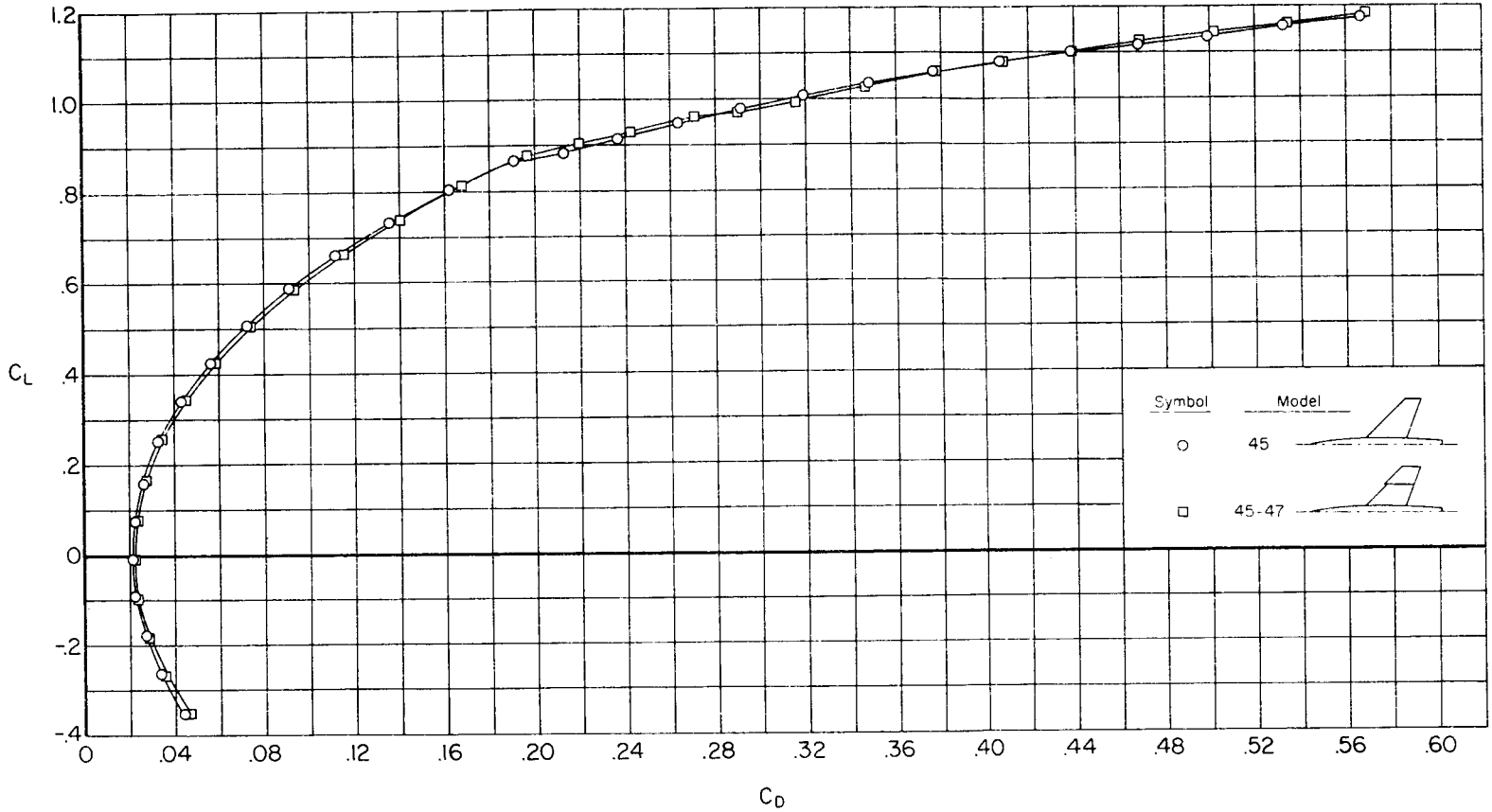

(g) M = 1.06

Figure 9.- Continued.

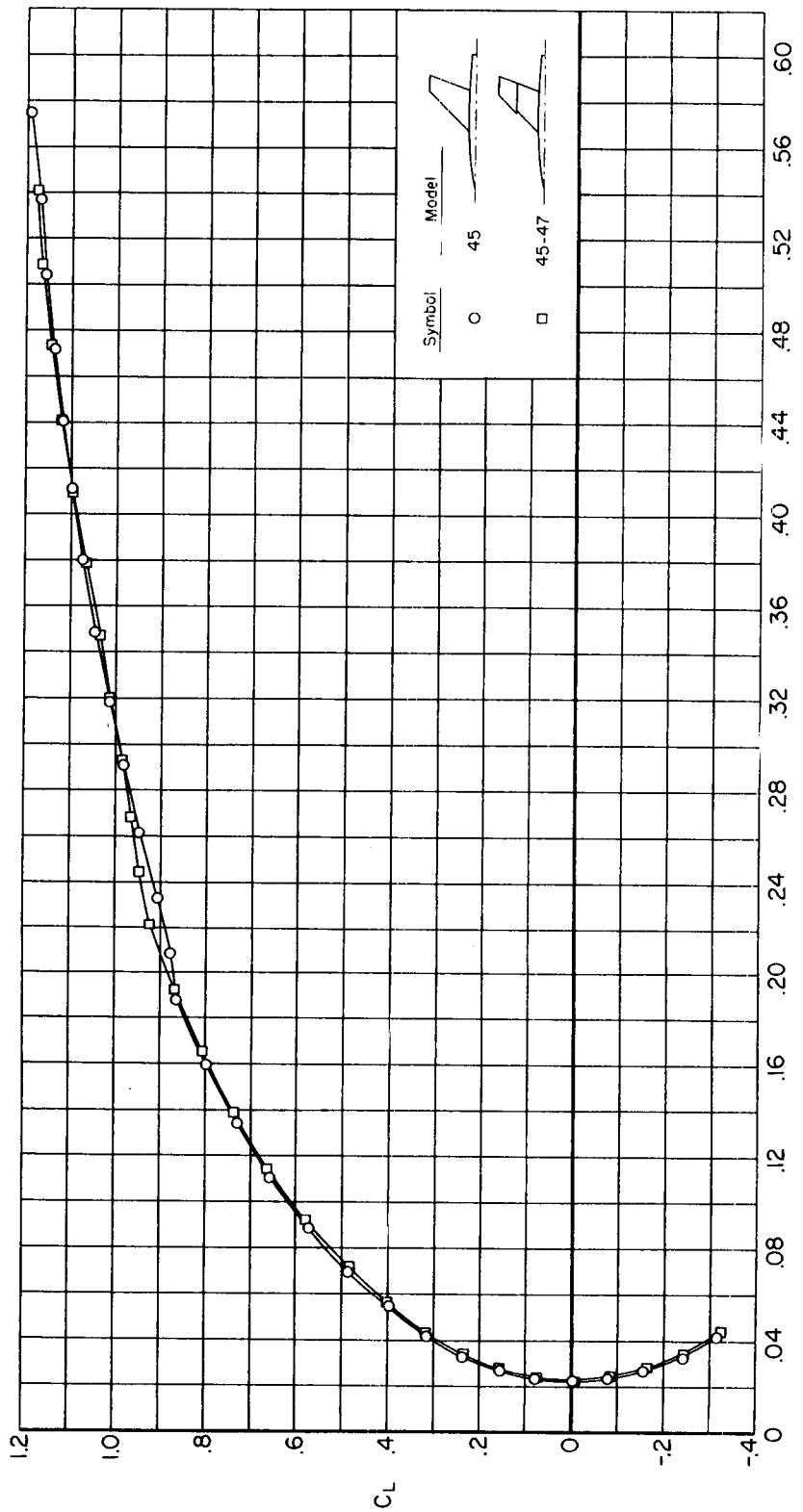

(h) M = 1.10

Figure 9.- Continued.

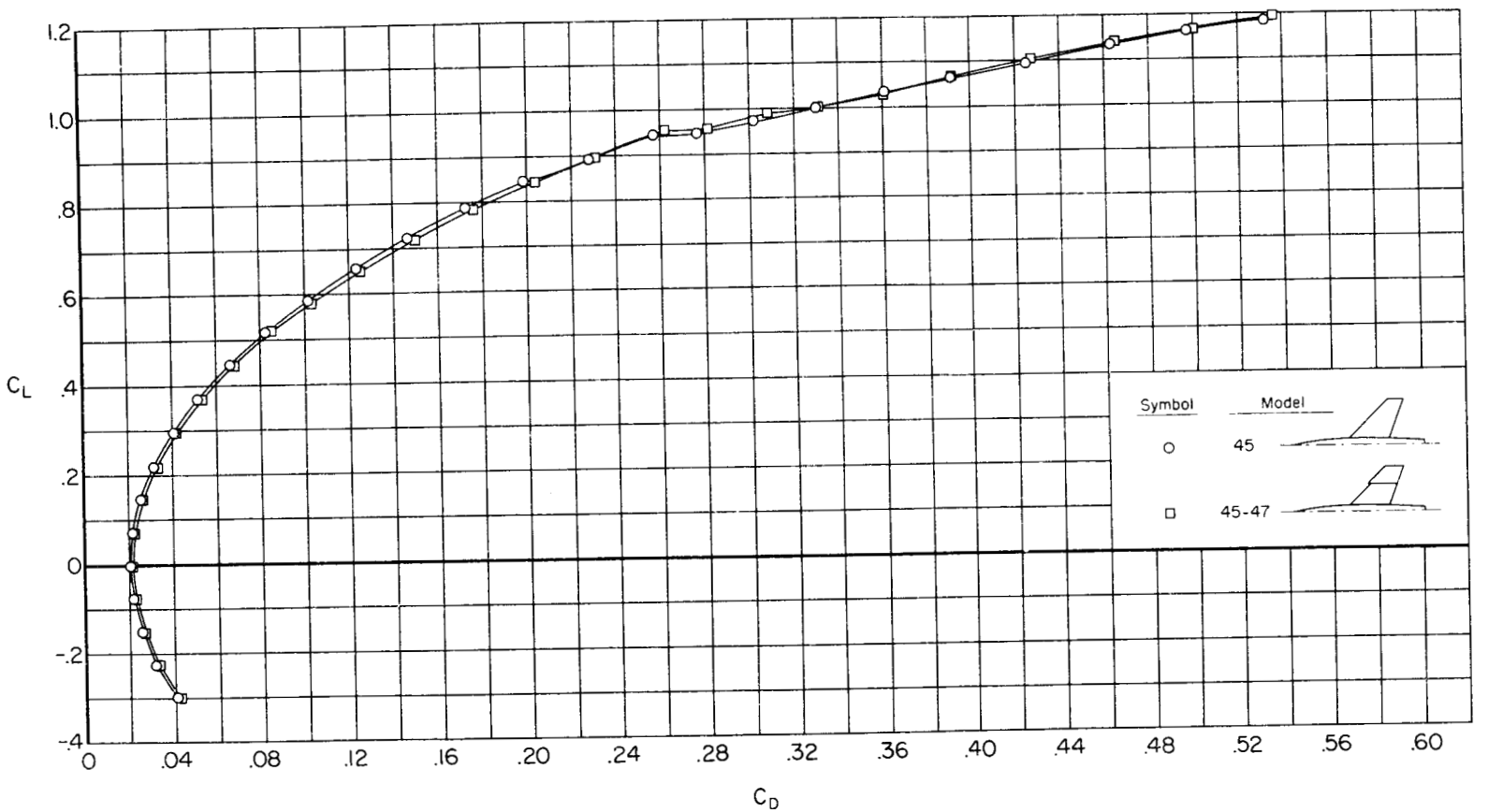

(i) M = 1.20

Figure 9.- Continued.

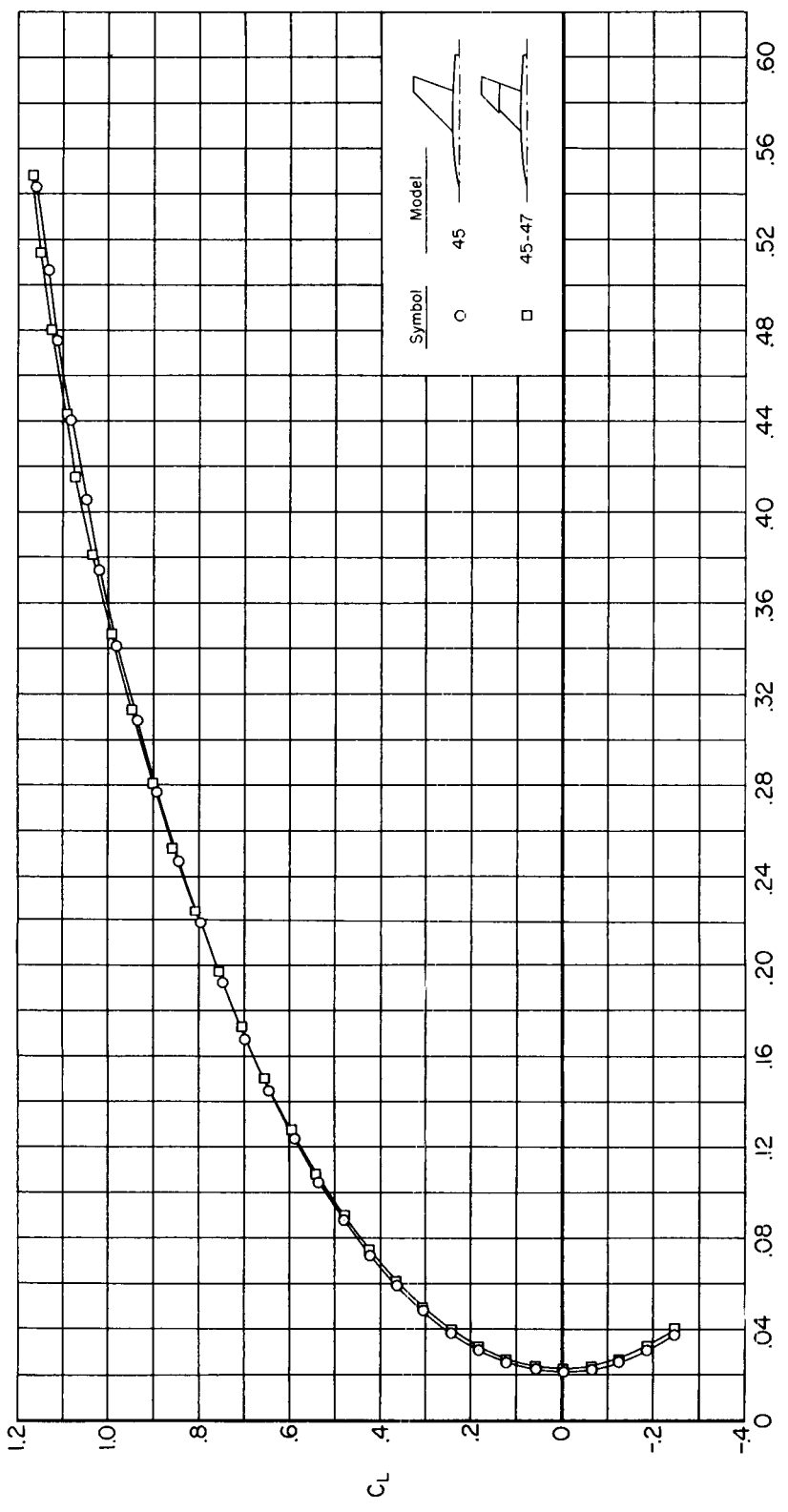

(j) M = 1.40

Figure 9.- Concluded.

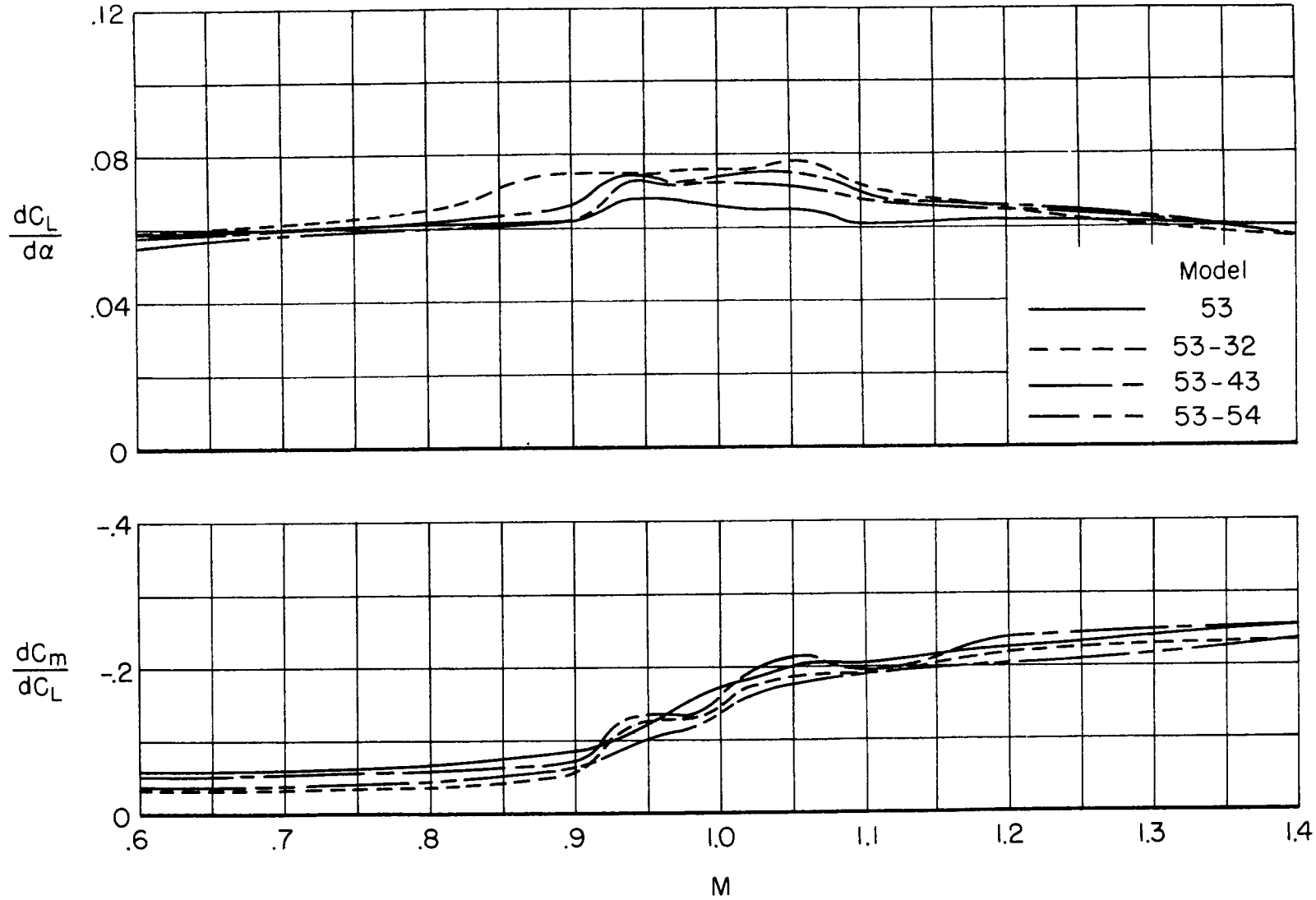

(a) 53 series models.

Figure 10.- Variation of $dC_L/d\alpha$ and dC_m/dC_L at $C_L = 0$ with Mach number for wing-body models.

CONFIDENTIAL

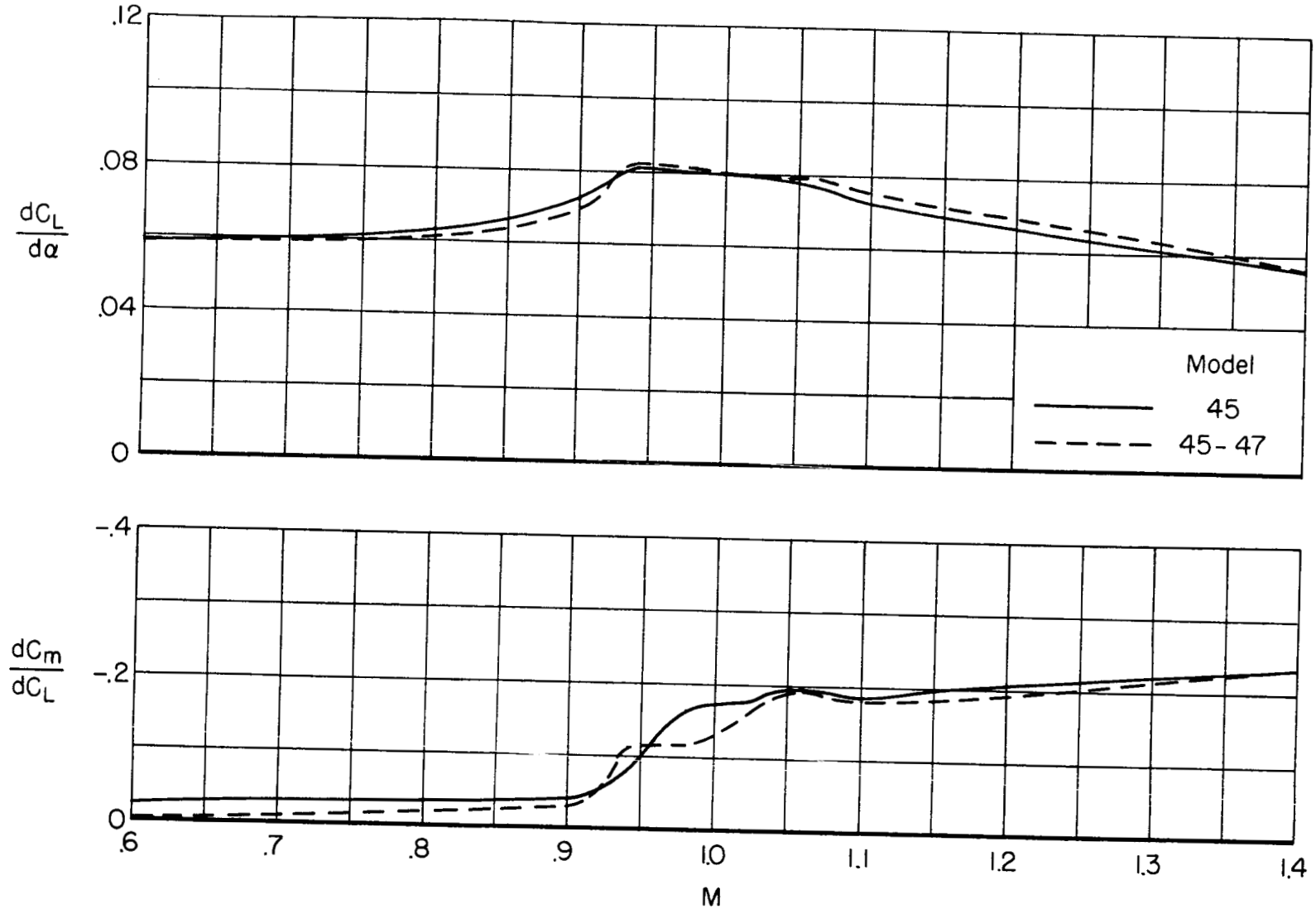

(b) 45 series models.

Figure 10.- Concluded.

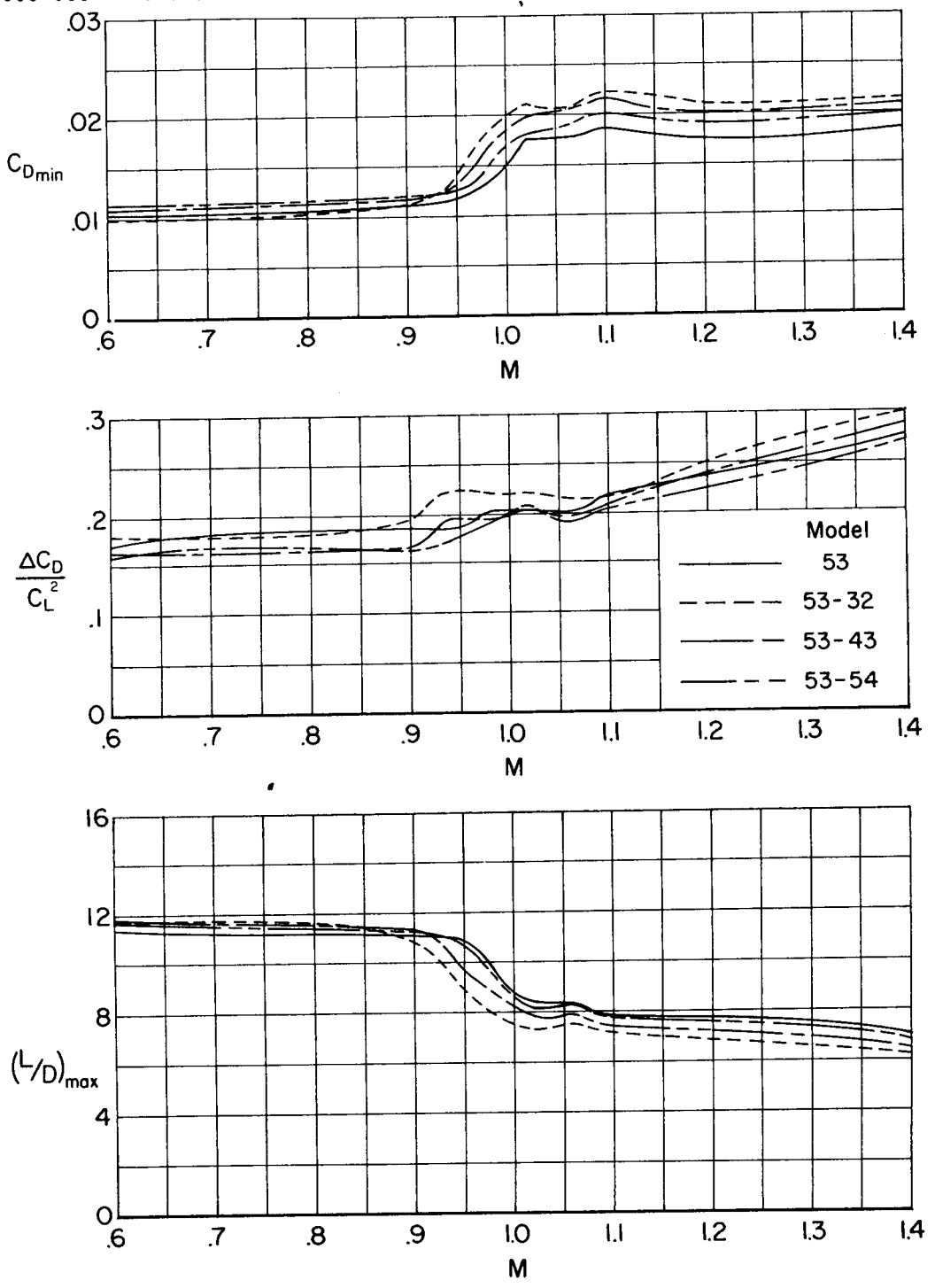

(a) 53 series models.

Figure 11.- Variation of minimum drag coefficient, drag rise factor and maximum lift-drag ratio with Mach number for wing-body models.

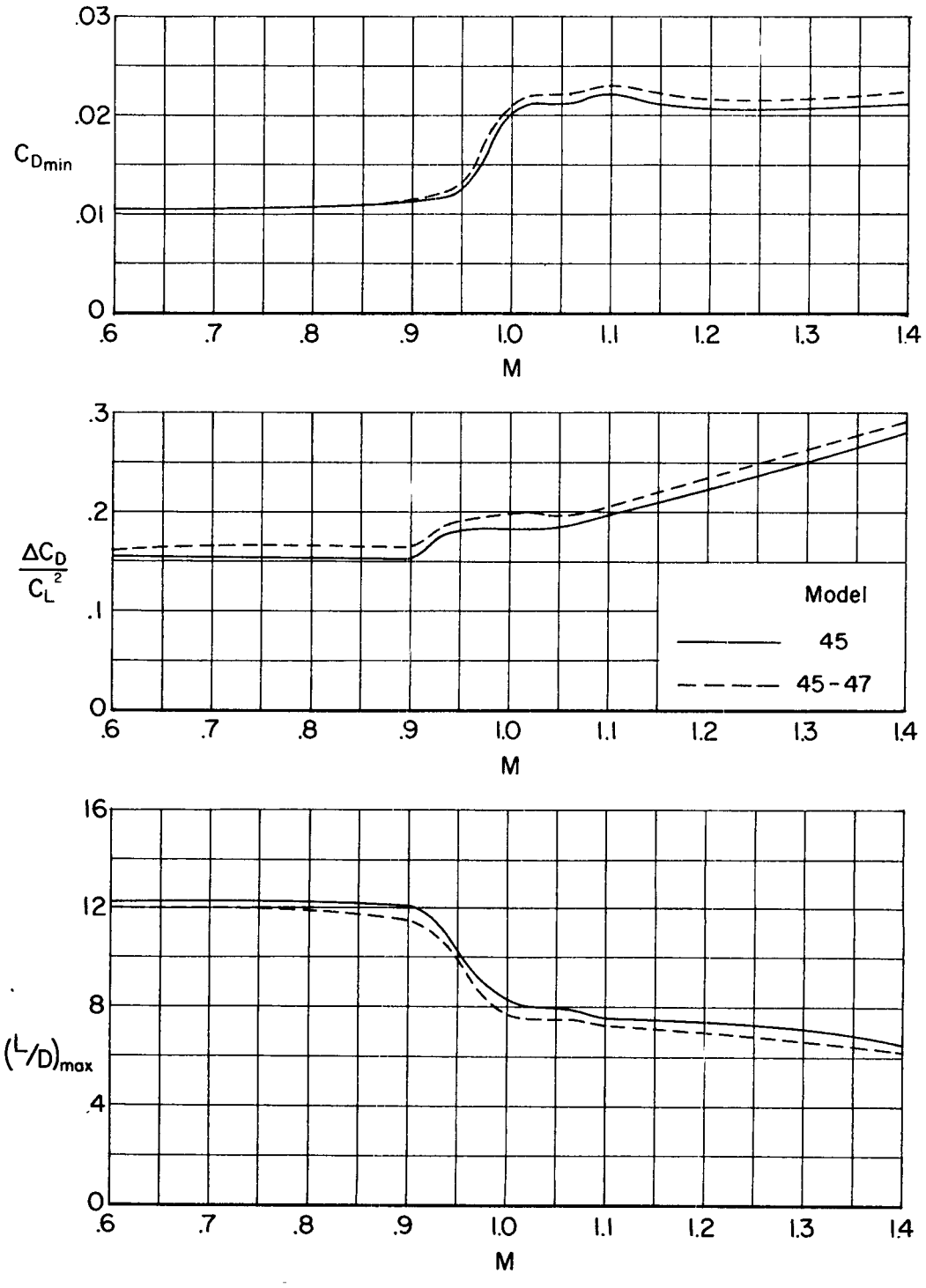

(b) 45 series models.

Figure 11.- Concluded.

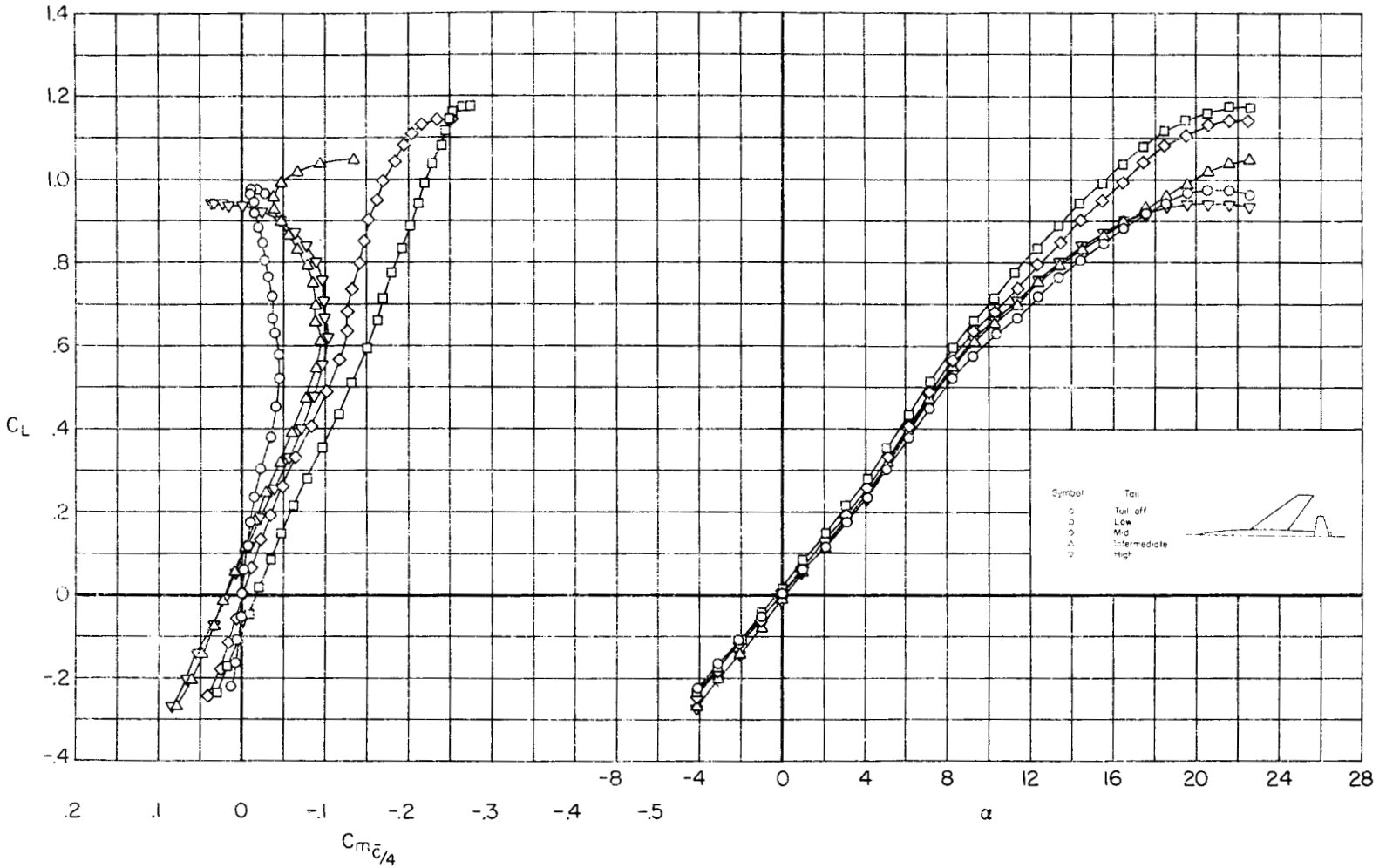

(a) M = 0.60

Figure 12.- Variation of lift coefficient with pitching-moment coefficient and angle of attack at constant Mach number for the 53 series wing-body-tail models.

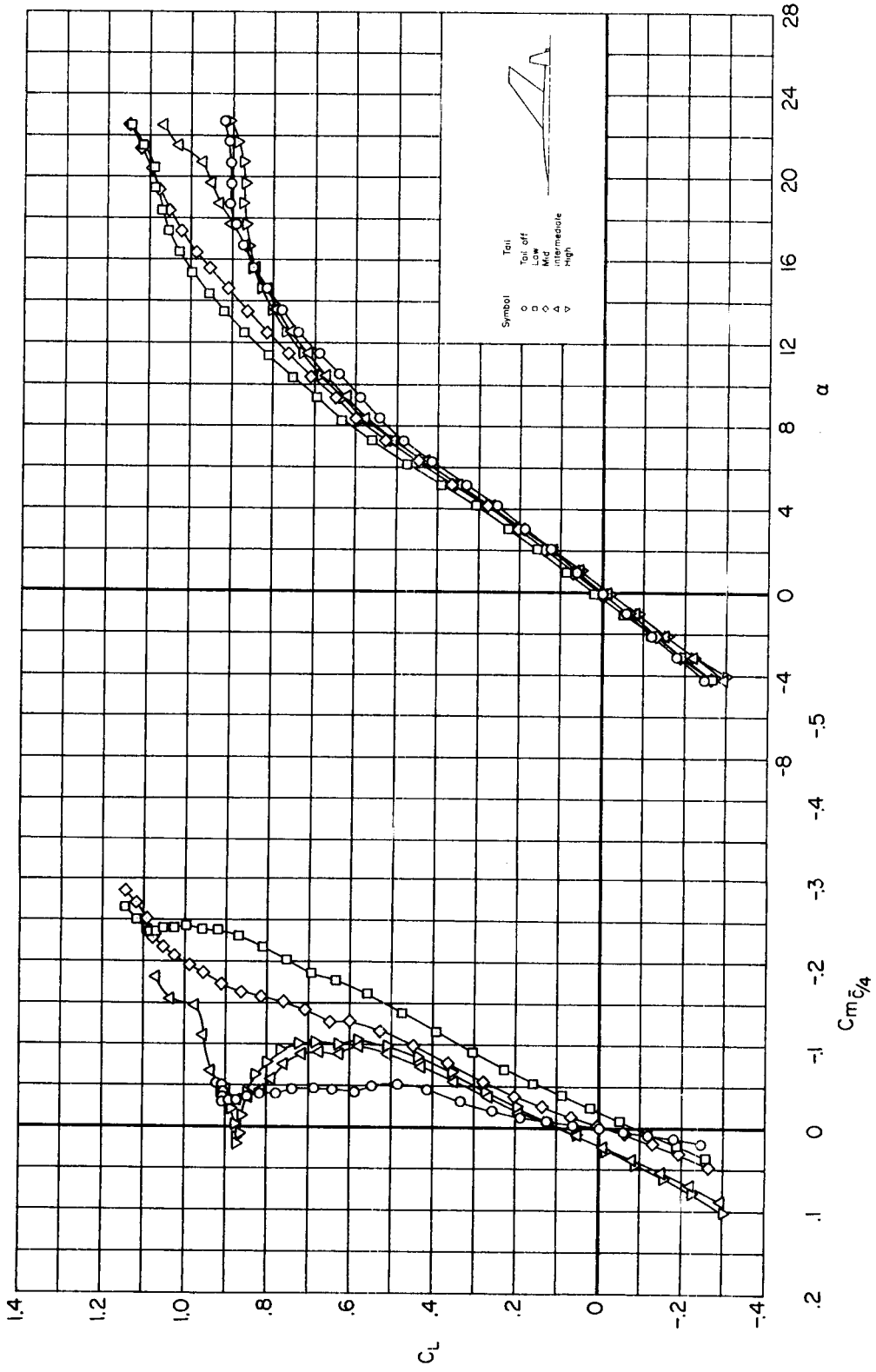

(b) M = 0.80

Figure 12.- Continued.

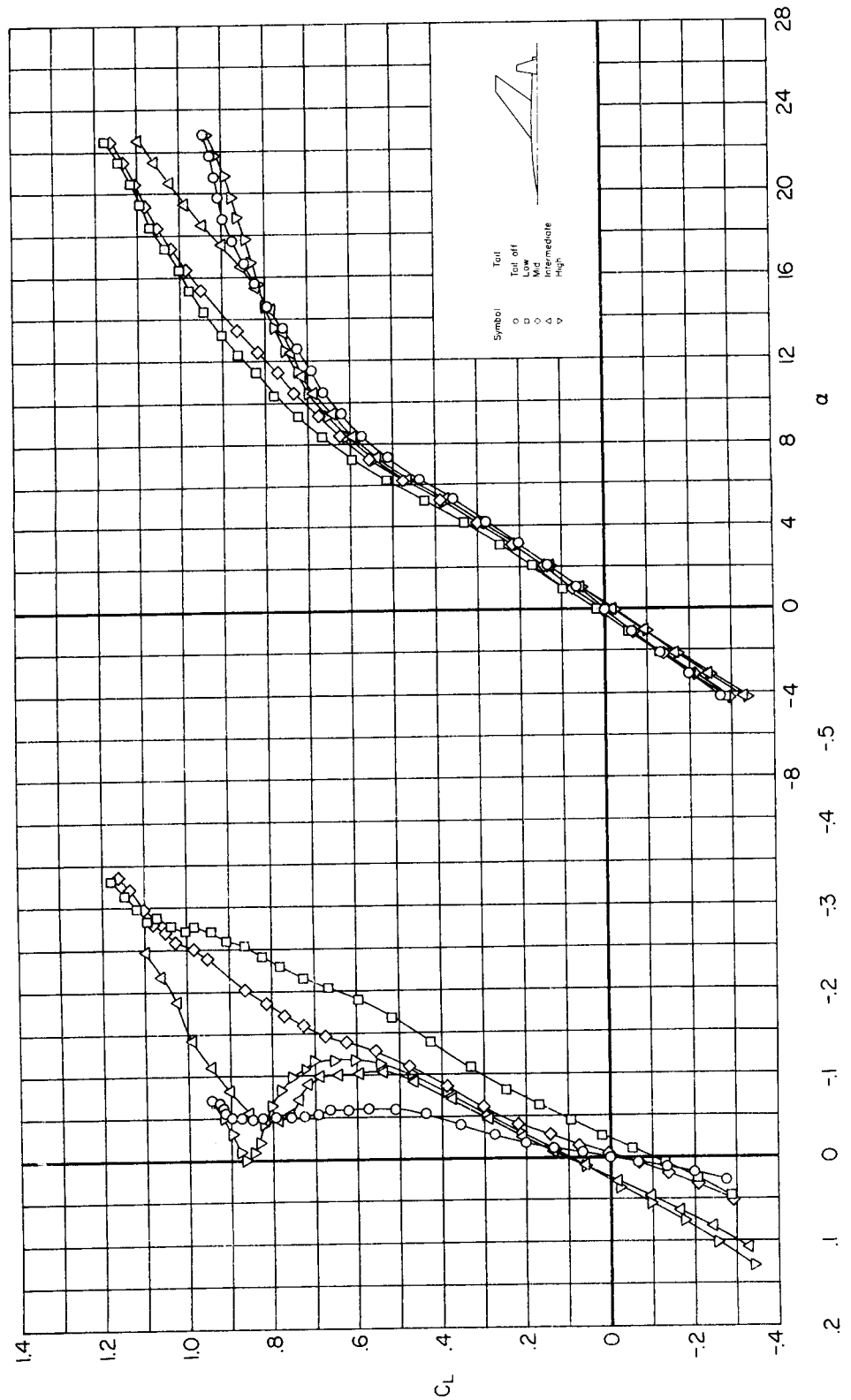

(c) M = 0.90

Figure 12.- Continued.

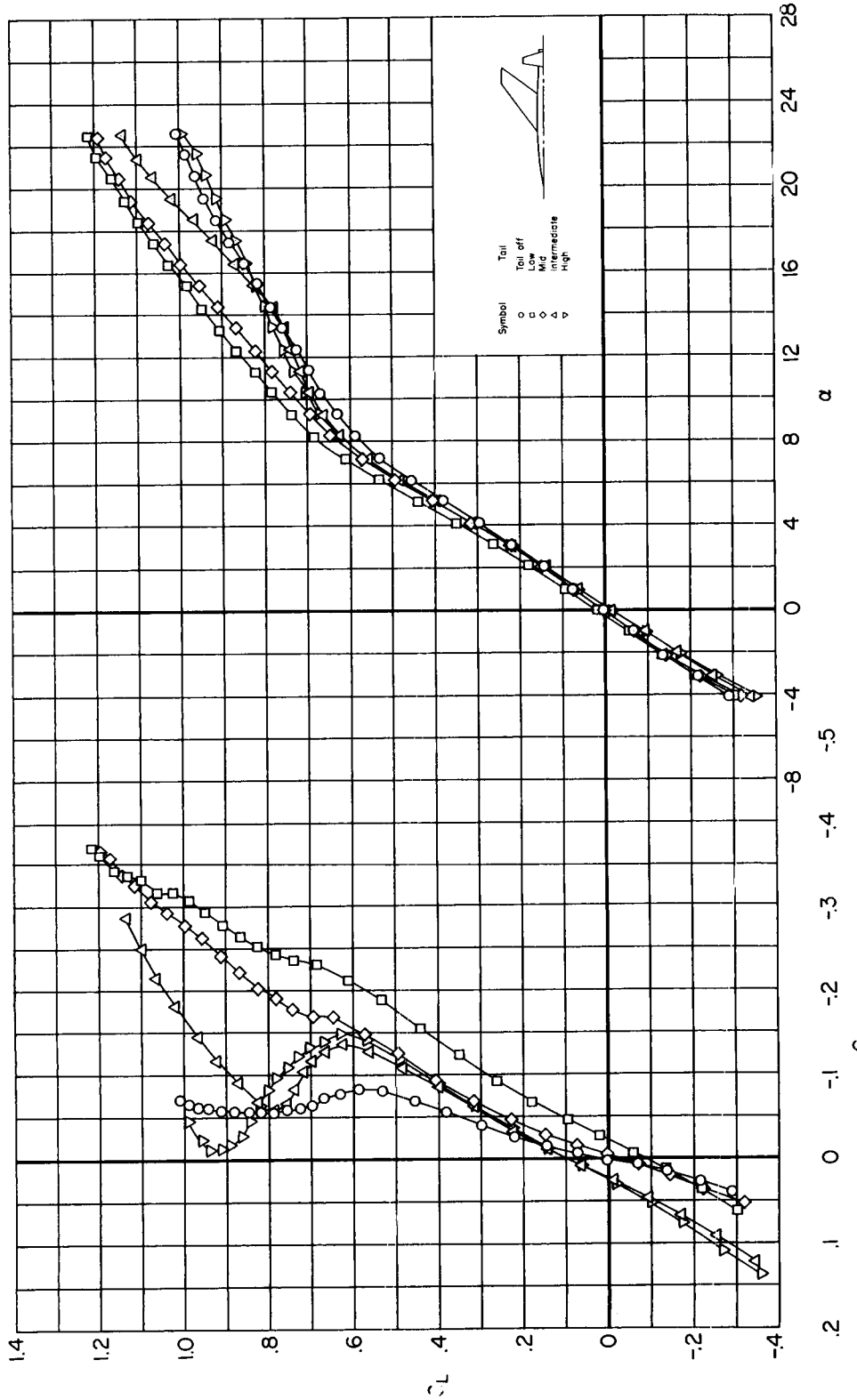

(d) M = 0.94

Figure 12.- Continued.

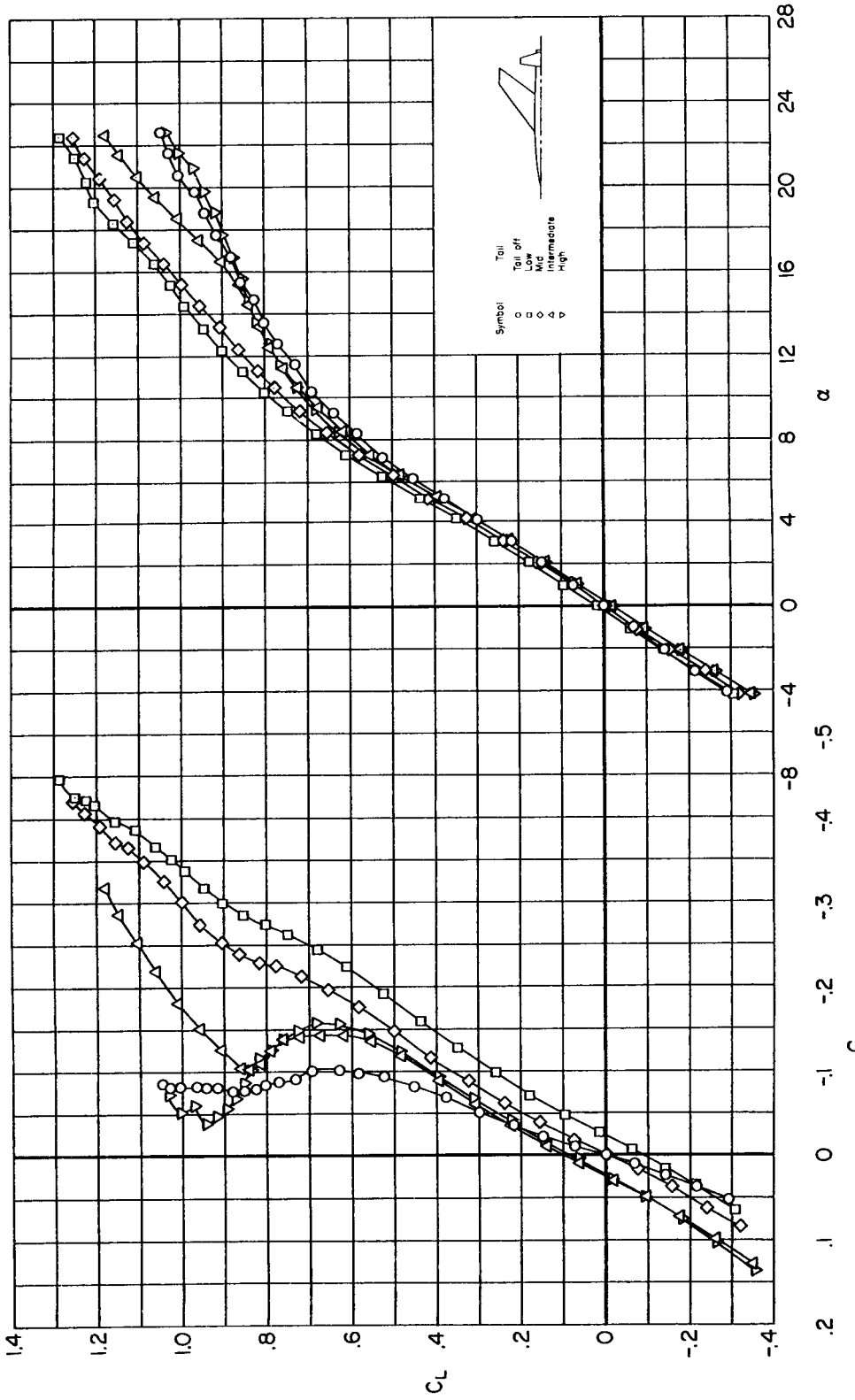

(e) M = 0.98

Figure 12.- Continued.

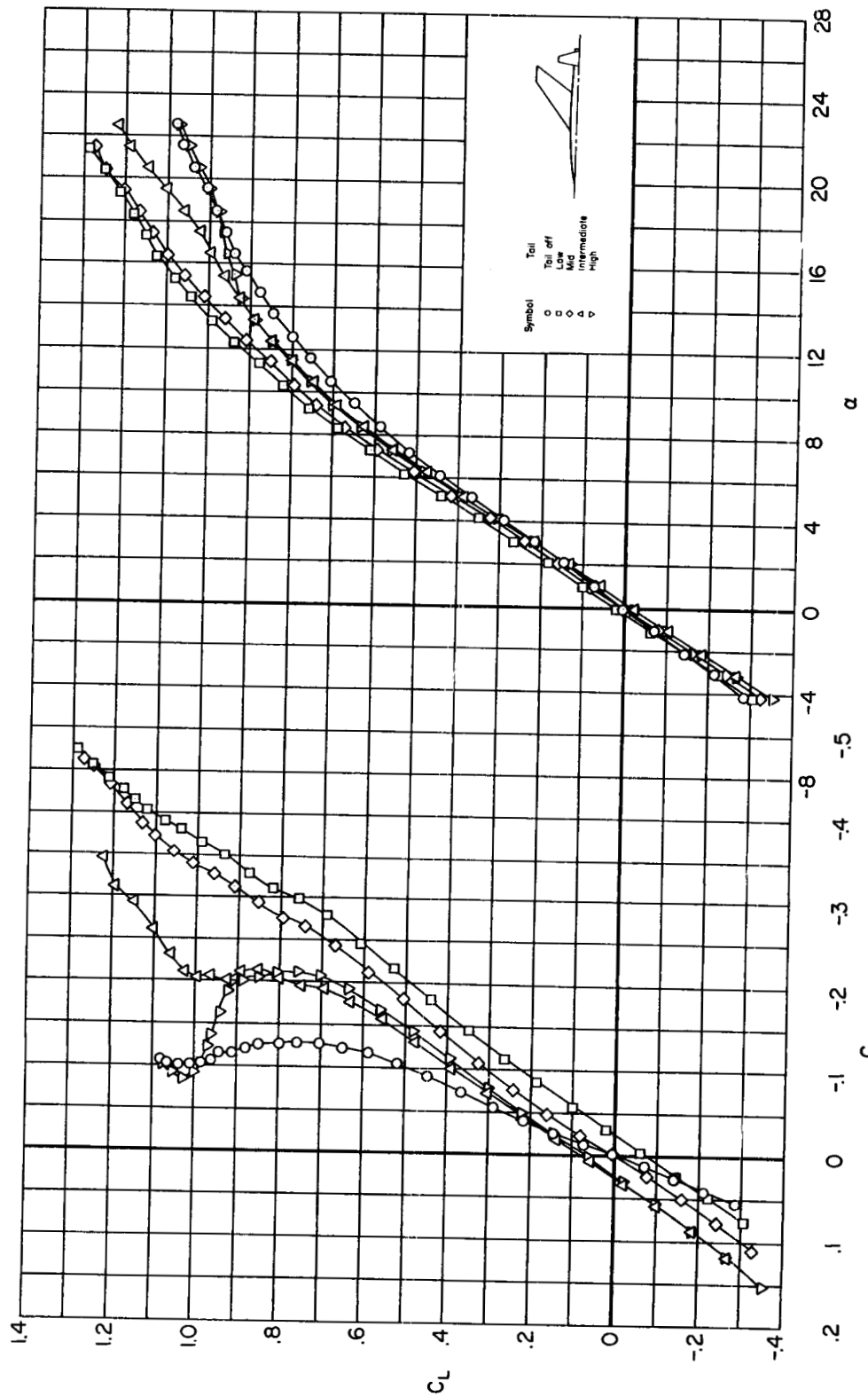

(f) M = 1.02

Figure 12.- Continued.

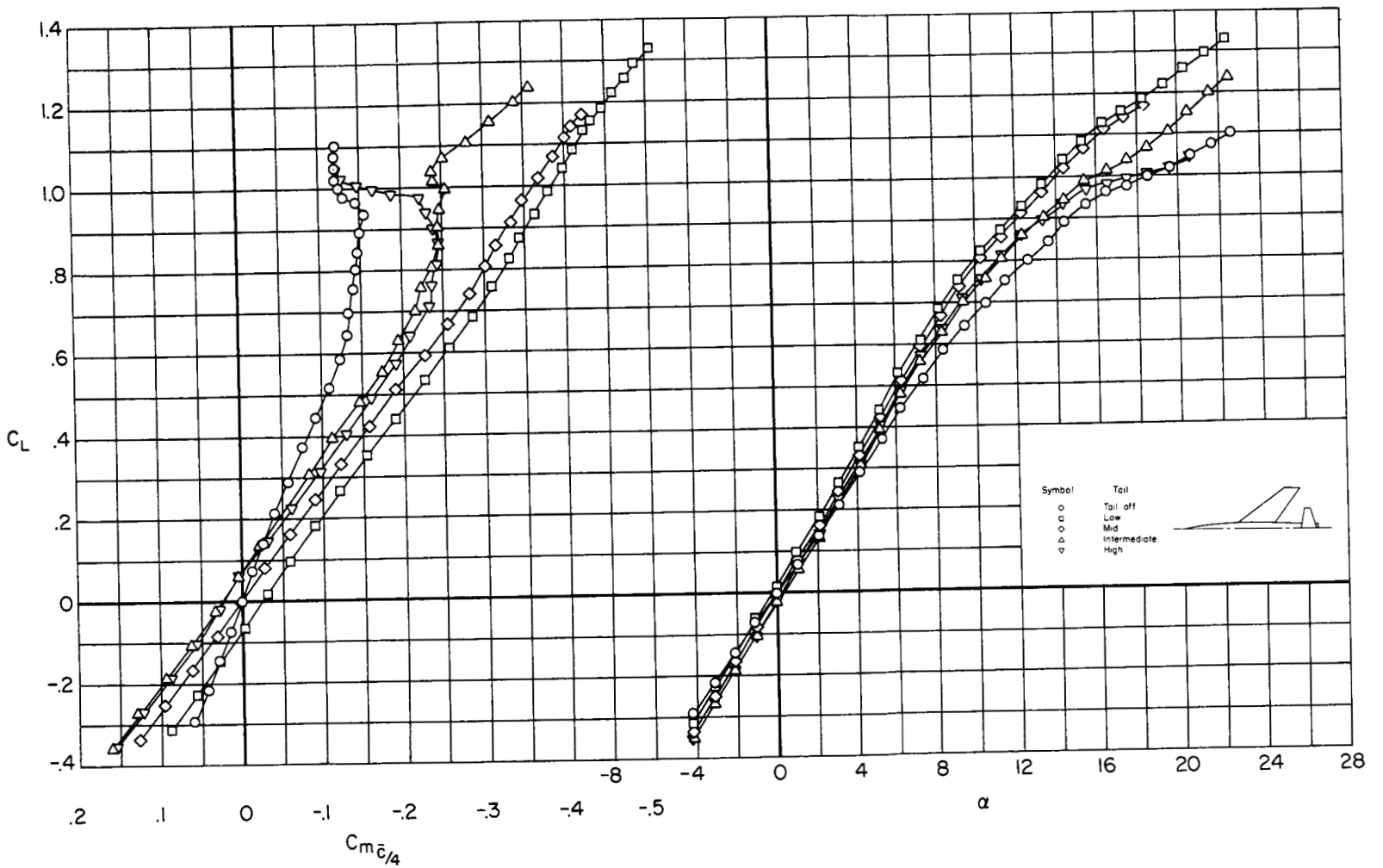

(g) M = 1.06

Figure 12.- Continued.

CONFIDENTIAL

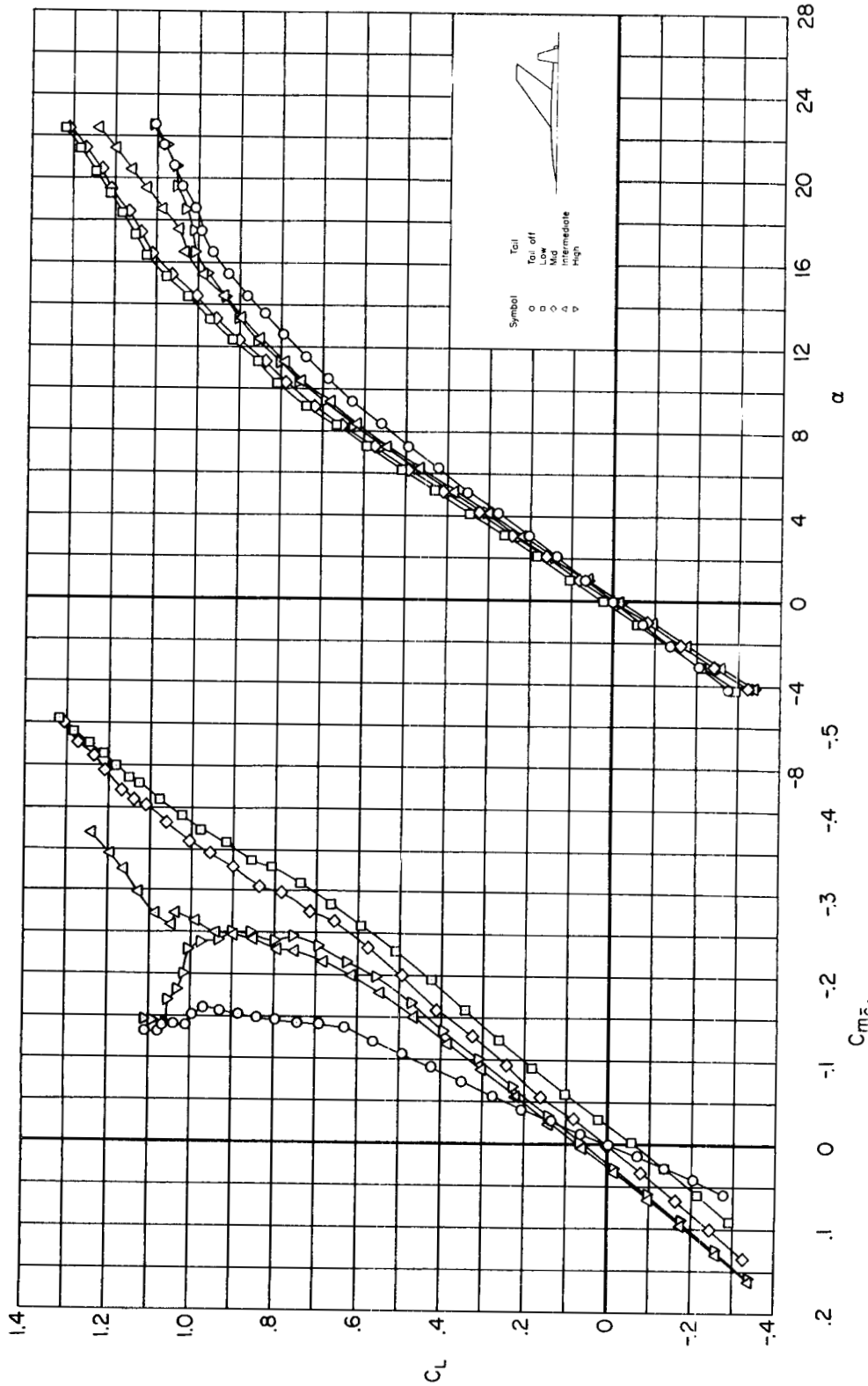

(h) M = 1.10

Figure 12.- Continued.

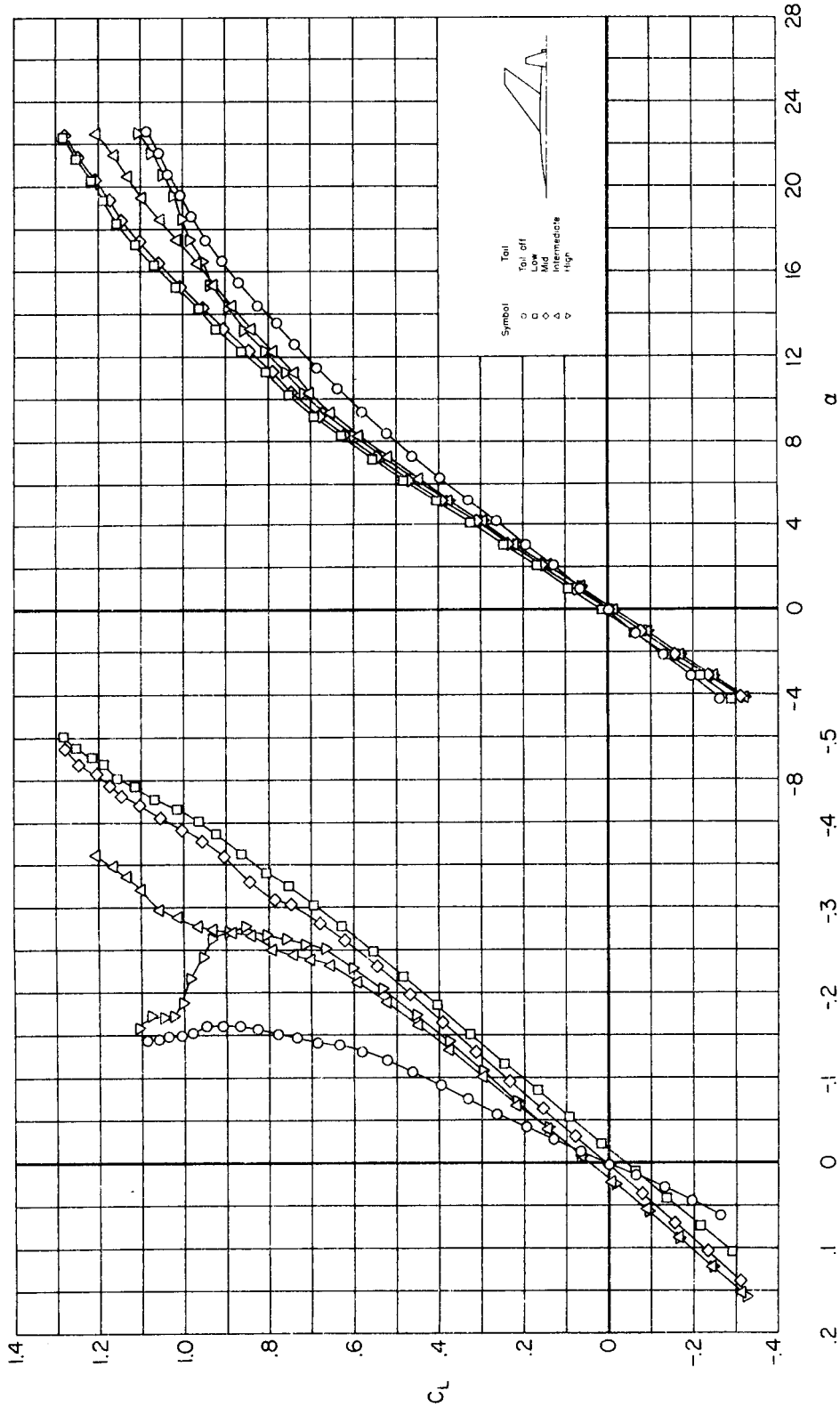

(i) M = 1.20

Figure 12.- Continued.

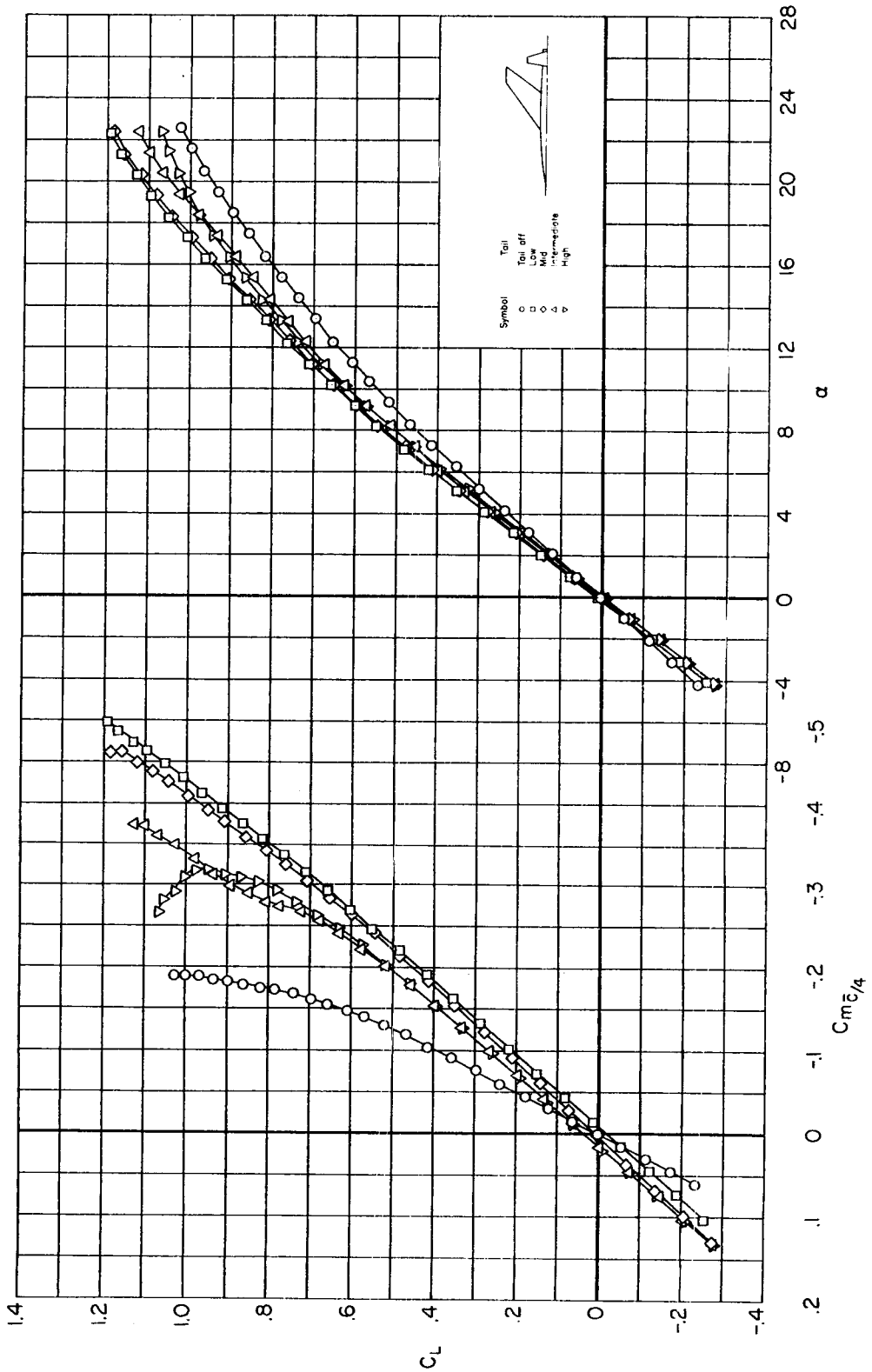

(j) M = 1.40

Figure 12.- Concluded.

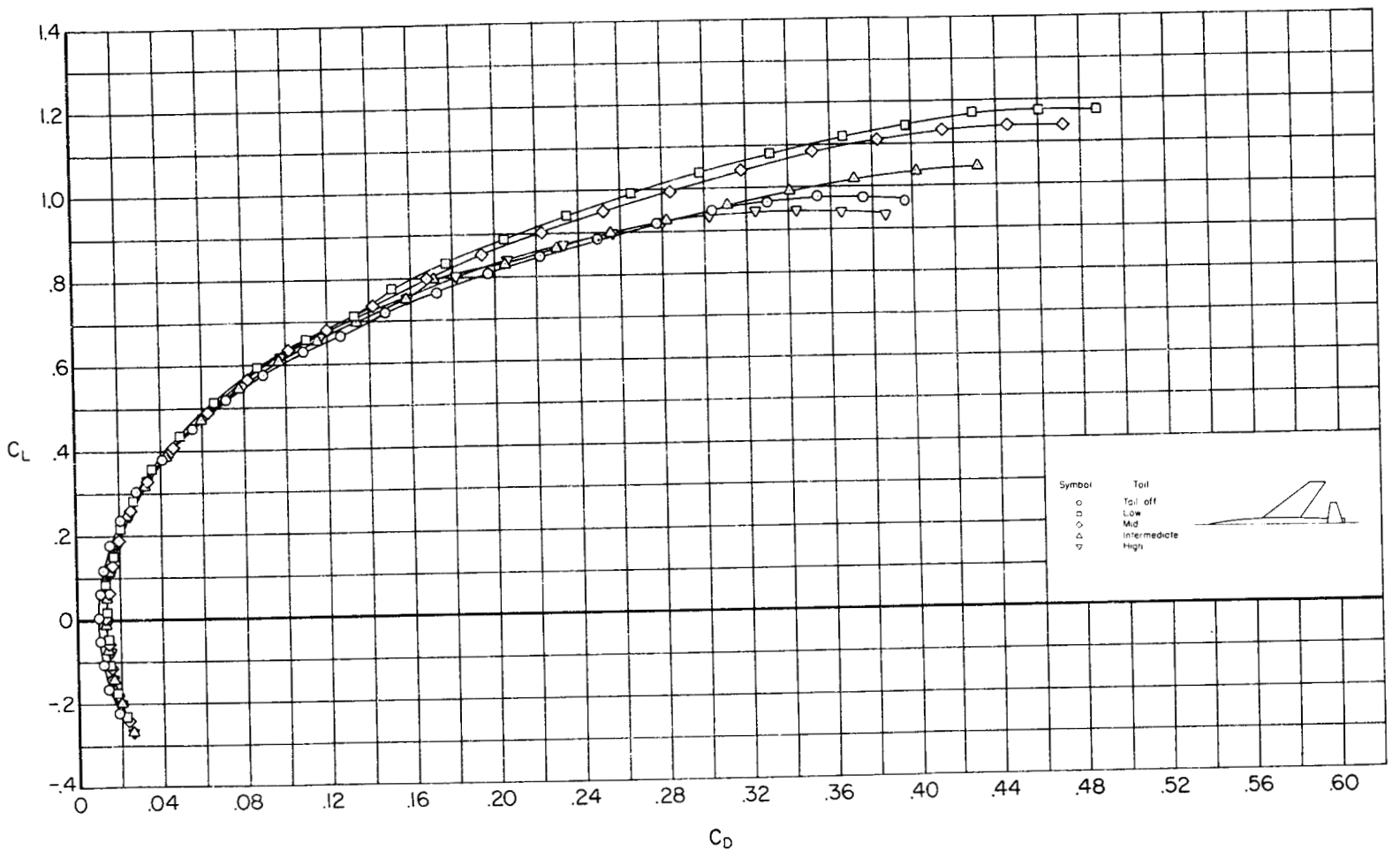

(a) M = 0.60

Figure 13.- Variation of lift coefficient with drag coefficient at constant Mach number for the 53 series wing-body-tail models.

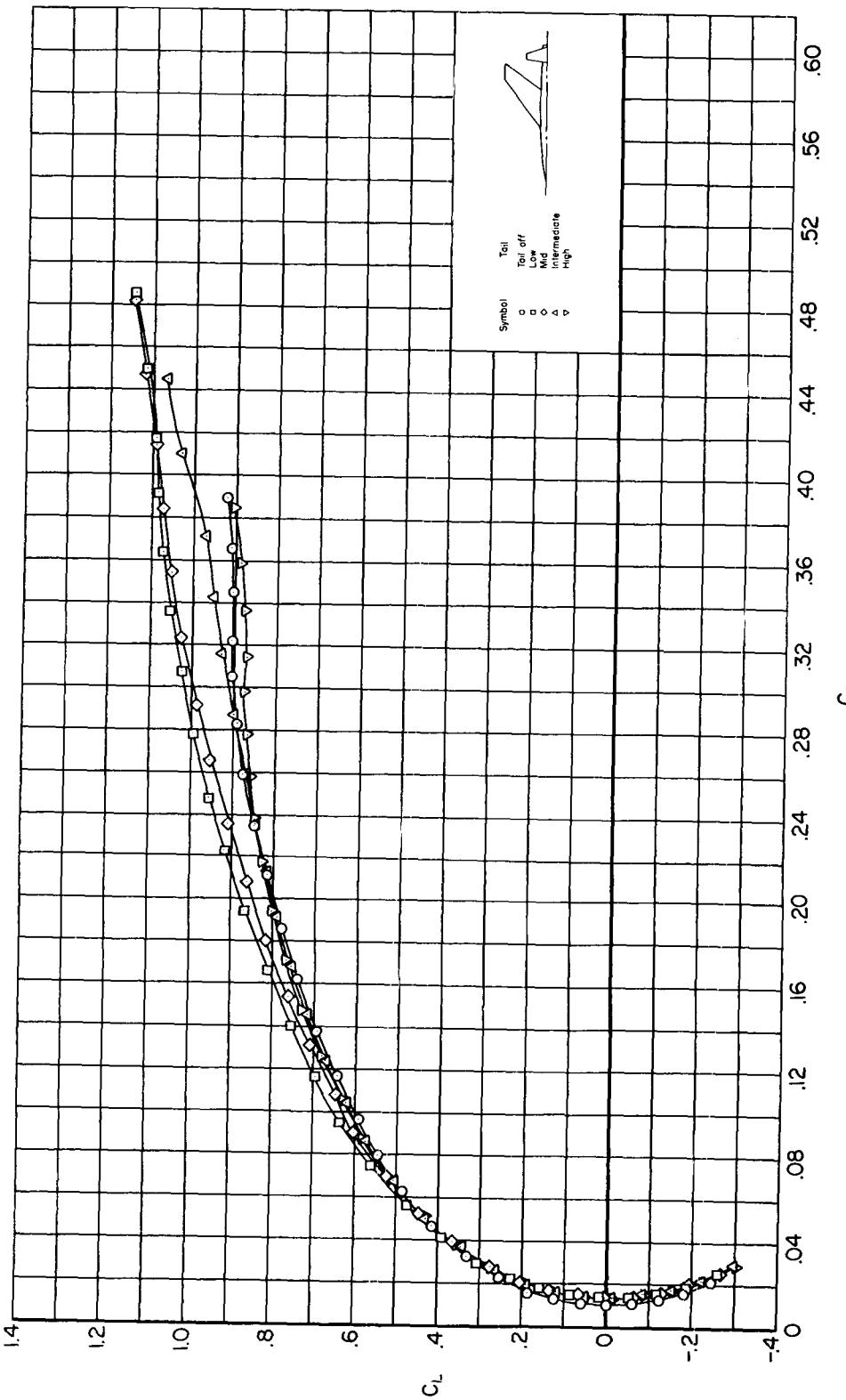

(b) M = 0.80

Figure 13.- Continued.

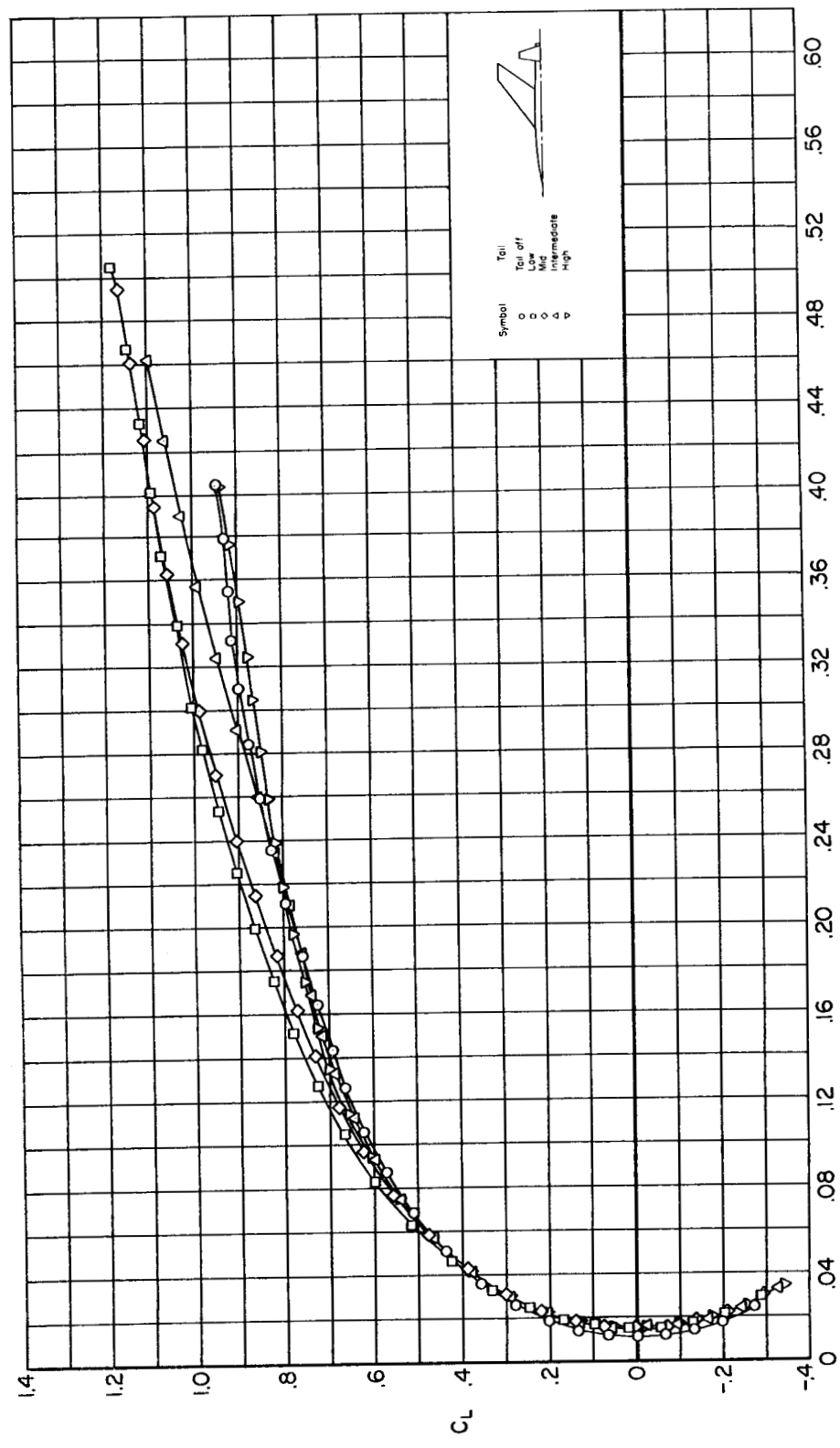

(c) M = 0.90

Figure 13.- Continued.

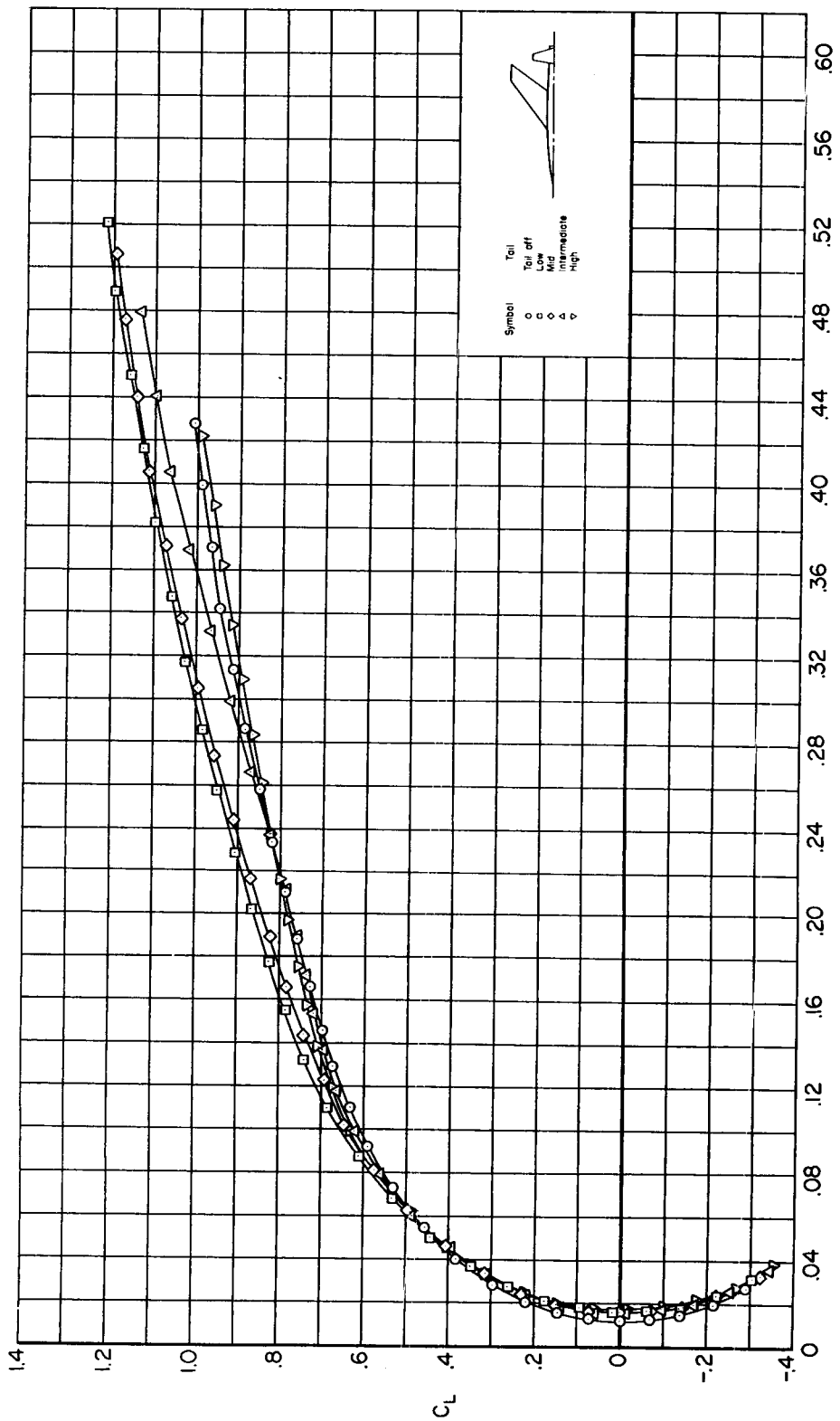

(d) M = 0.94

Figure 13.- Continued.

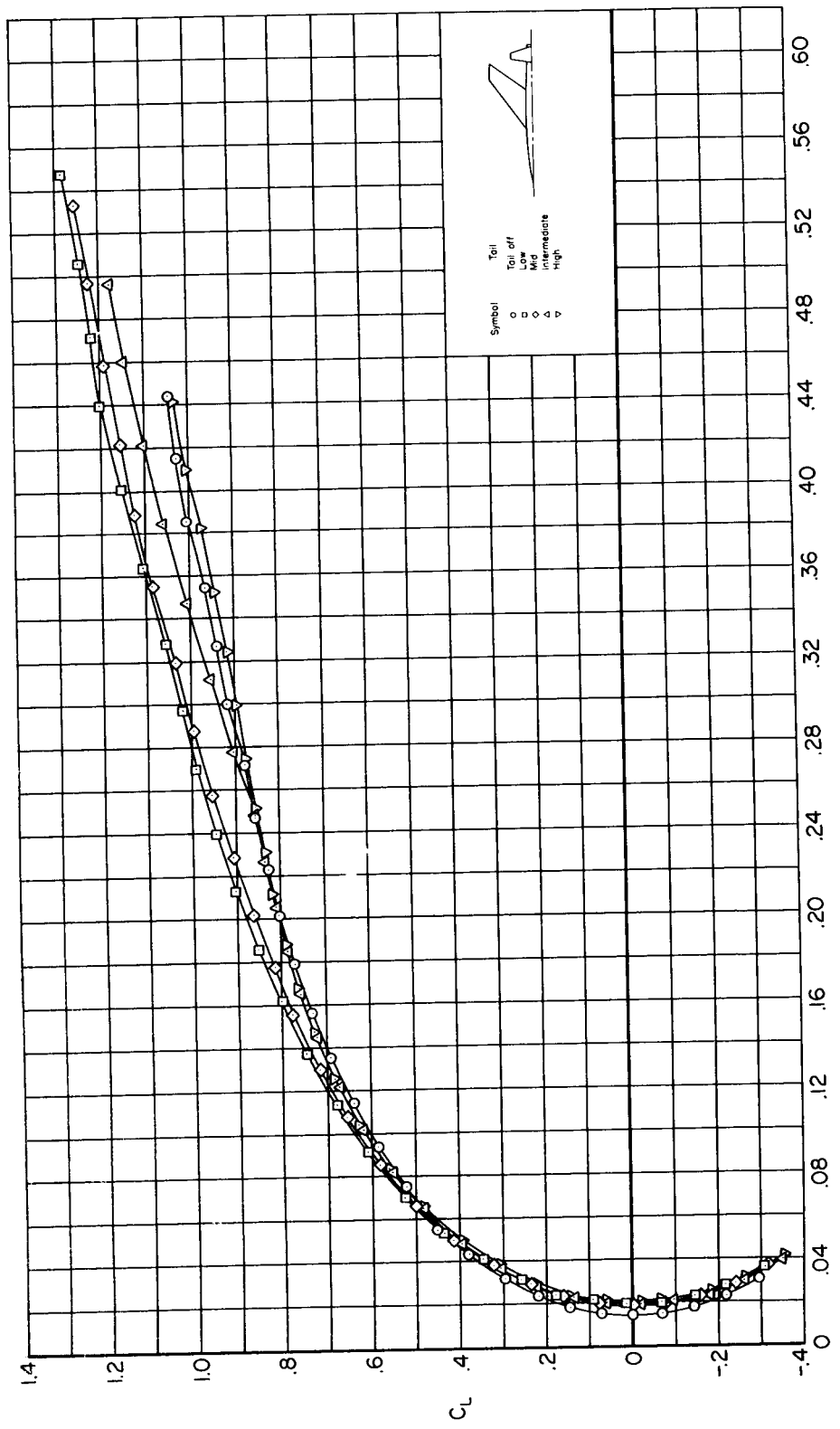

(e) M = 0.98

Figure 13.- Continued.

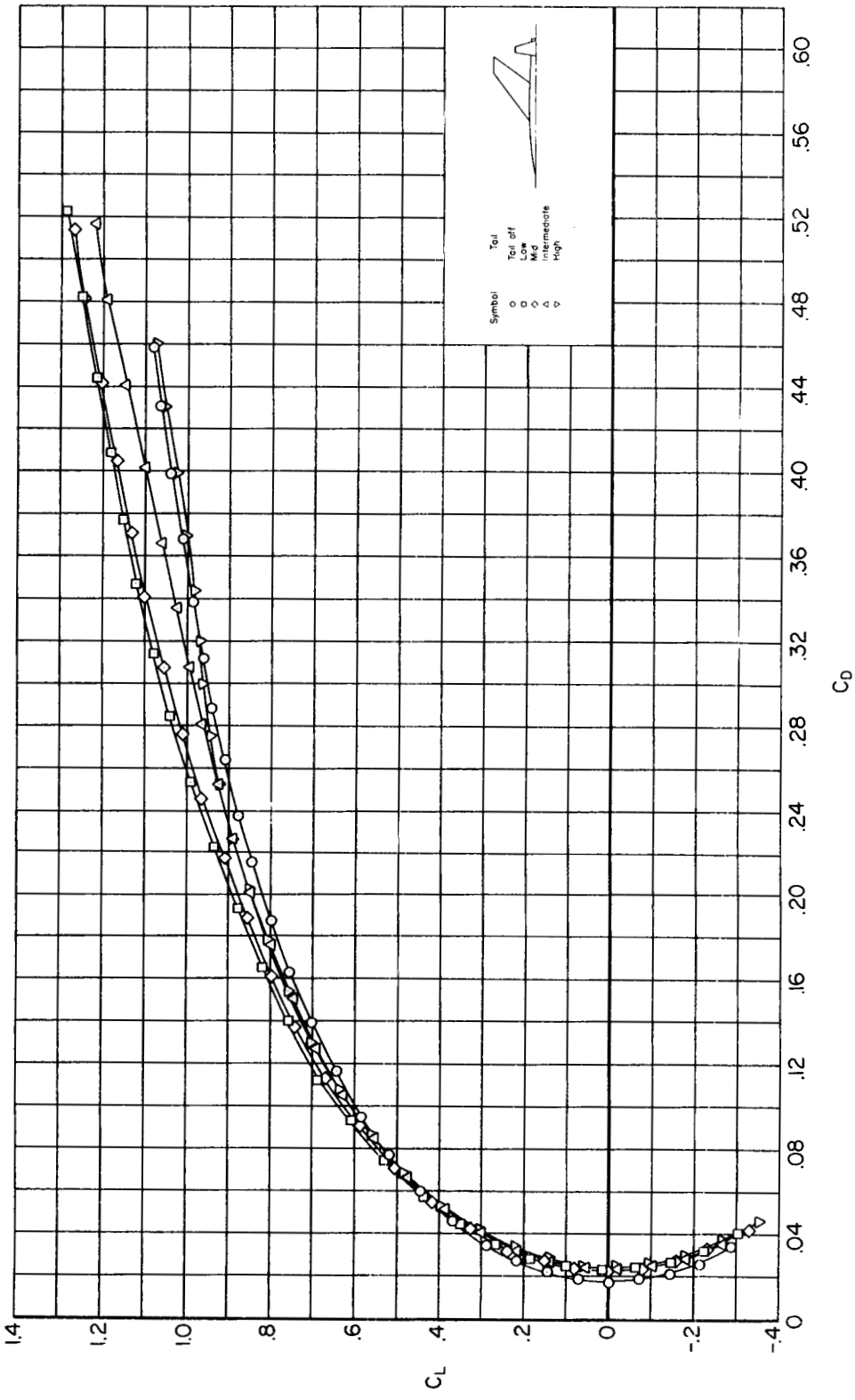

(f) M = 1.02

Figure 13.- Continued.

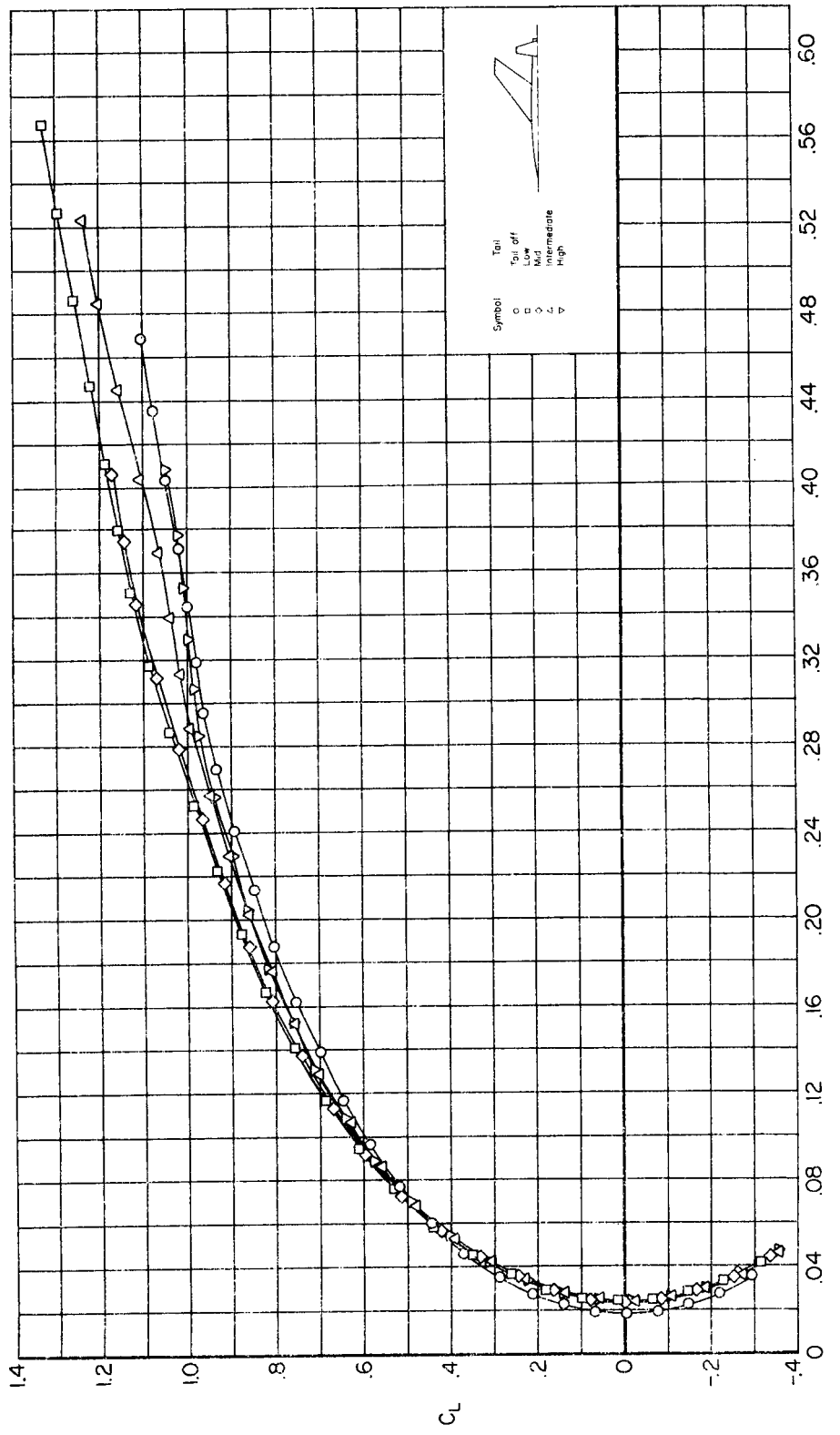

(g) M = 1.06

Figure 13.- Continued.

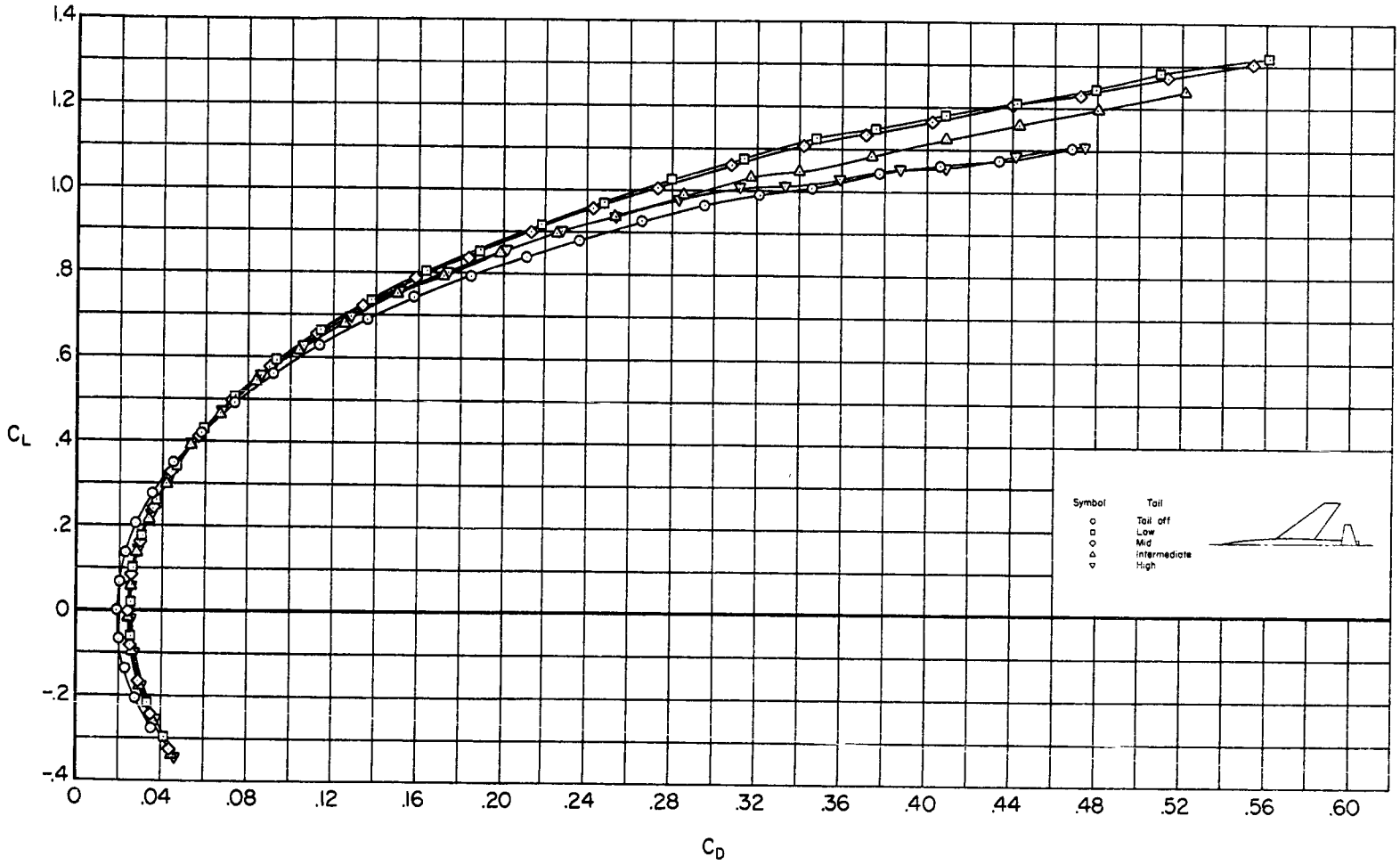

(h) M = 1.10

Figure 13.- Continued.

CONFIDENTIAL

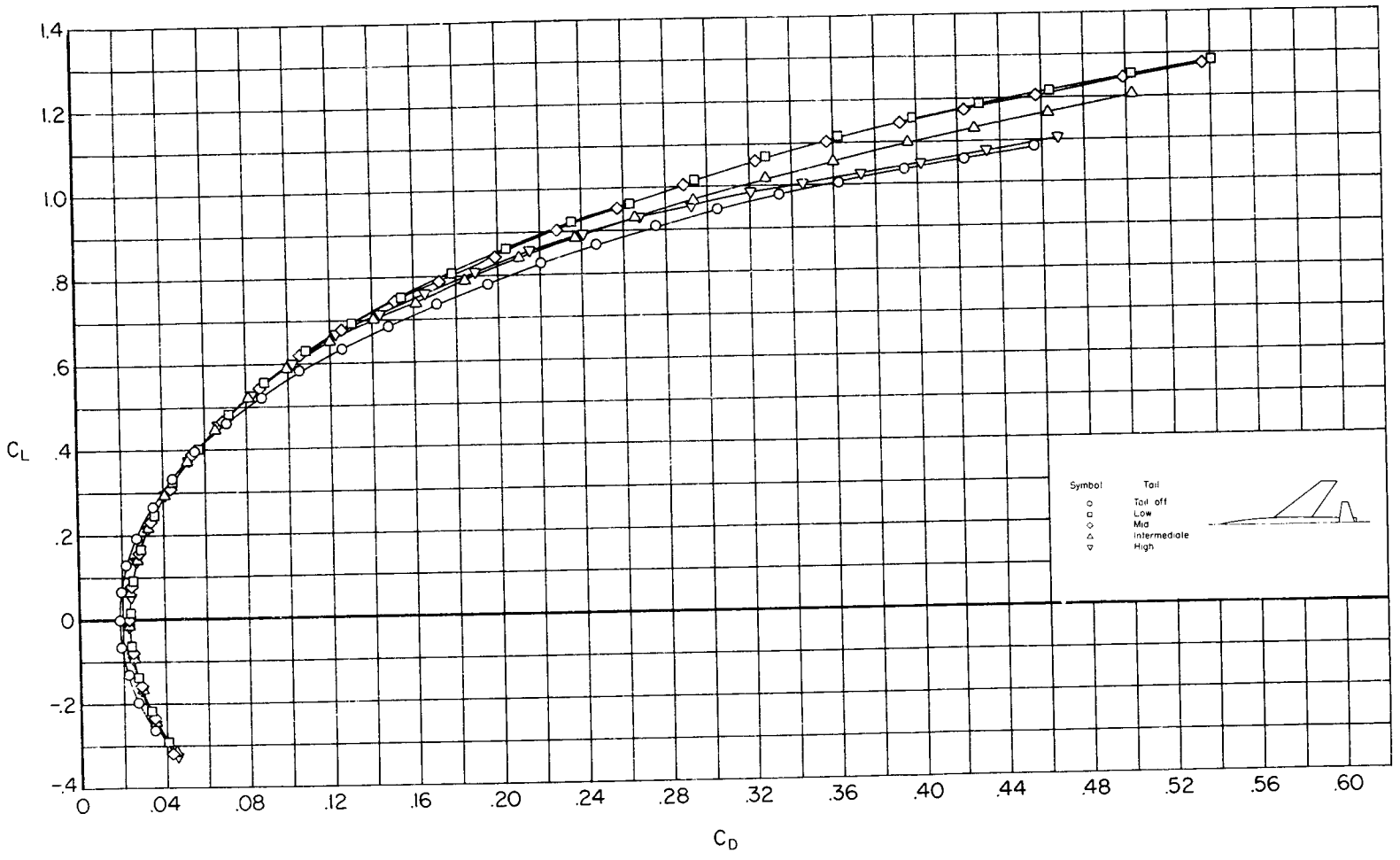

(i) M = 1.20

Figure 13.- Continued.

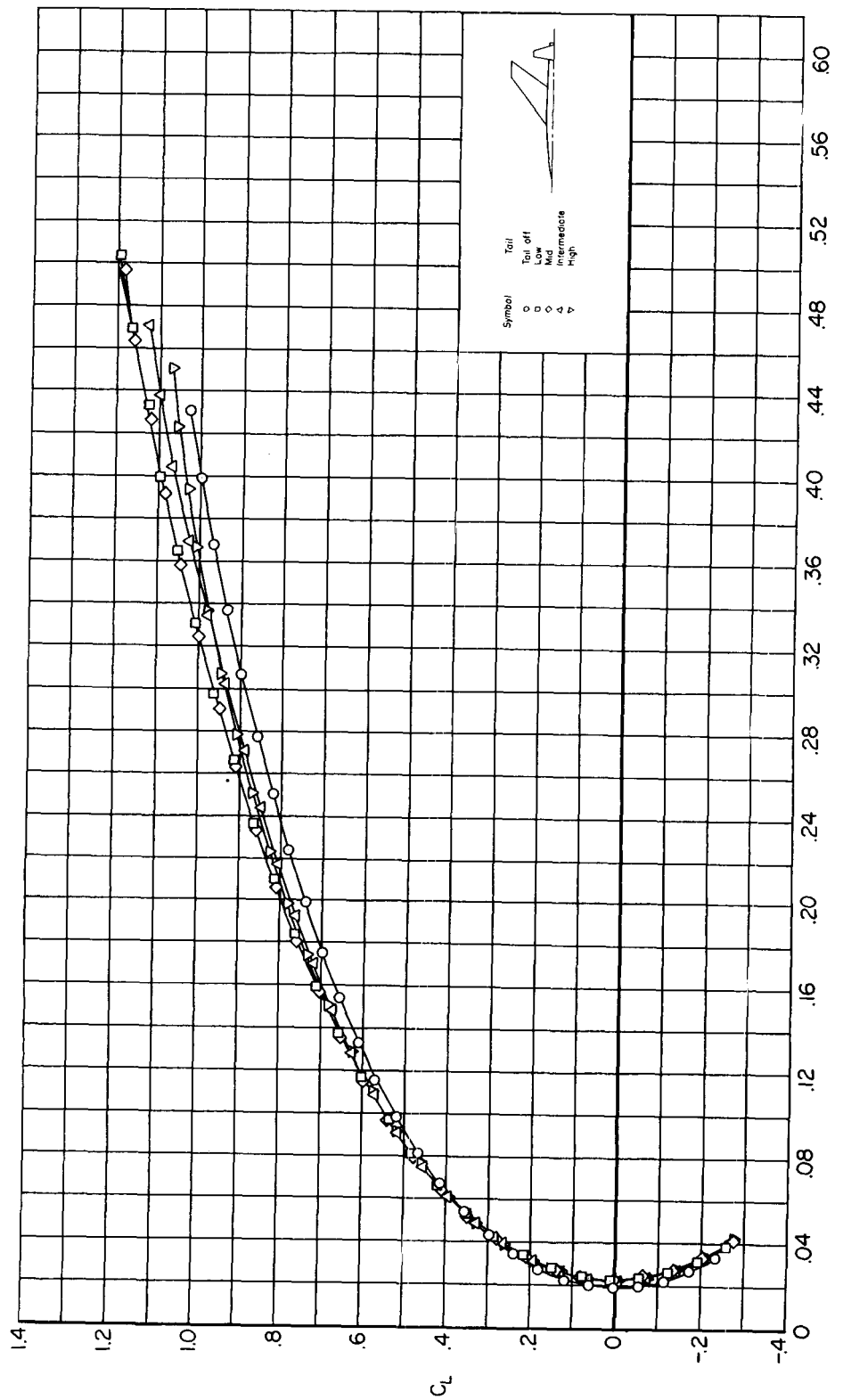

(j) M = 1.40

Figure 13.- Concluded.

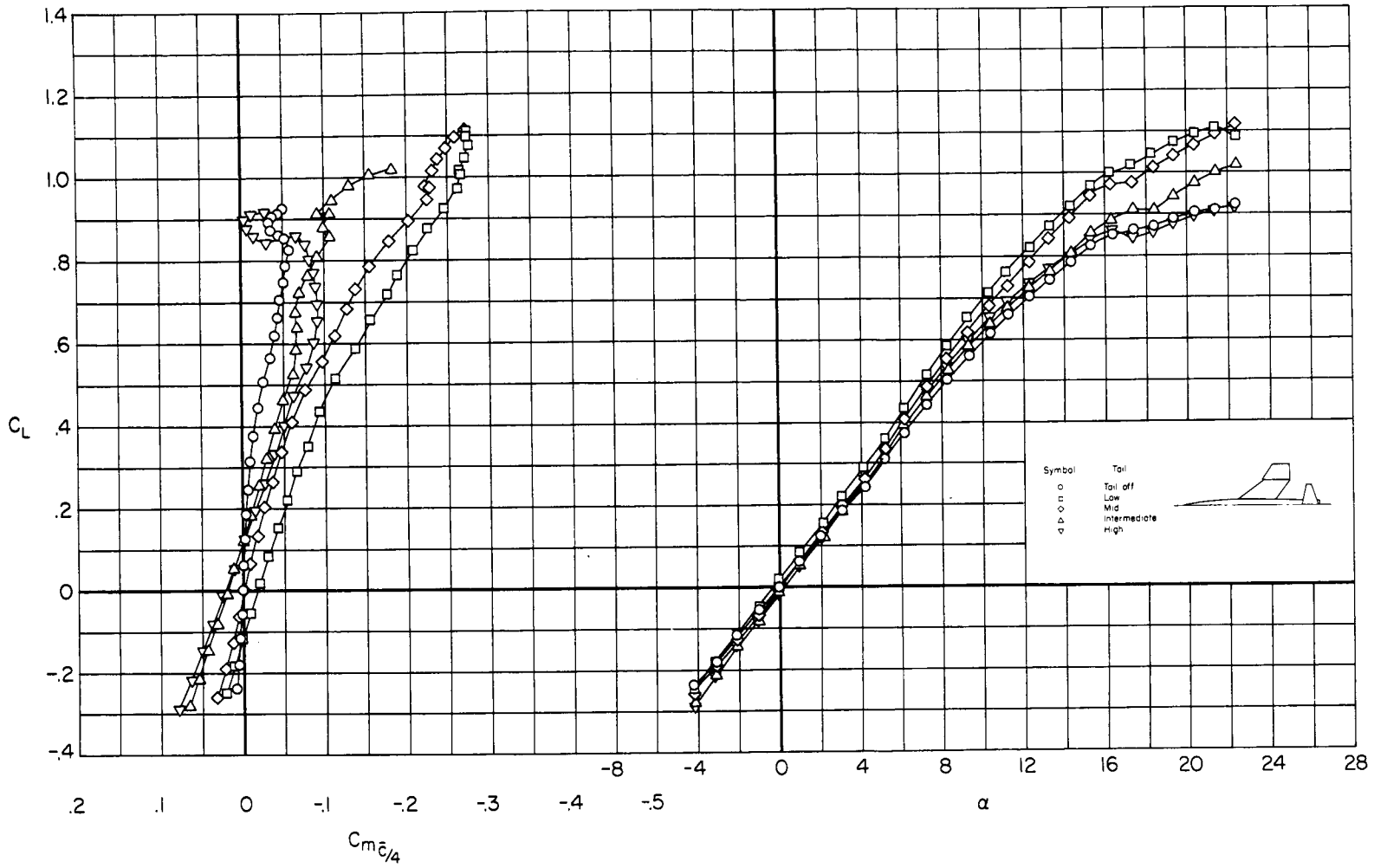

(a) M = 0.60

Figure 14.- Variation of lift coefficient with pitching-moment coefficient and angle of attack at constant Mach number for the 53-32 series wing-body-tail models.

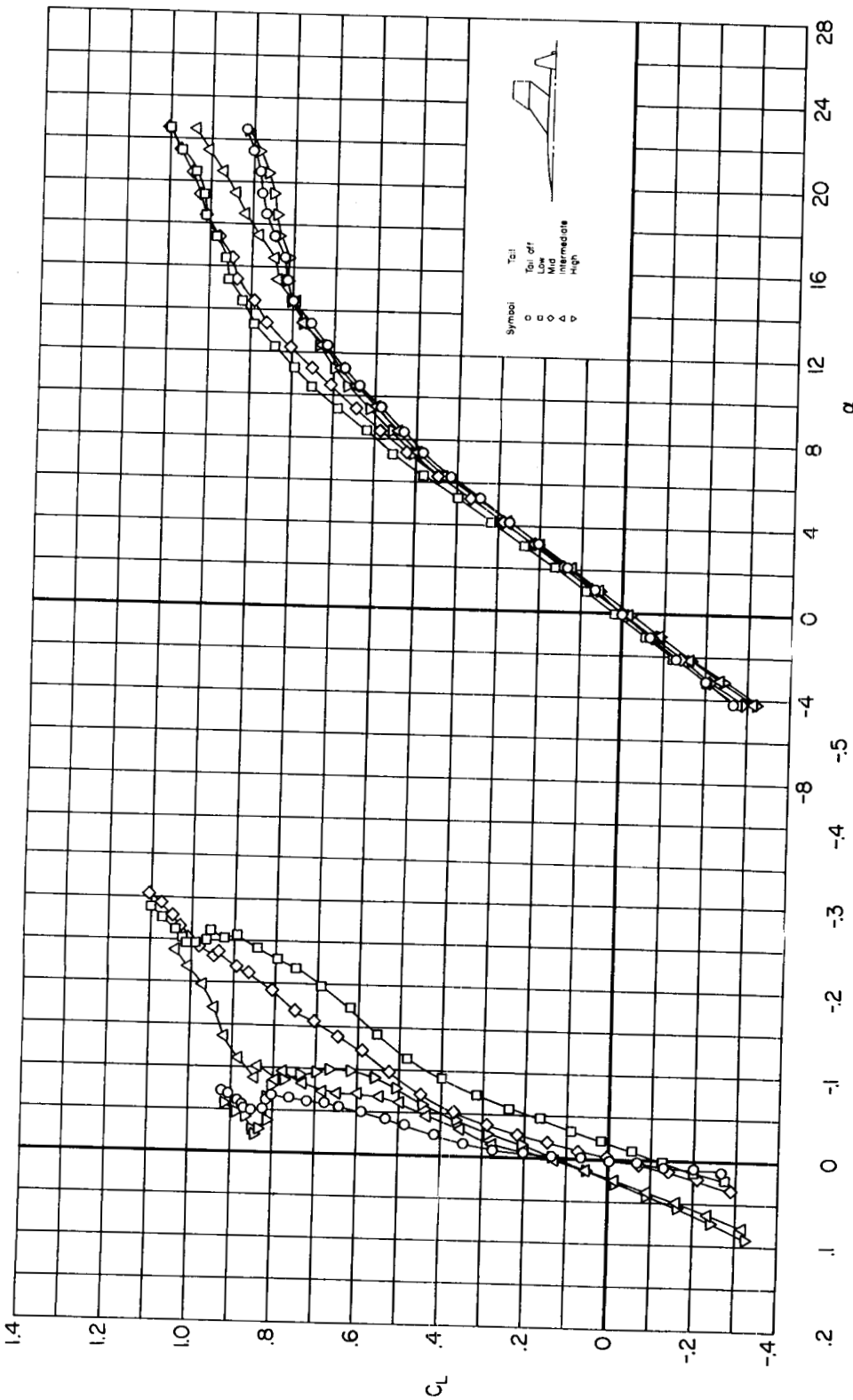

(b) M = 0.80

Figure 14.- Continued.

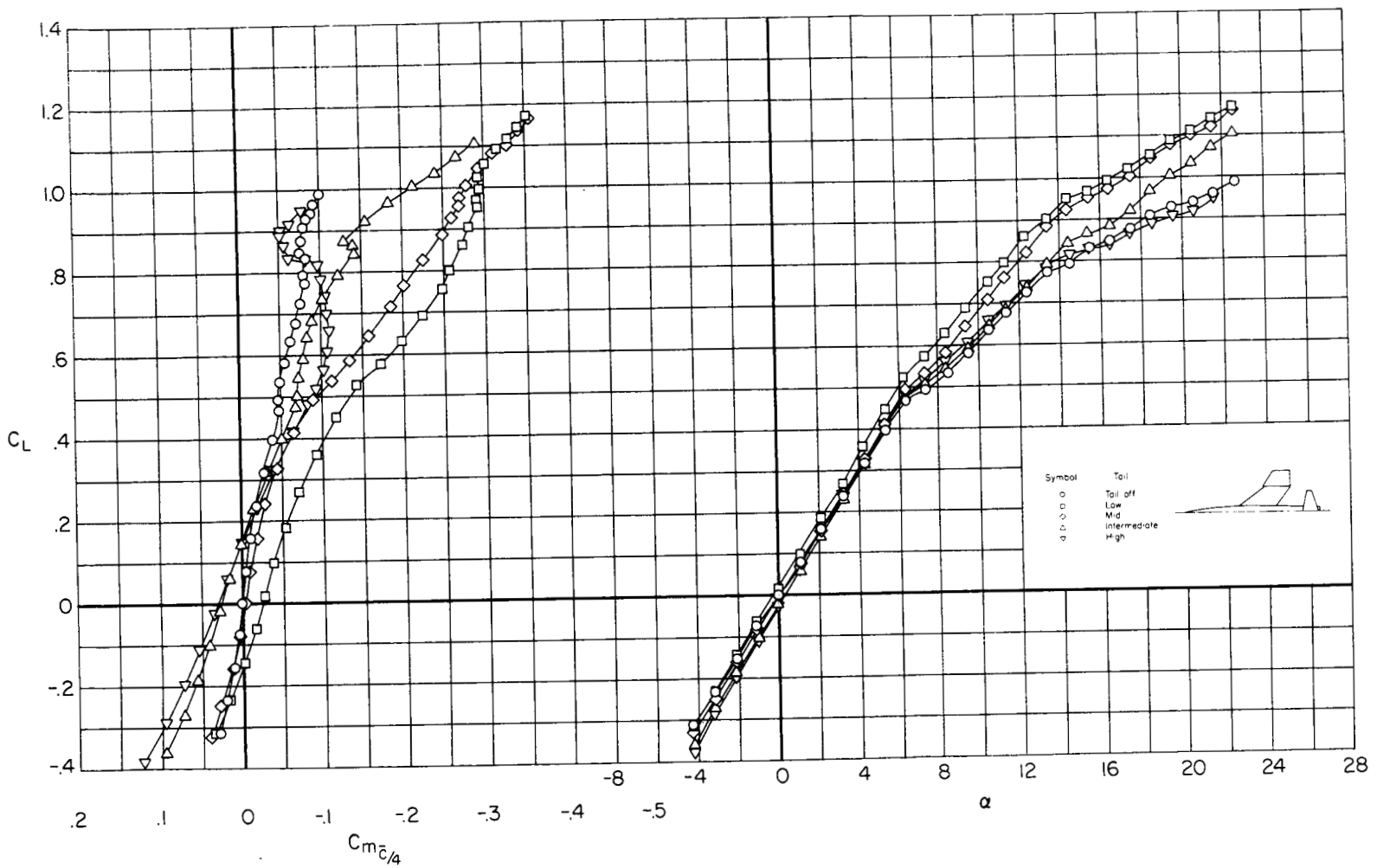

(c) M = 0.90

Figure 14.- Continued.

CONFIDENTIAL

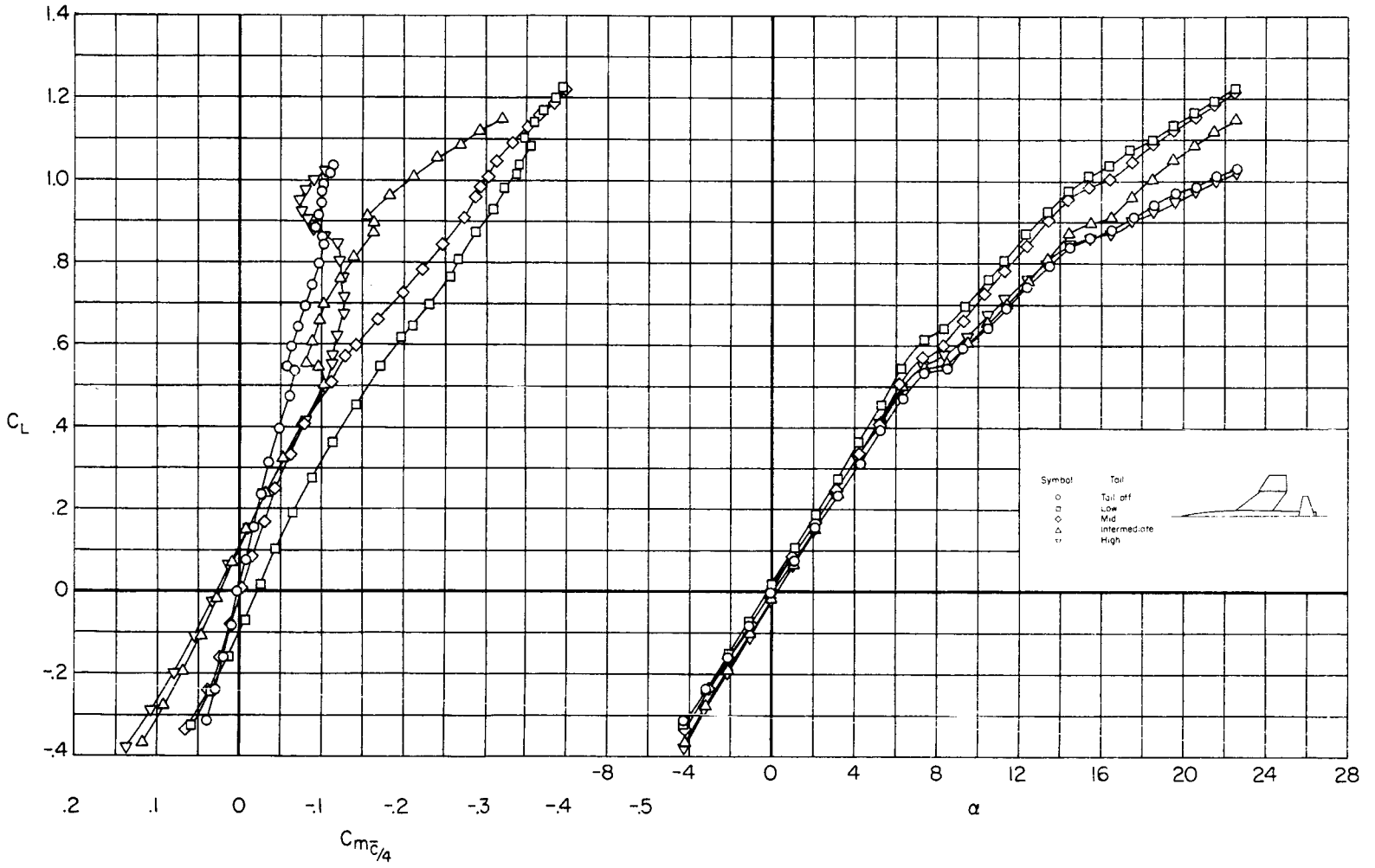

(d) M = 0.94

Figure 14.- Continued.

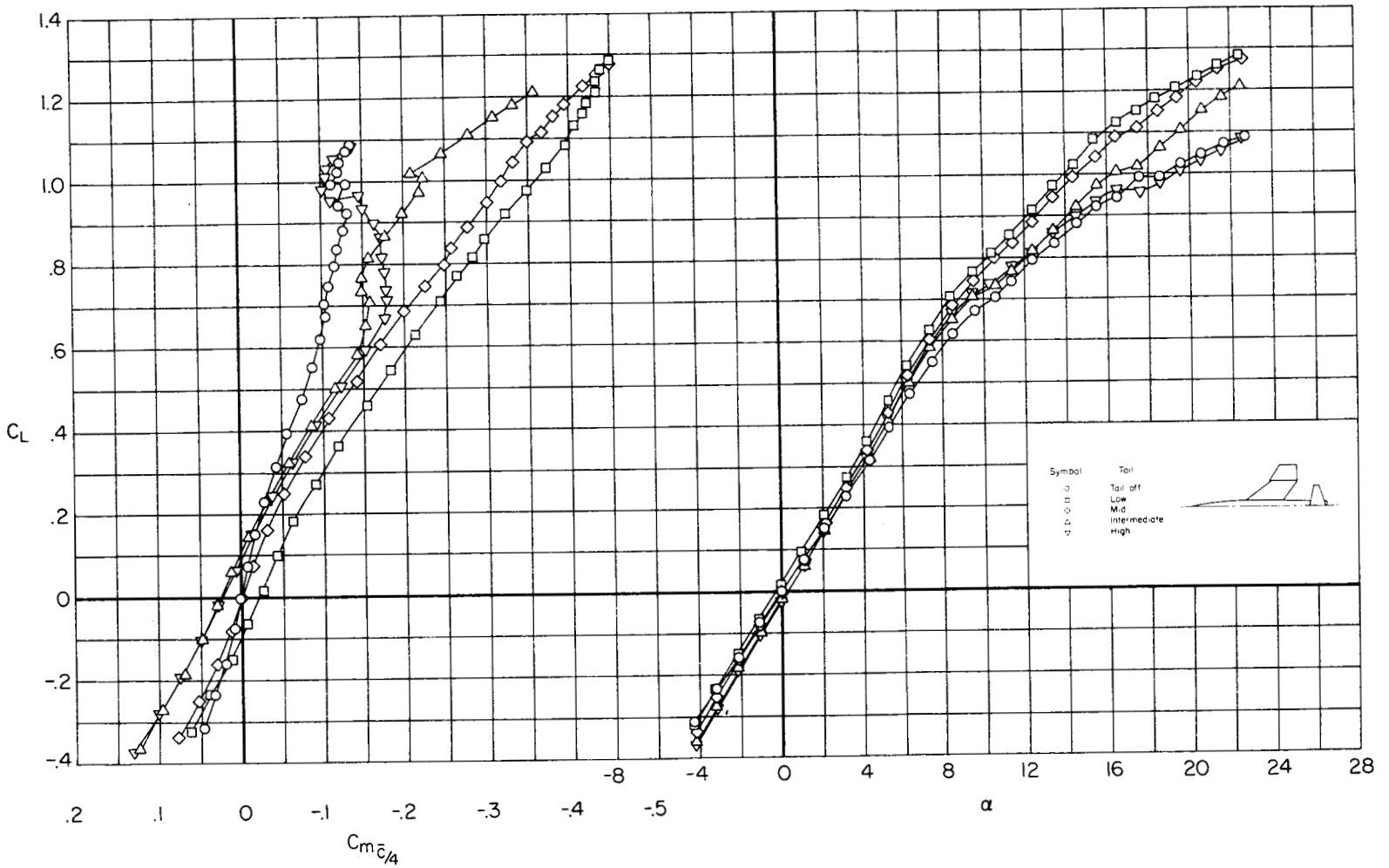

(e) M = 0.98

Figure 14.- Continued.

CONFIDENTIAL

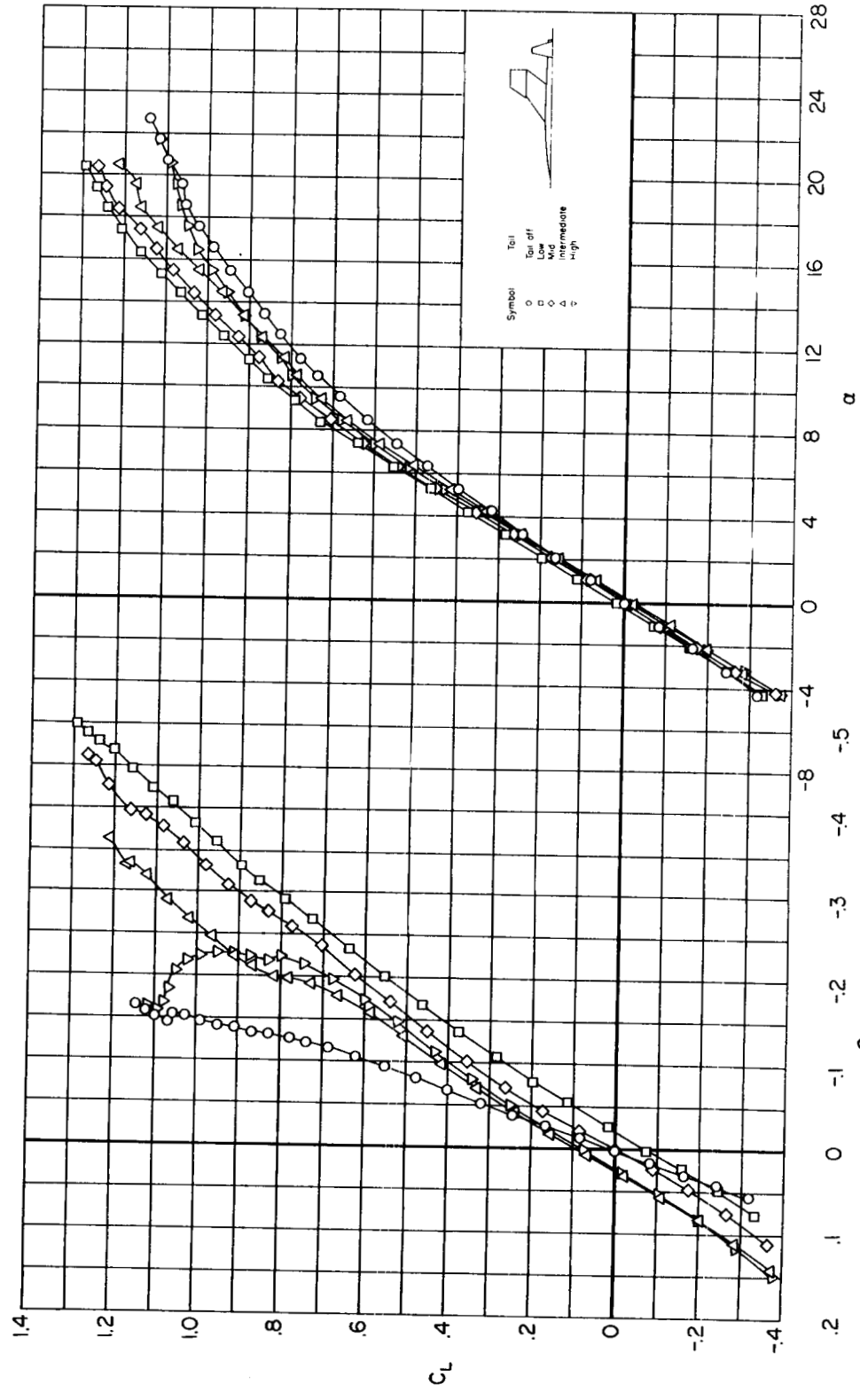

(f) M = 1.02

Figure 14.- Continued.

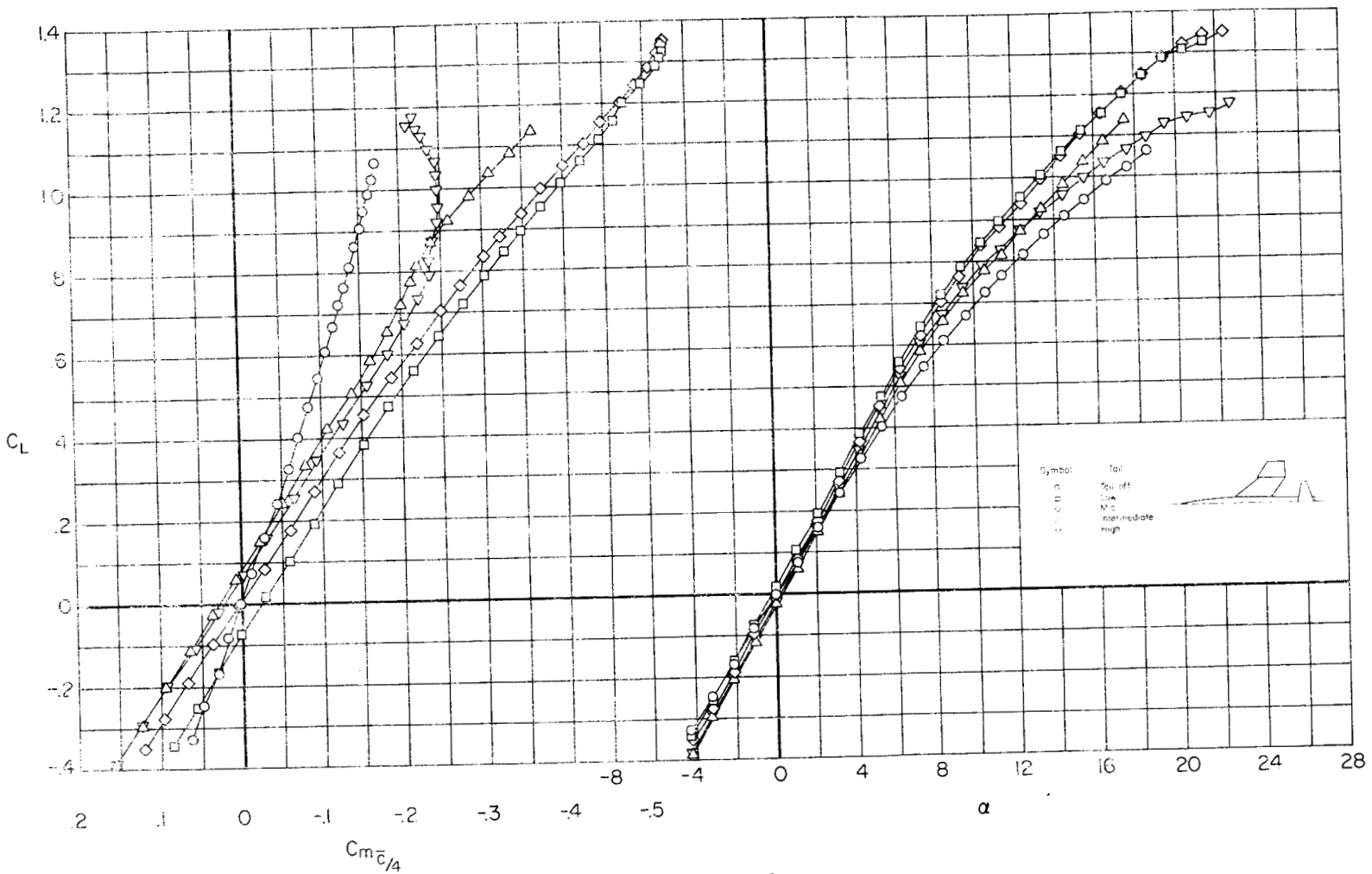

(g) M = 1.06

Figure 14.- Continued.

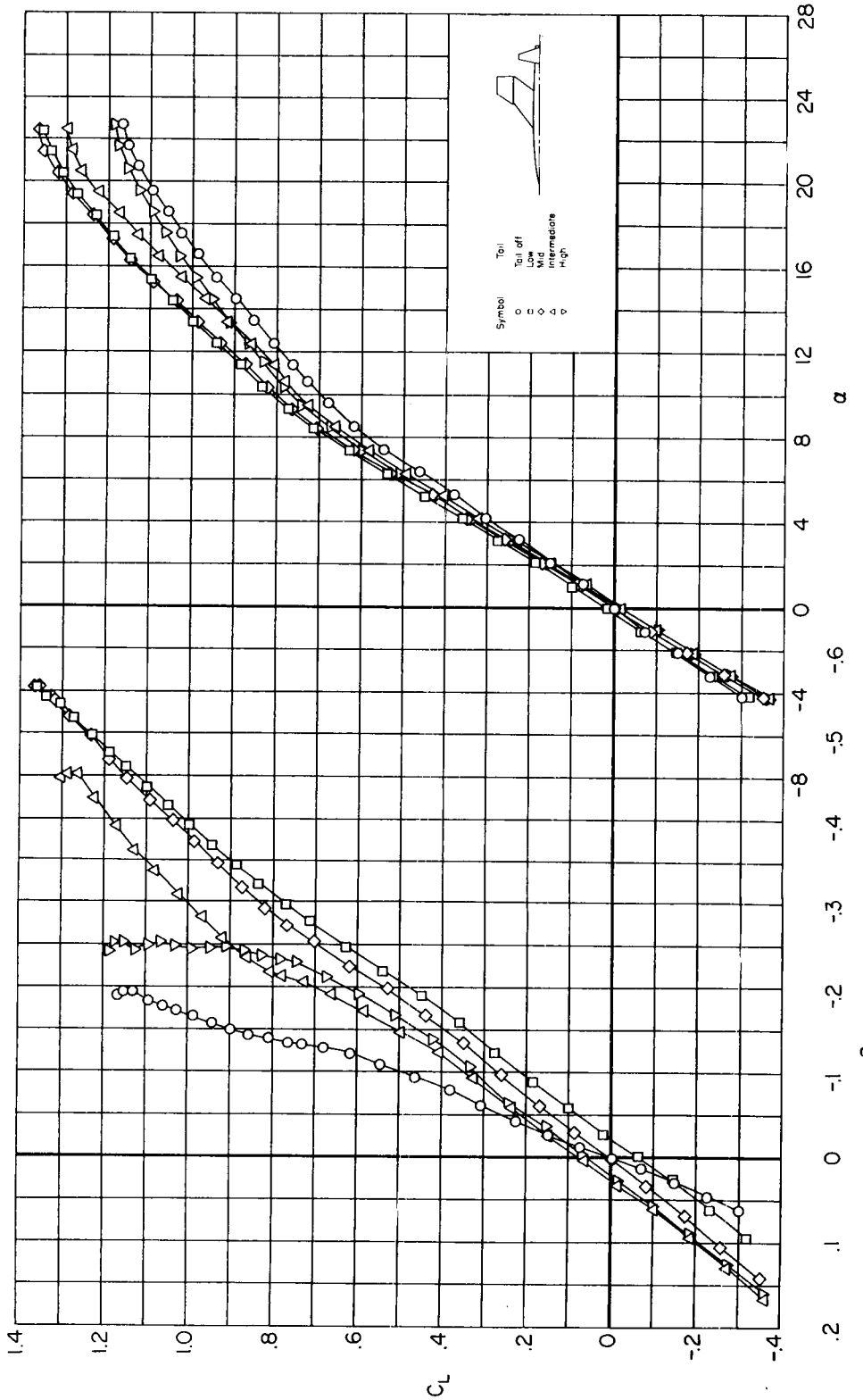

(h) M = 1.10

Figure 14.- Continued.

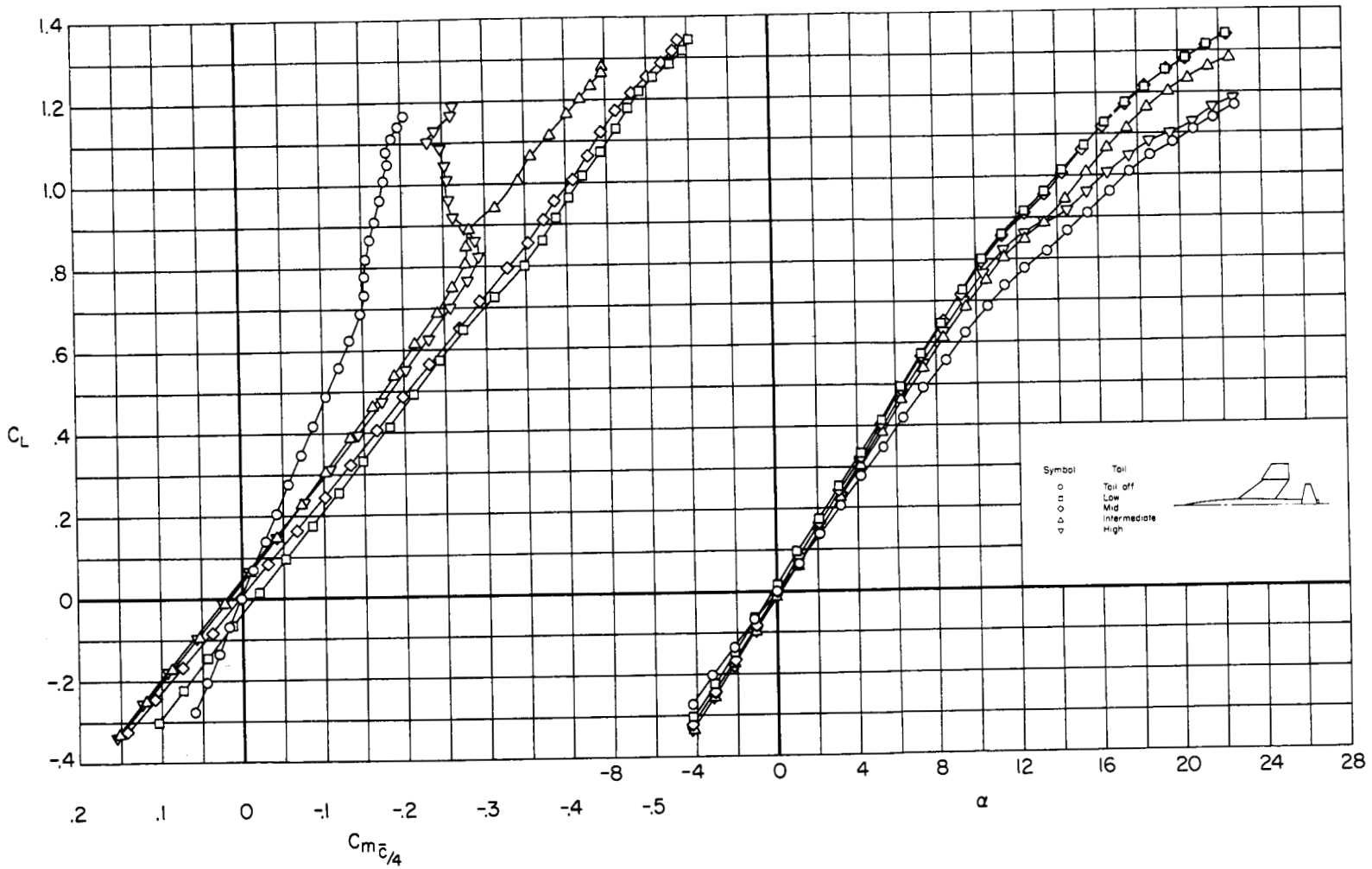

(i) M = 1.20

Figure 14.- Continued.

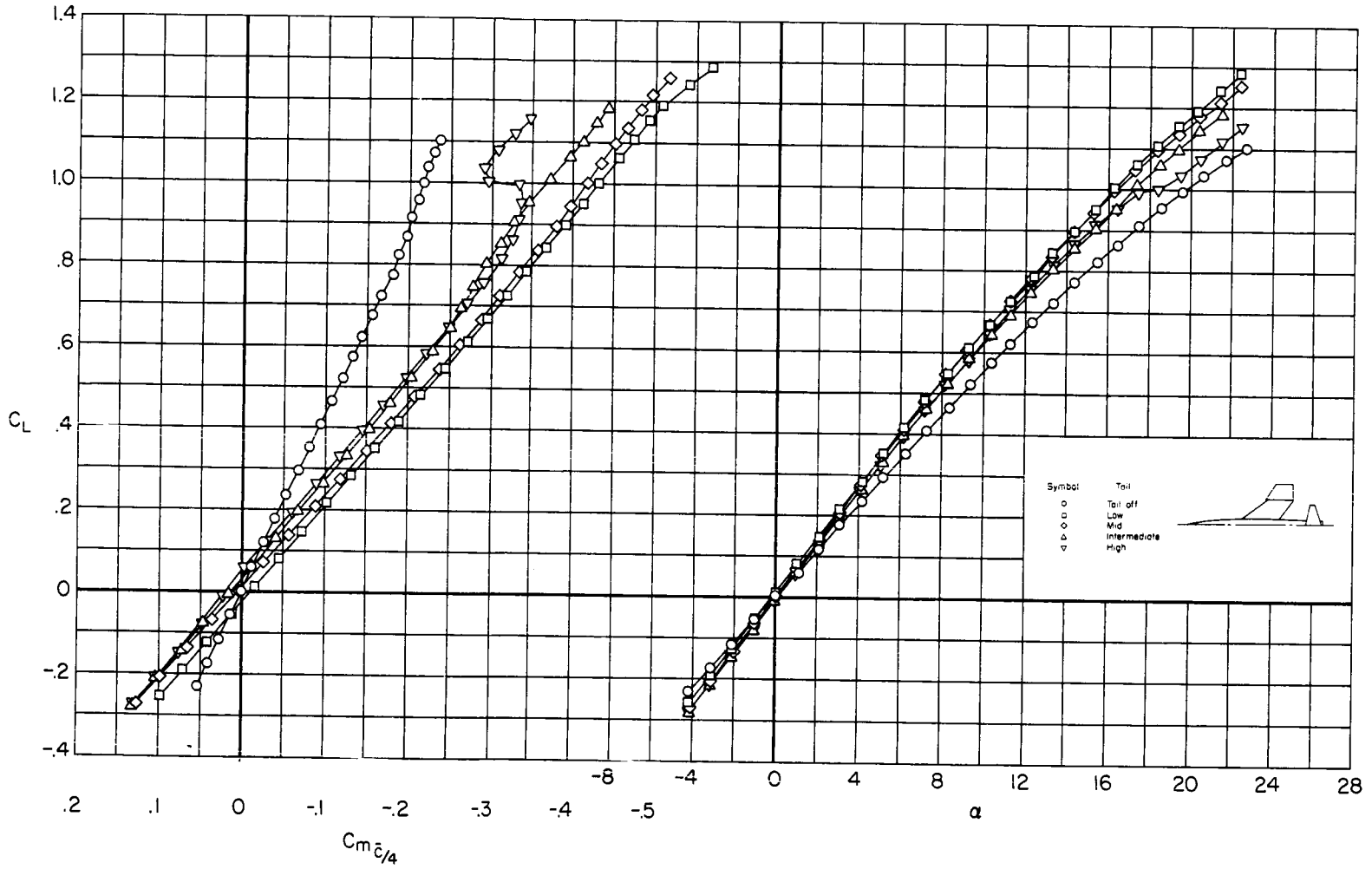

(j) M = 1.40

Figure 14.- Concluded.

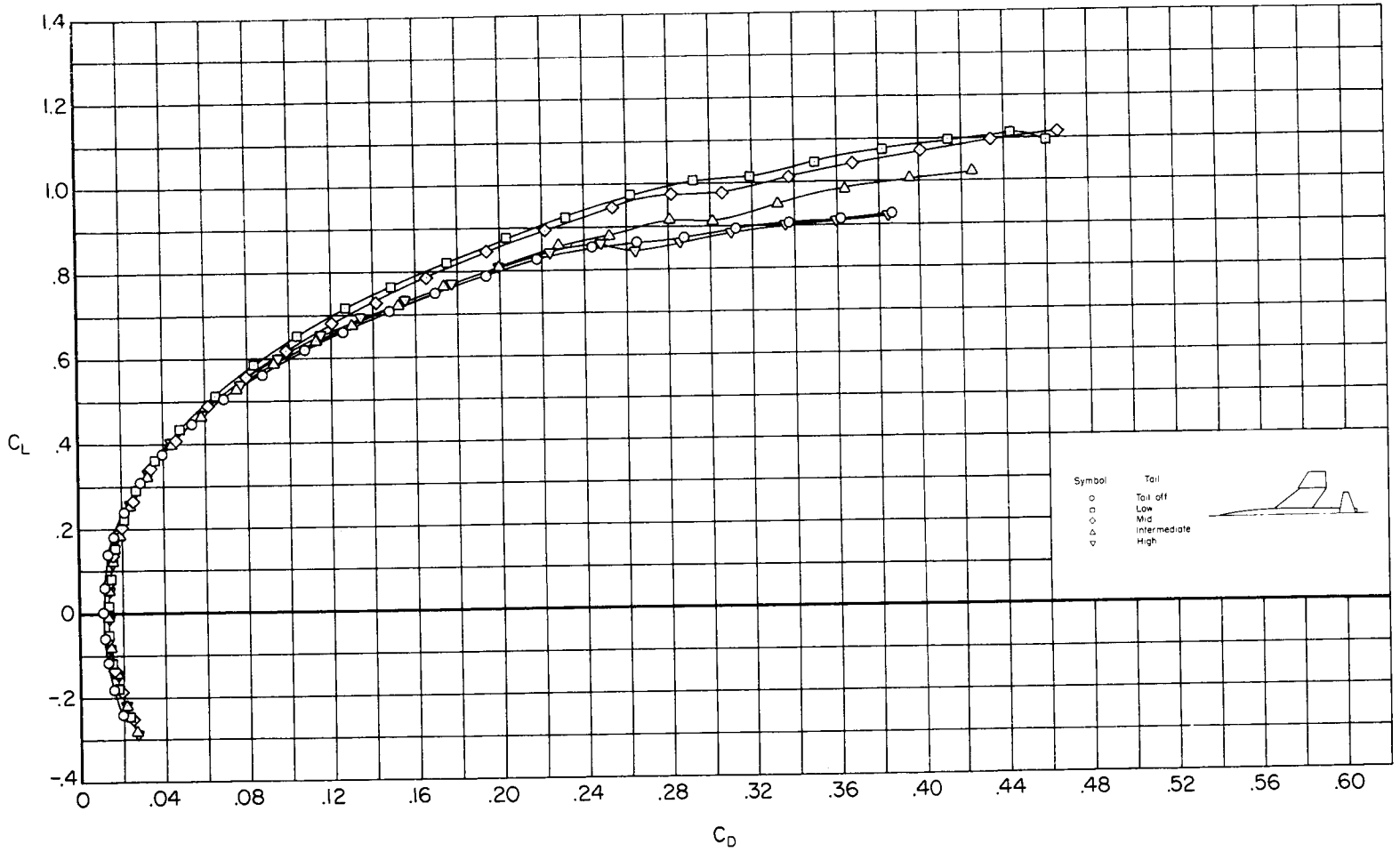

(a) M = 0.60

Figure 15.- Variation of lift coefficient with drag coefficient at constant Mach number for the 53-32 series wing-body-tail models.

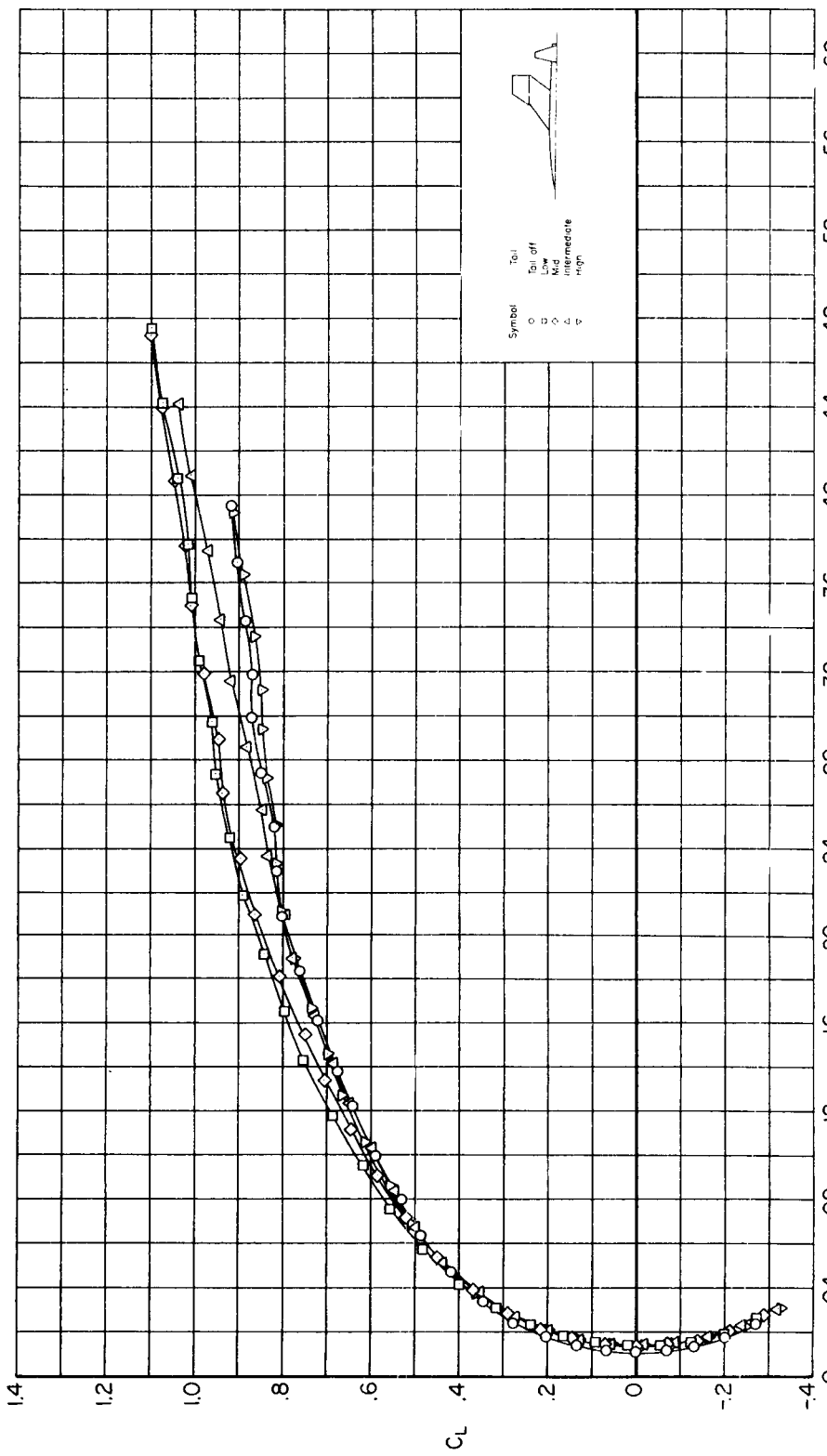

(b) M = 0.80

Figure 15.- Continued.

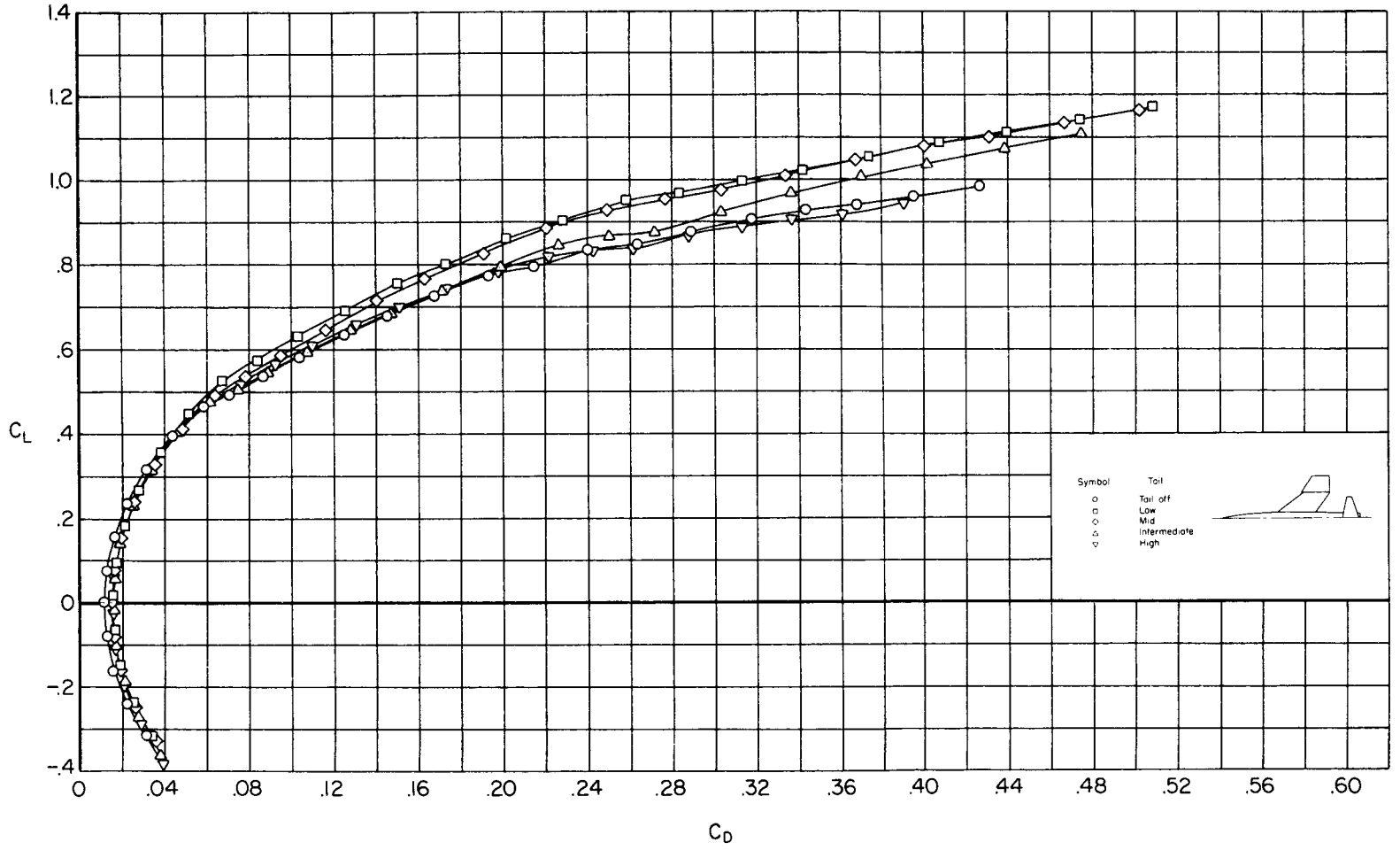

(c) M = 0.90

Figure 15.- Continued.

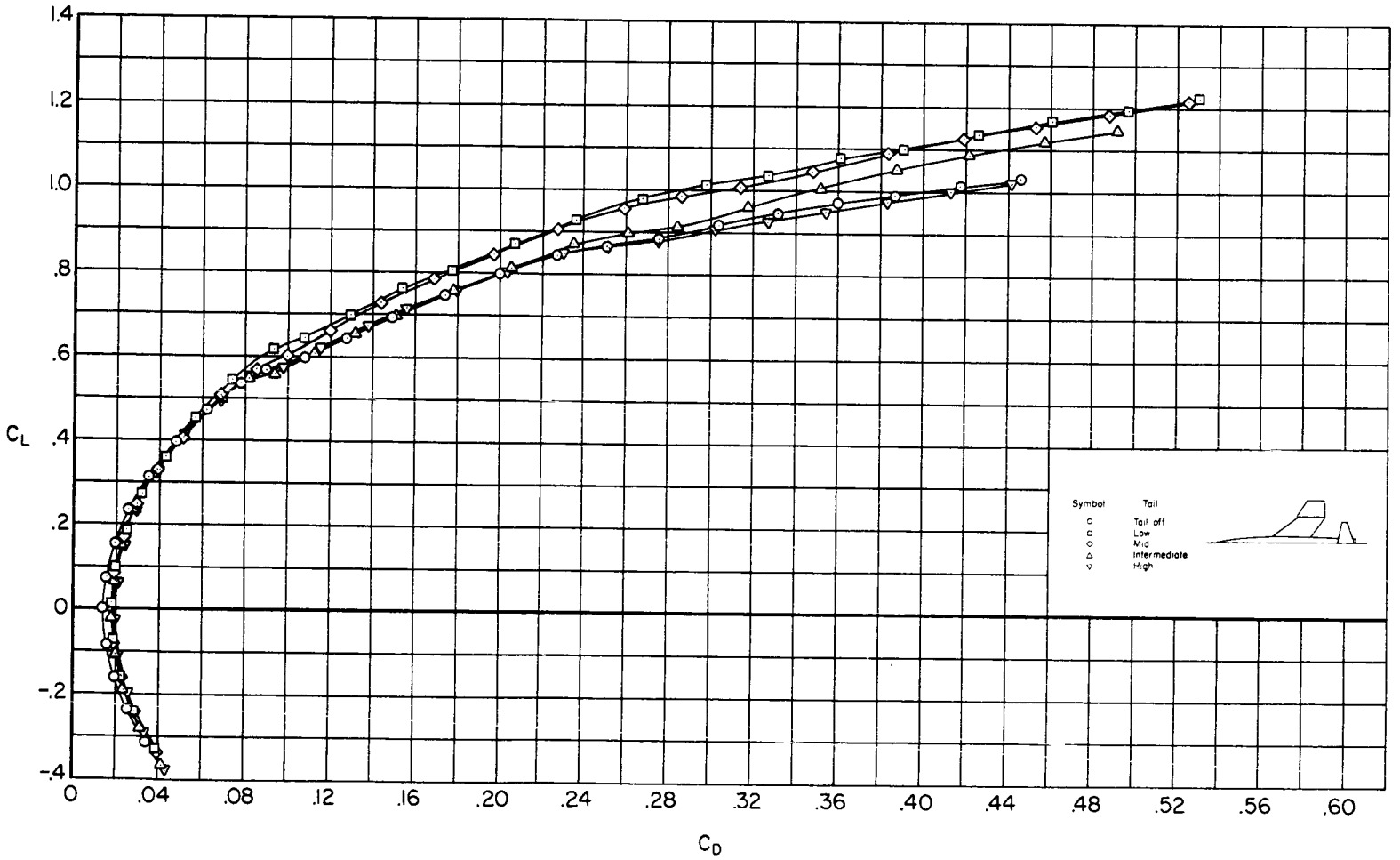

(d) M = 0.94

Figure 15.- Continued.

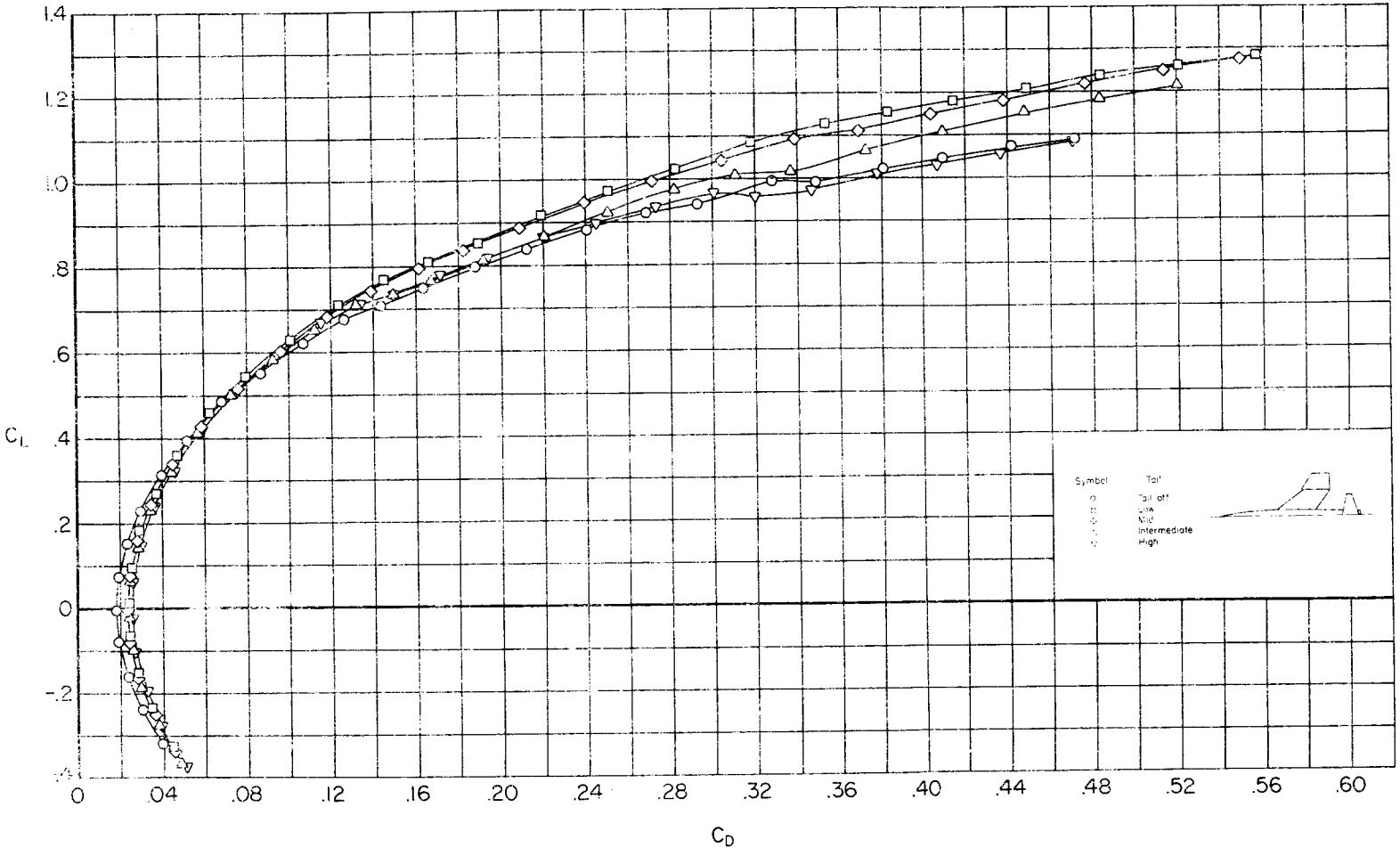

(e) M = 0.98

Figure 15.- Continued.

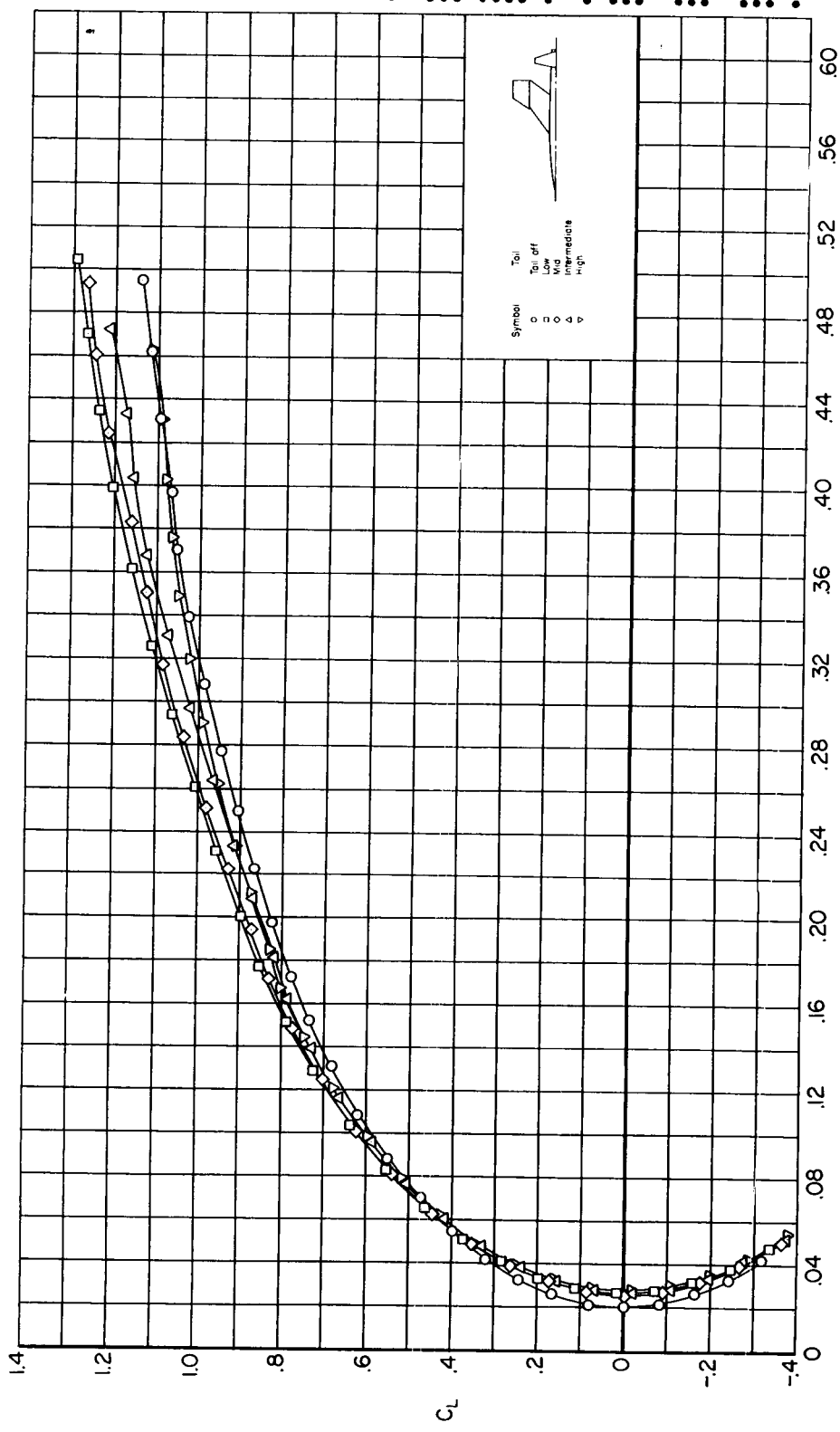

(f) M = 1.02

Figure 15.- Continued.

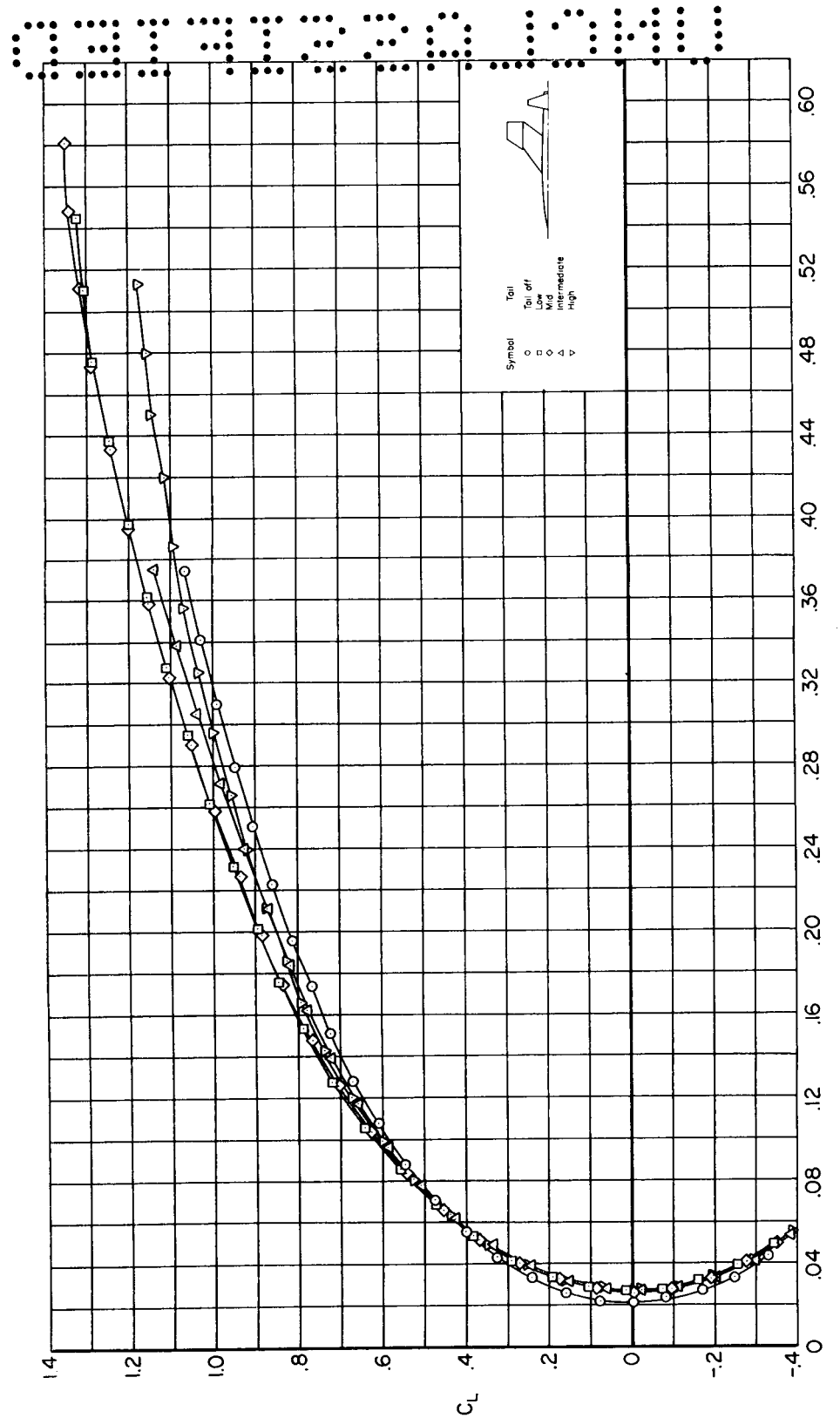

(g) M = 1.06

Figure 15.- Continued.

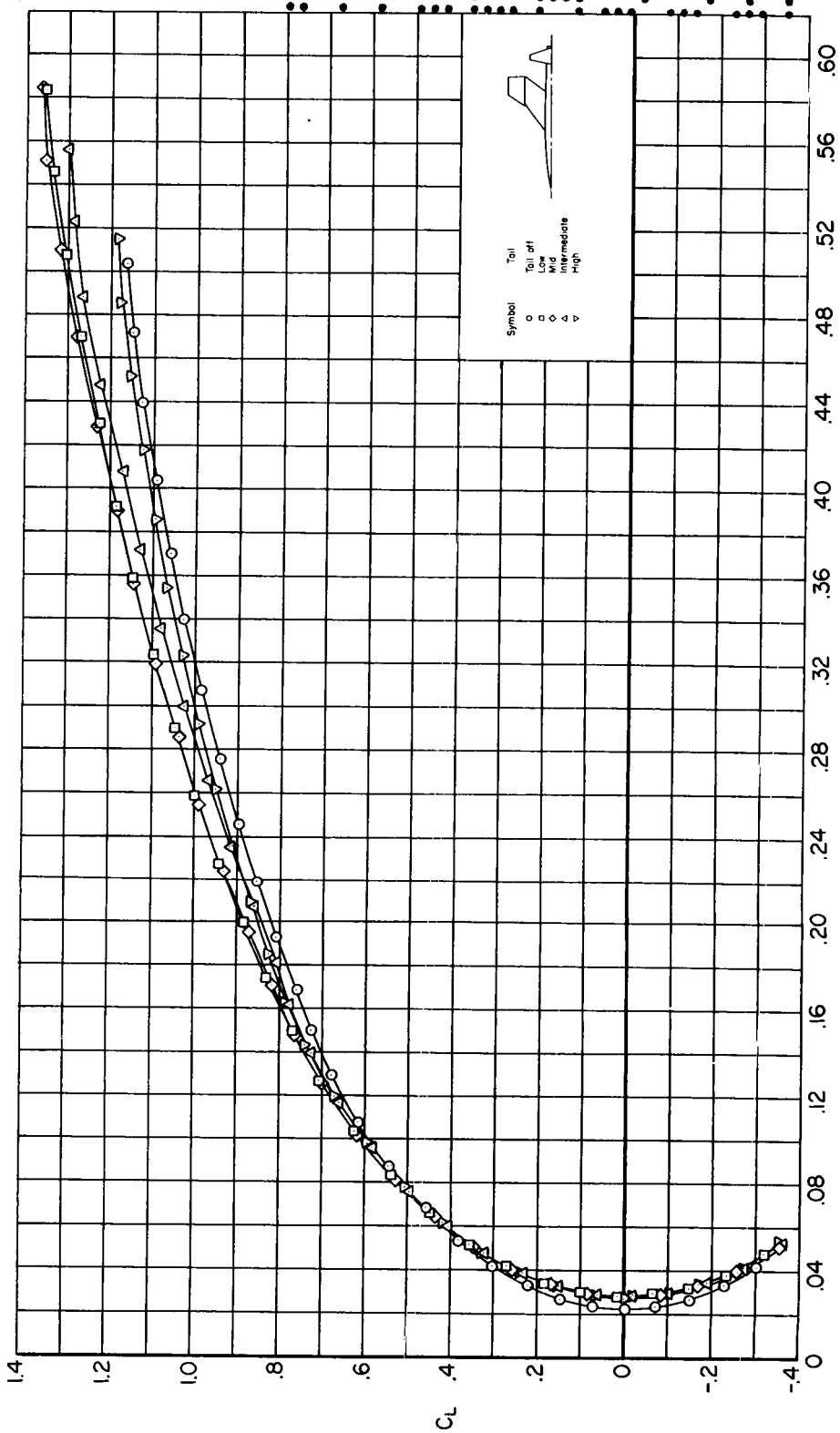

(h) M = 1.10

Figure 15.- Continued.

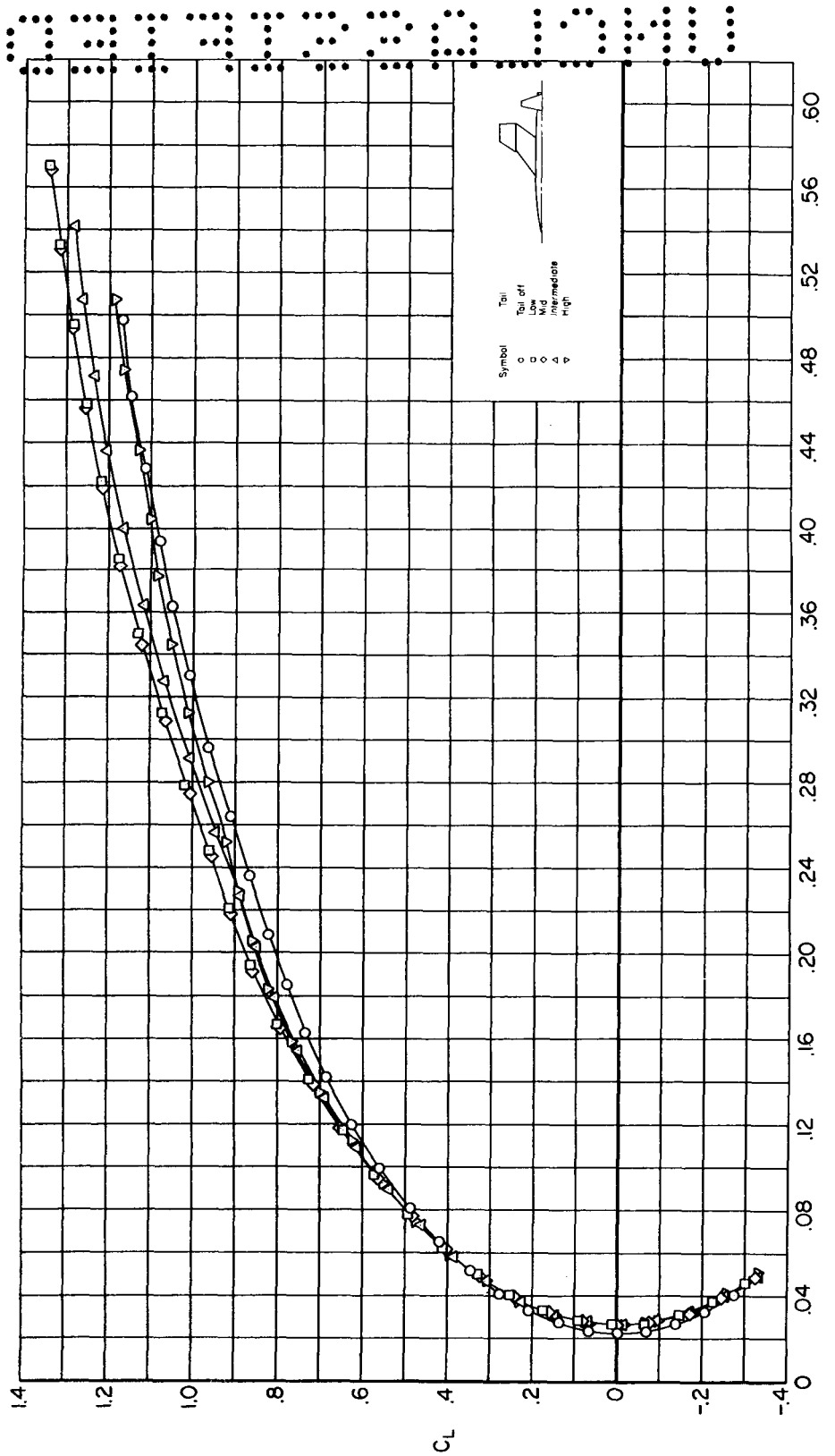

(i) M = 1.20

Figure 15.- Continued.

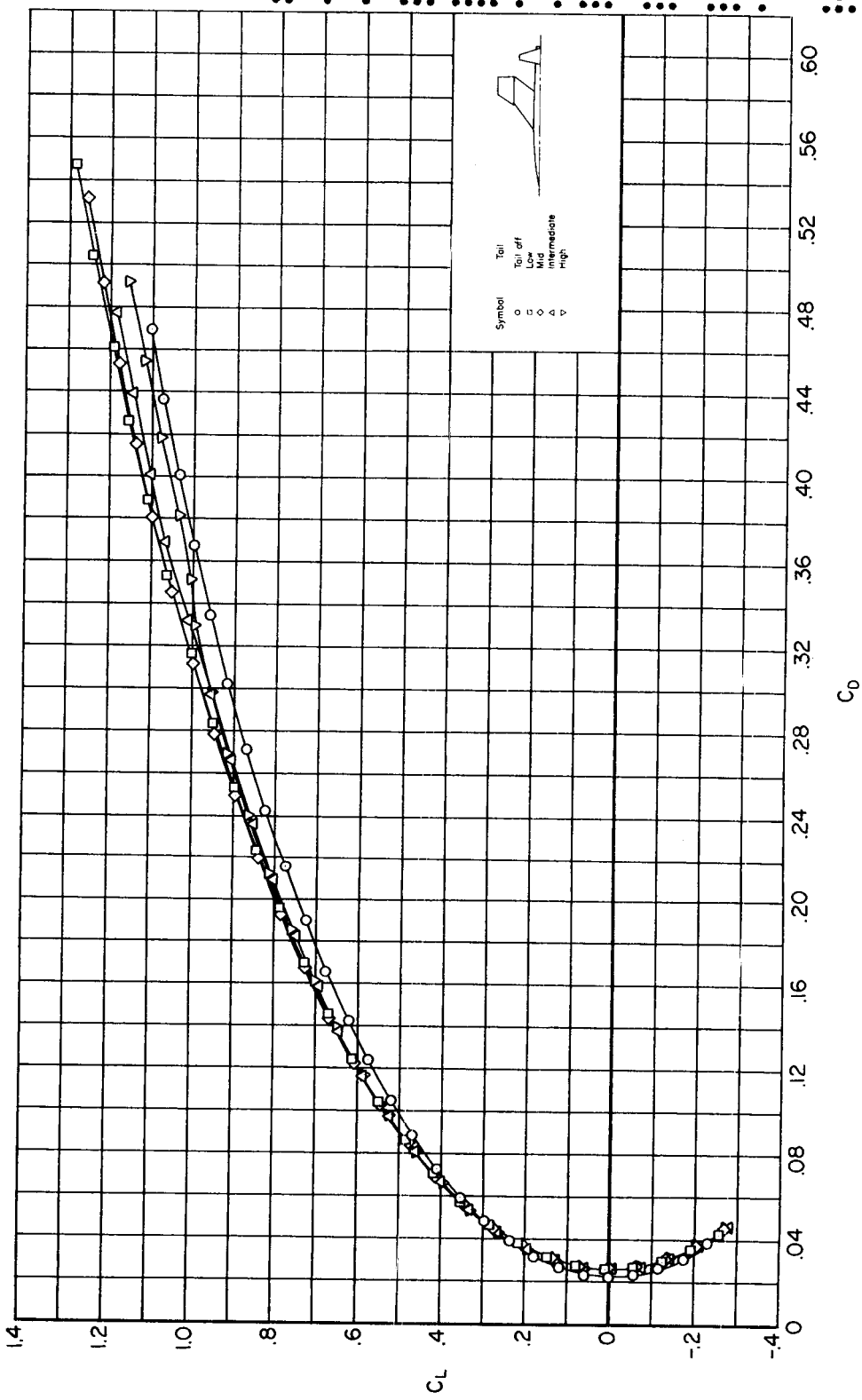

(j) M = 1.40

Figure 15.- Concluded.

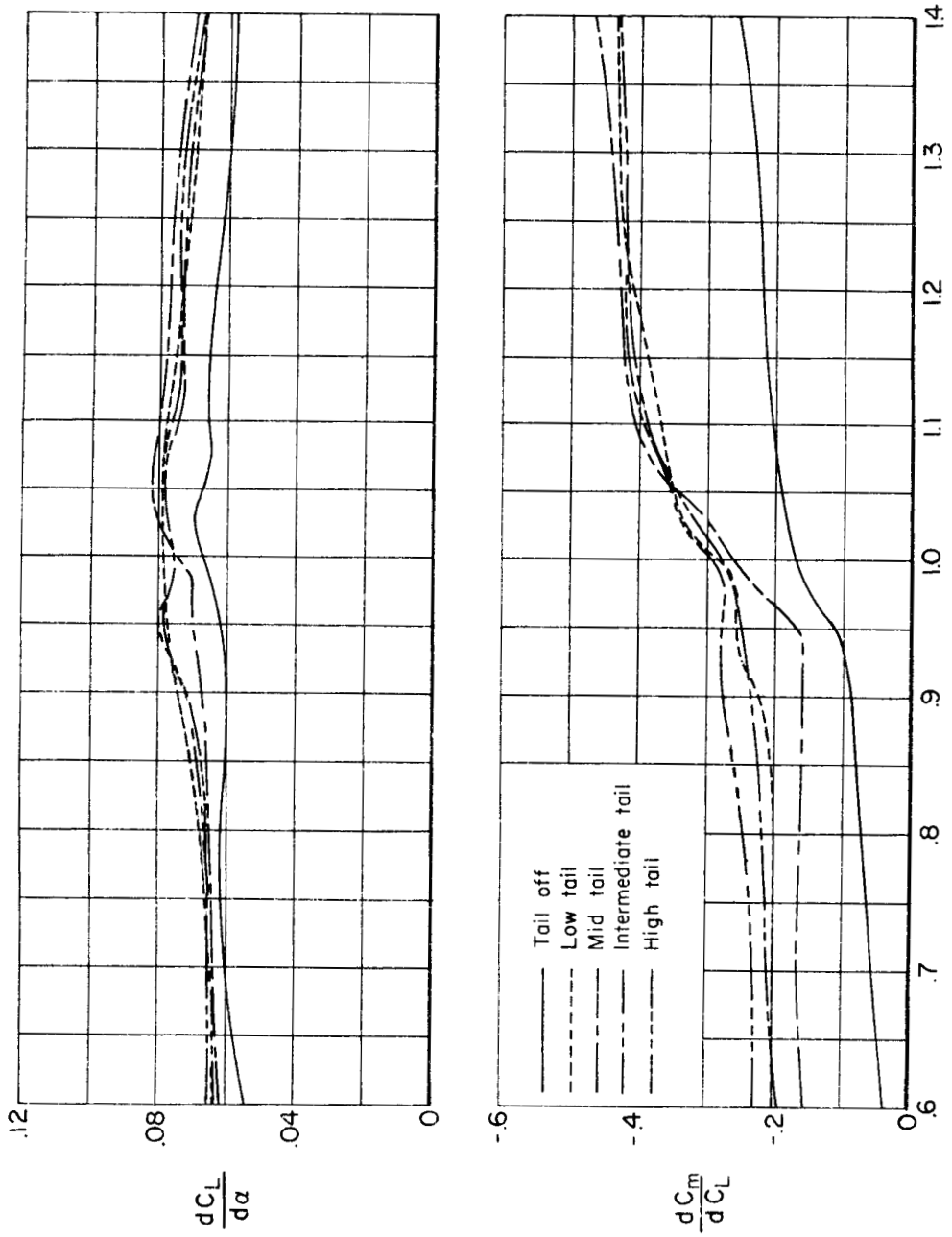

(a) 53 series wing-body-tail models.

Figure 16.- Variation of $dC_L/d\alpha$ and dC_m/dC_L at $C_L = 0$ with Mach number for wing-body-tail models.

UNCLASSIFIED

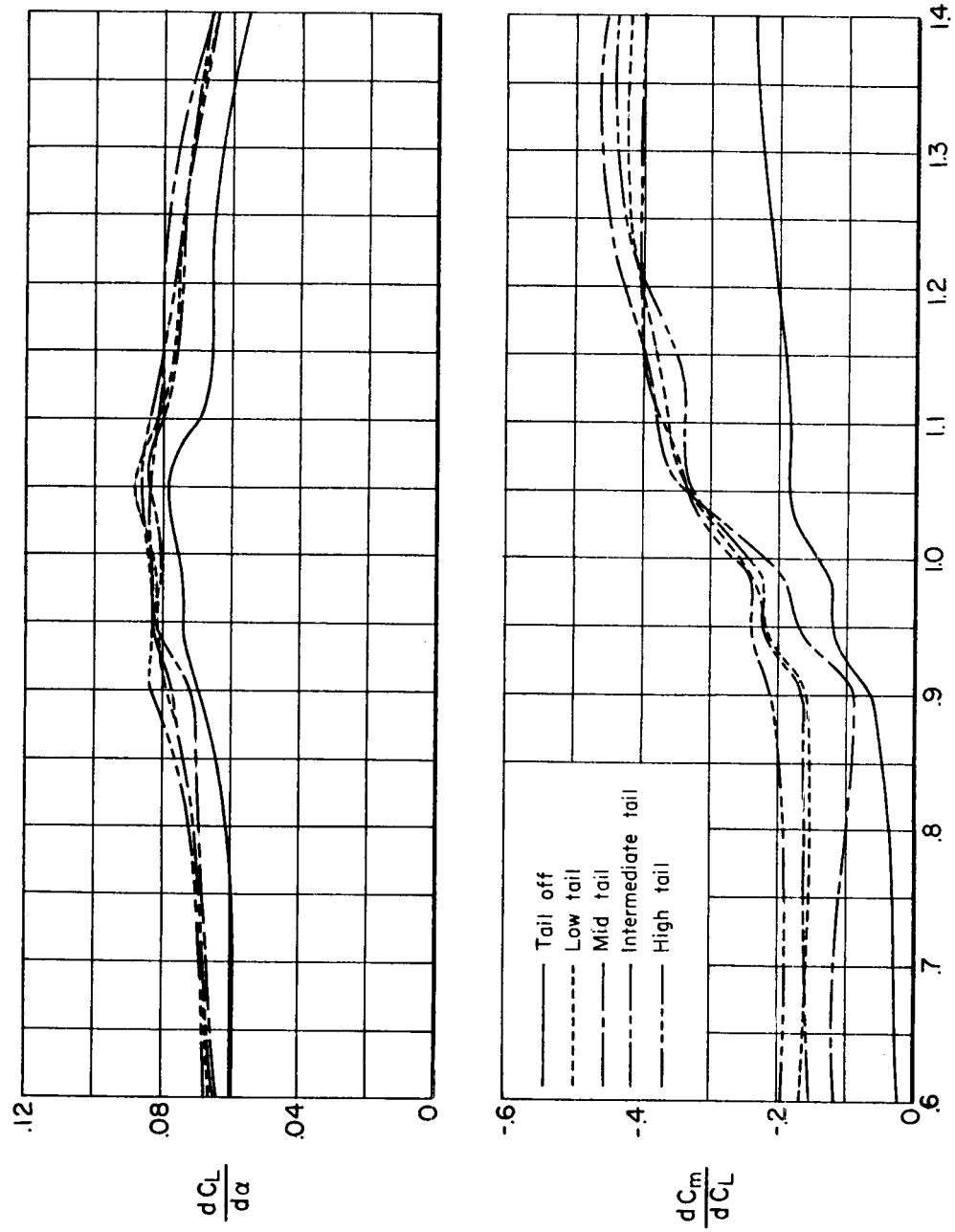

(b) 53-32 series wing-body-tail models.

Figure 16.- Concluded.

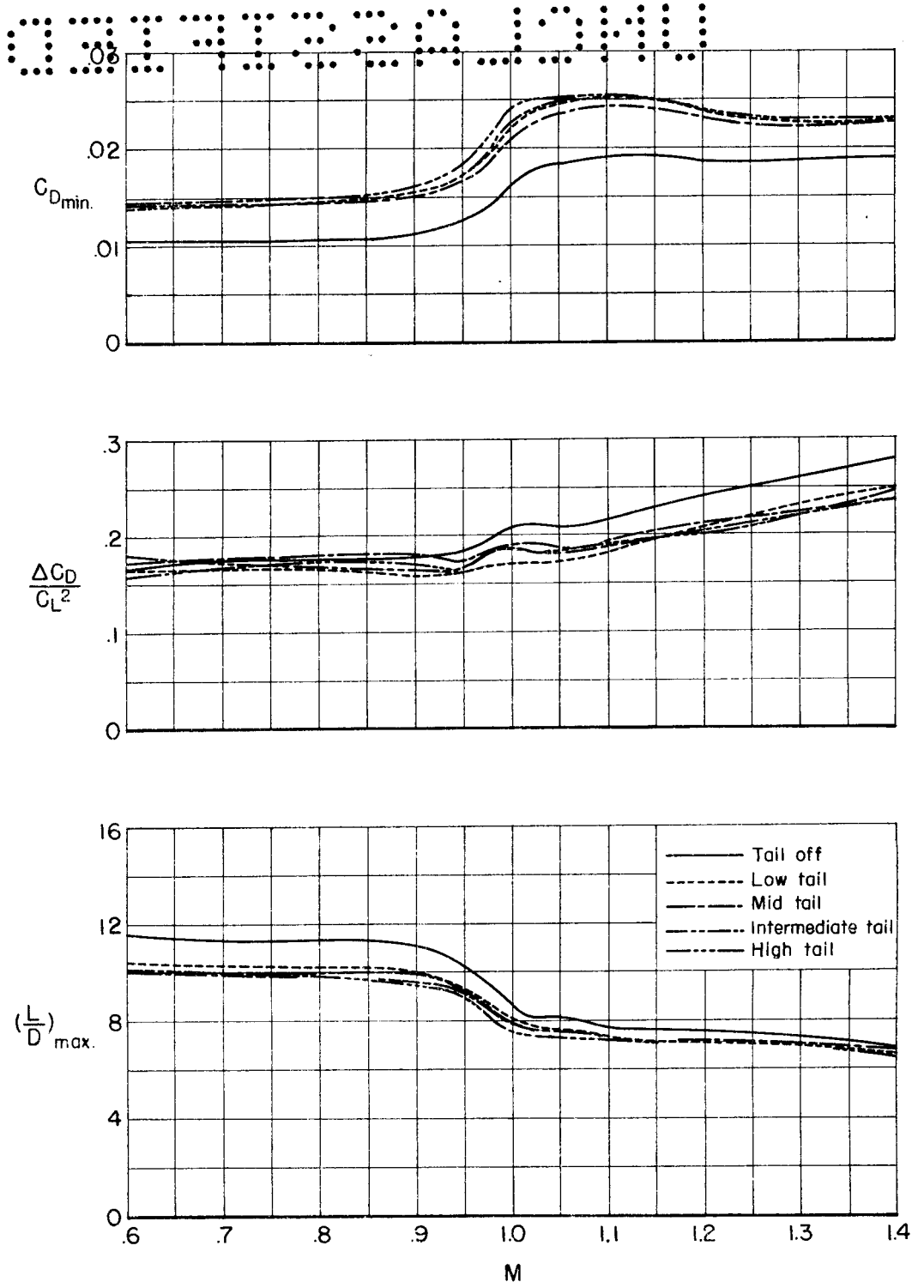

(a) 53 series wing-body-tail models.

Figure 17.- Variation of minimum drag coefficient, drag rise factor and maximum lift-drag ratio with Mach number for wing-body-tail models.

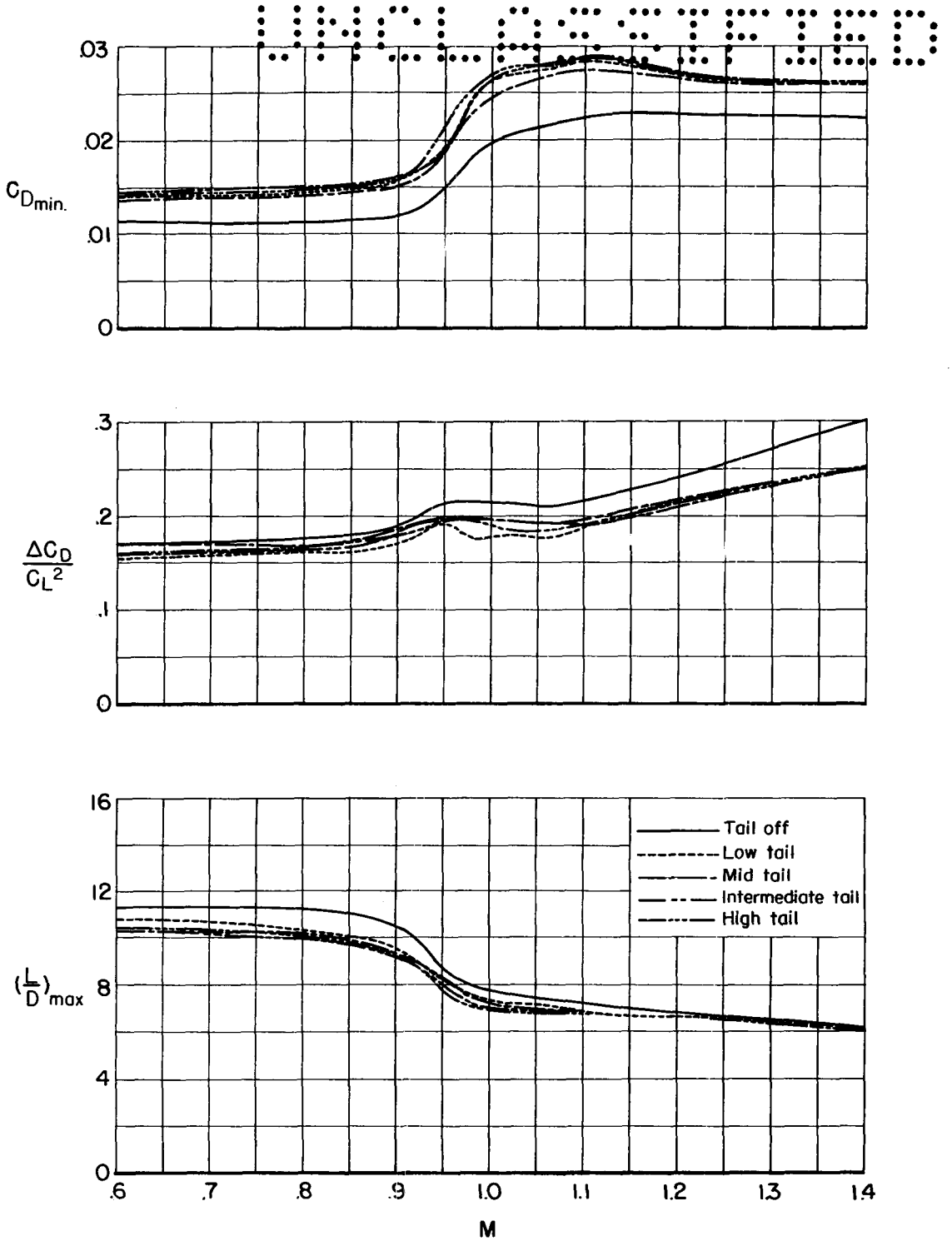

(b) 53-32 series wing-body-tail models.

Figure 17.- Concluded.

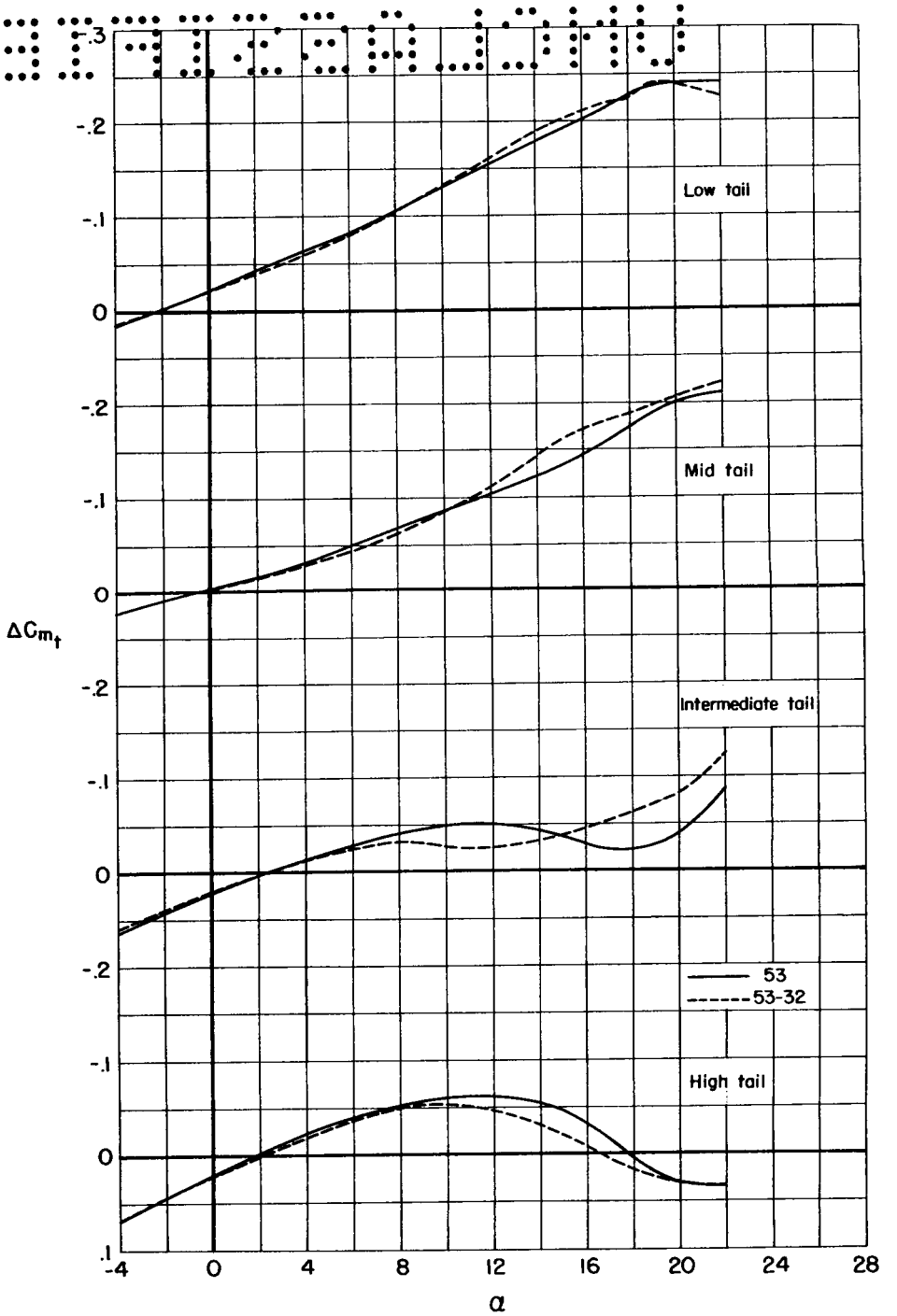

(a) M = 0.60

Figure 18.- Variation of the contribution of pitching moment of horizontal tails of various heights with angle of attack for wing-body-tail models.

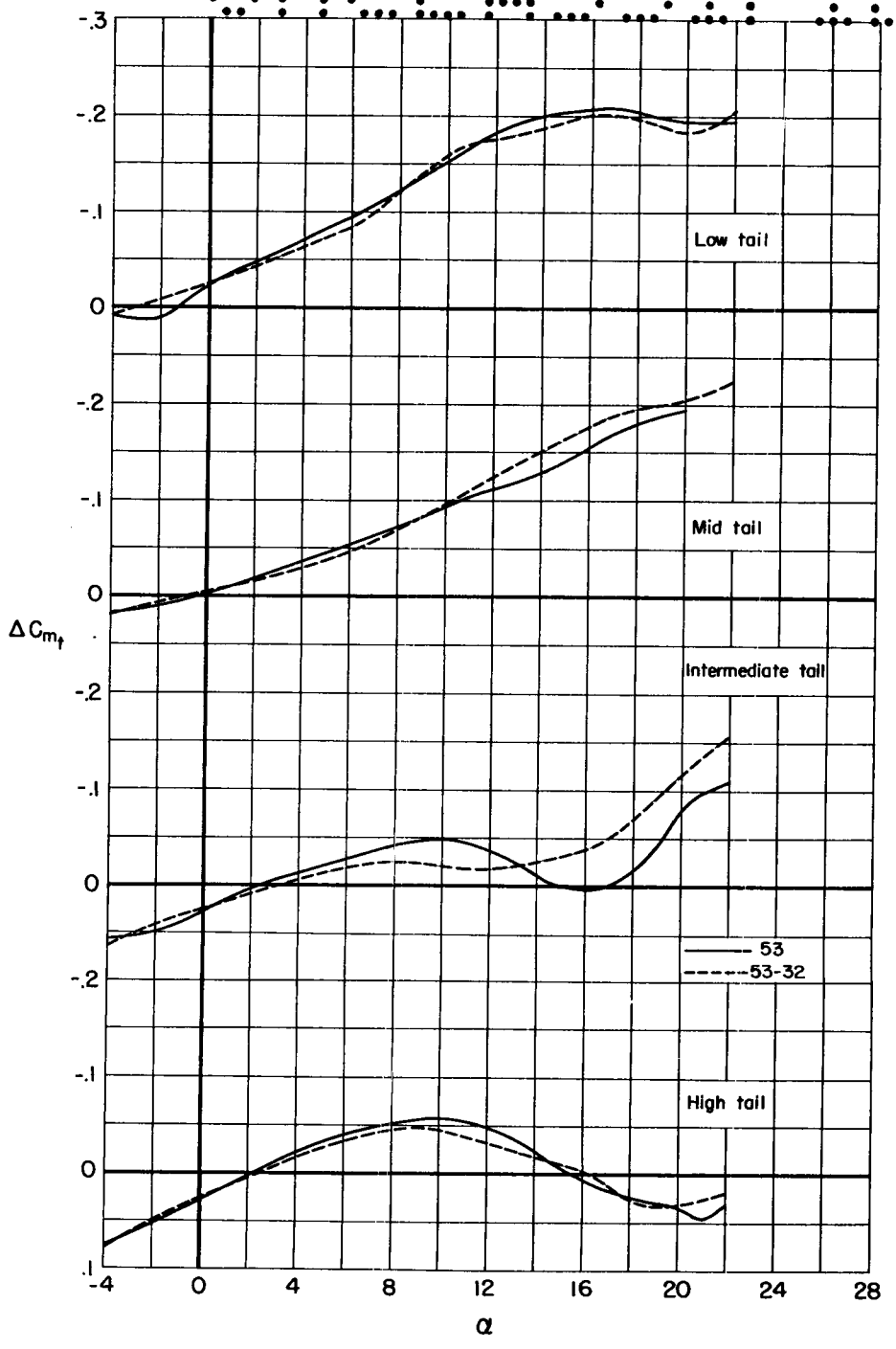

(b) M = 0.80

Figure 18.- Continued.

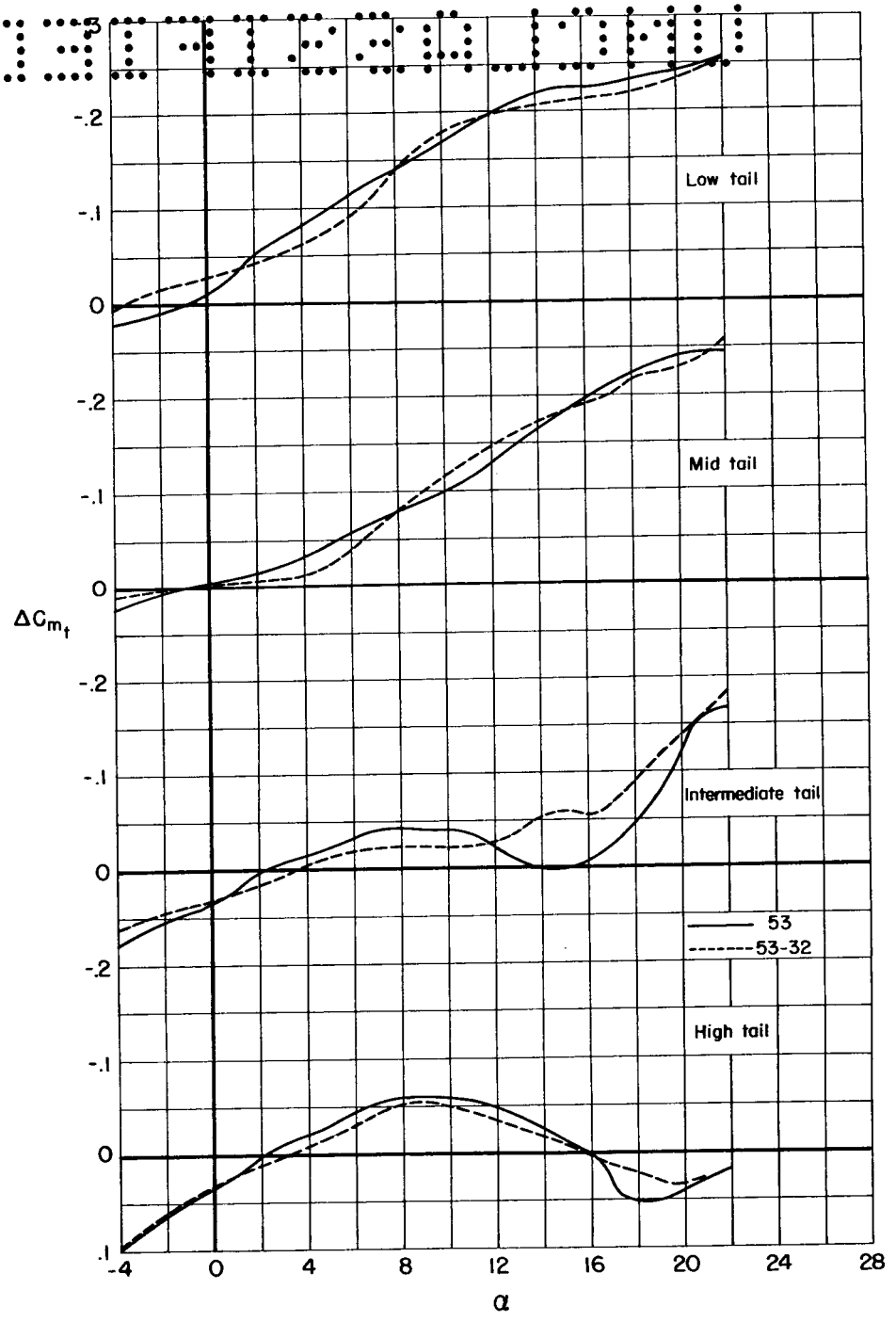

(c) M = 0.90

Figure 18.- Continued.

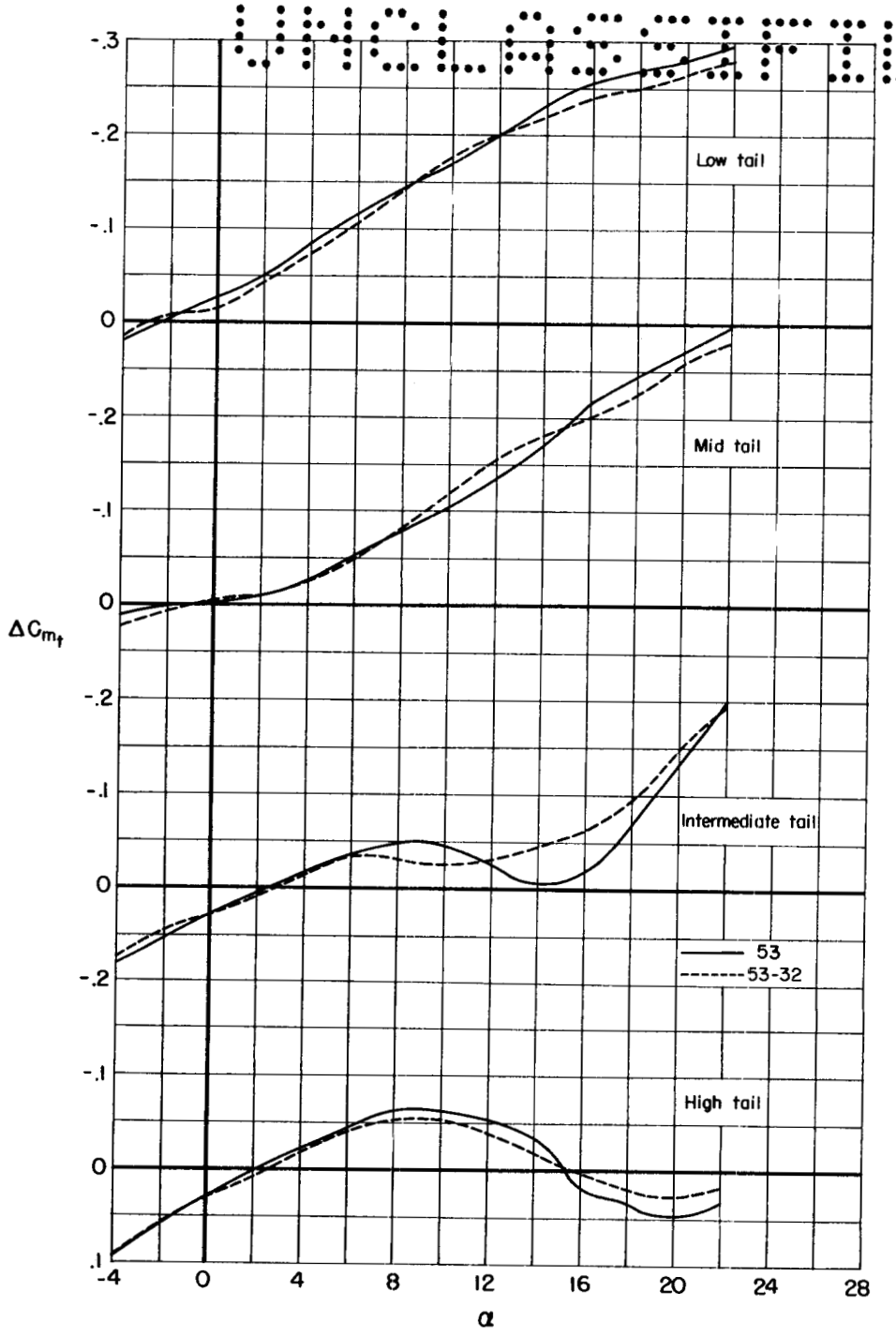

(d) M = 0.94

Figure 18.- Continued.

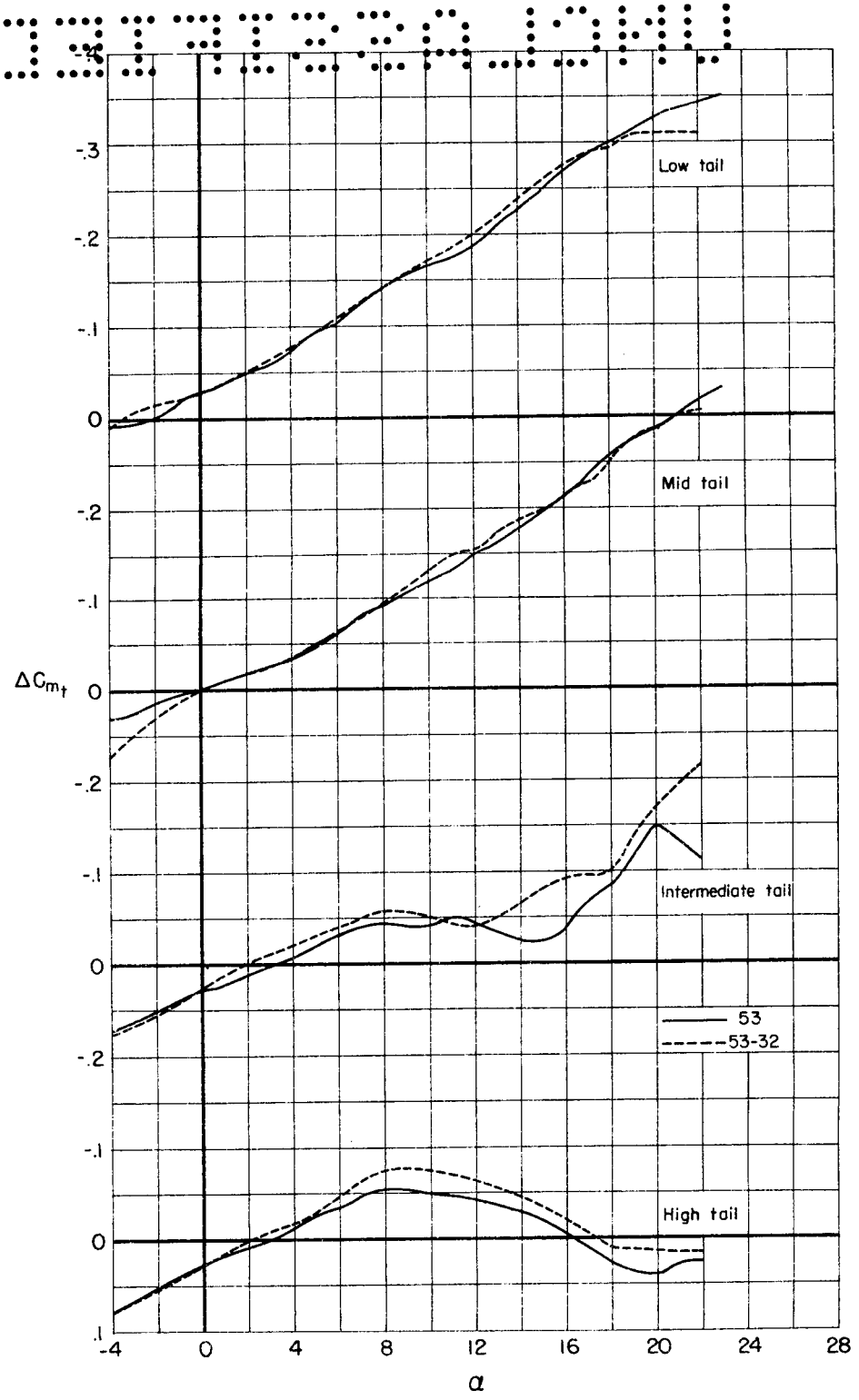

(e) M = 0.98

Figure 18.- Continued.

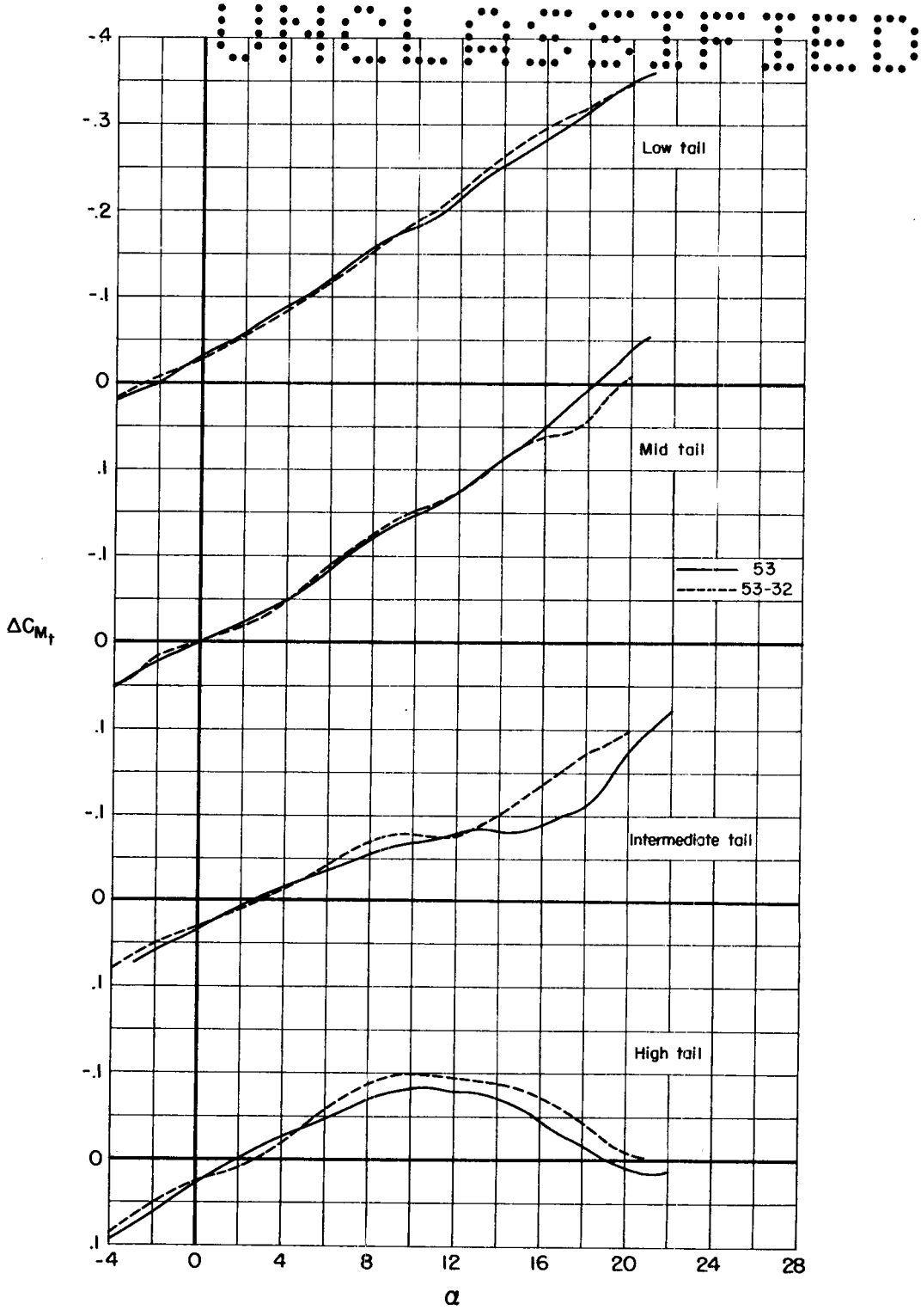

(f) M = 1.02

Figure 18.- Continued.

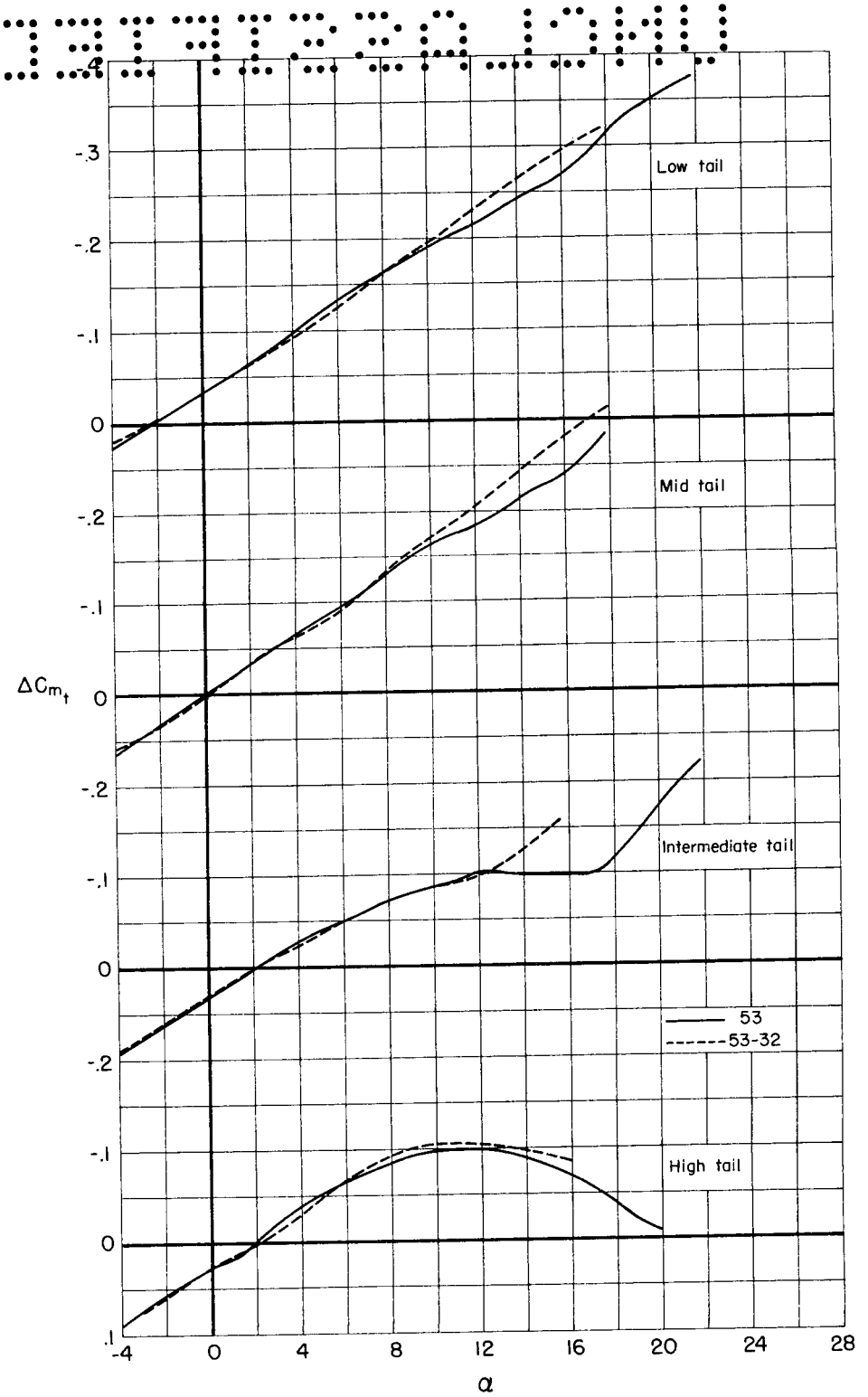

(g) M = 1.06

Figure 18.- Continued.

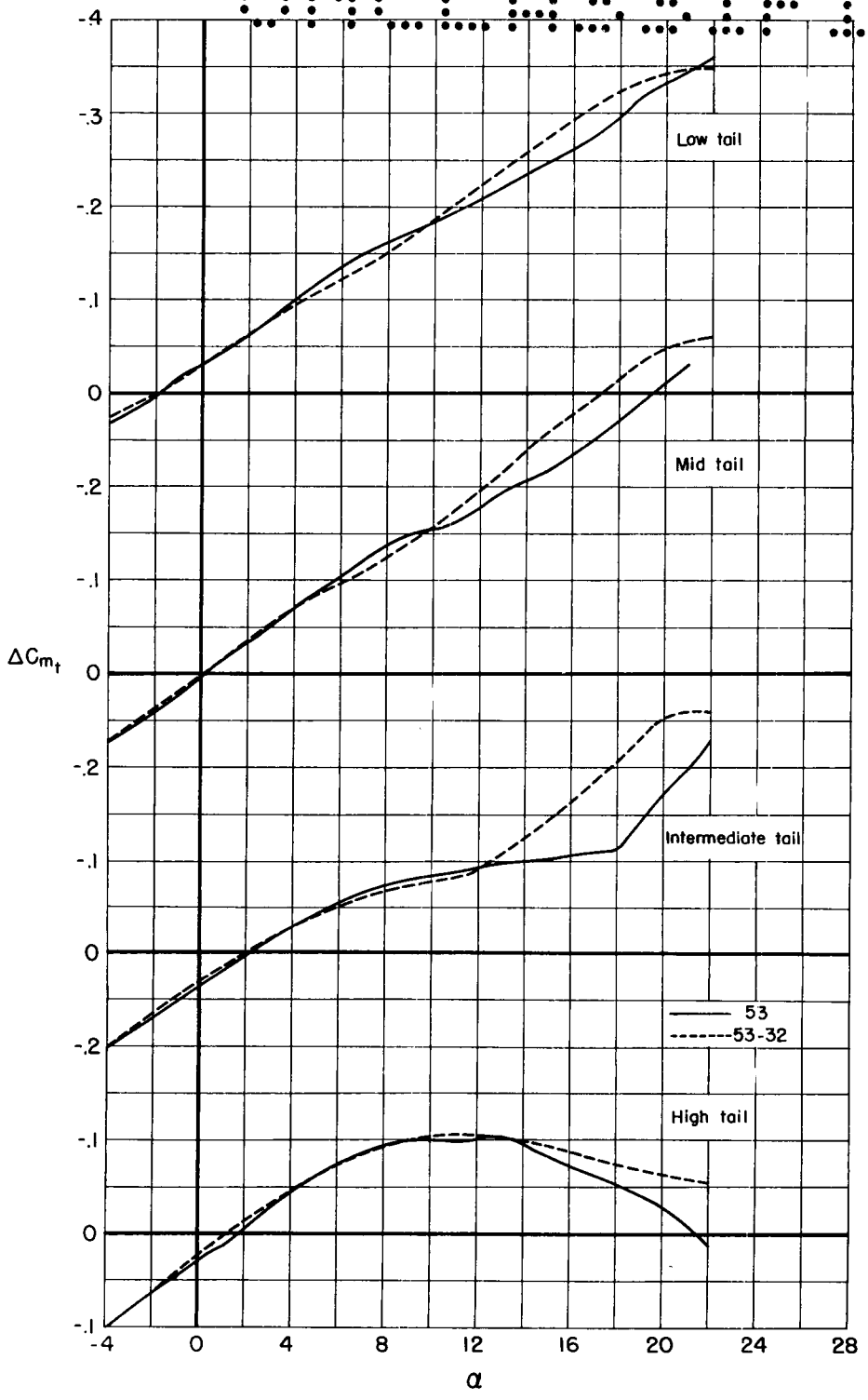

(h) M = 1.10

Figure 18.- Continued.

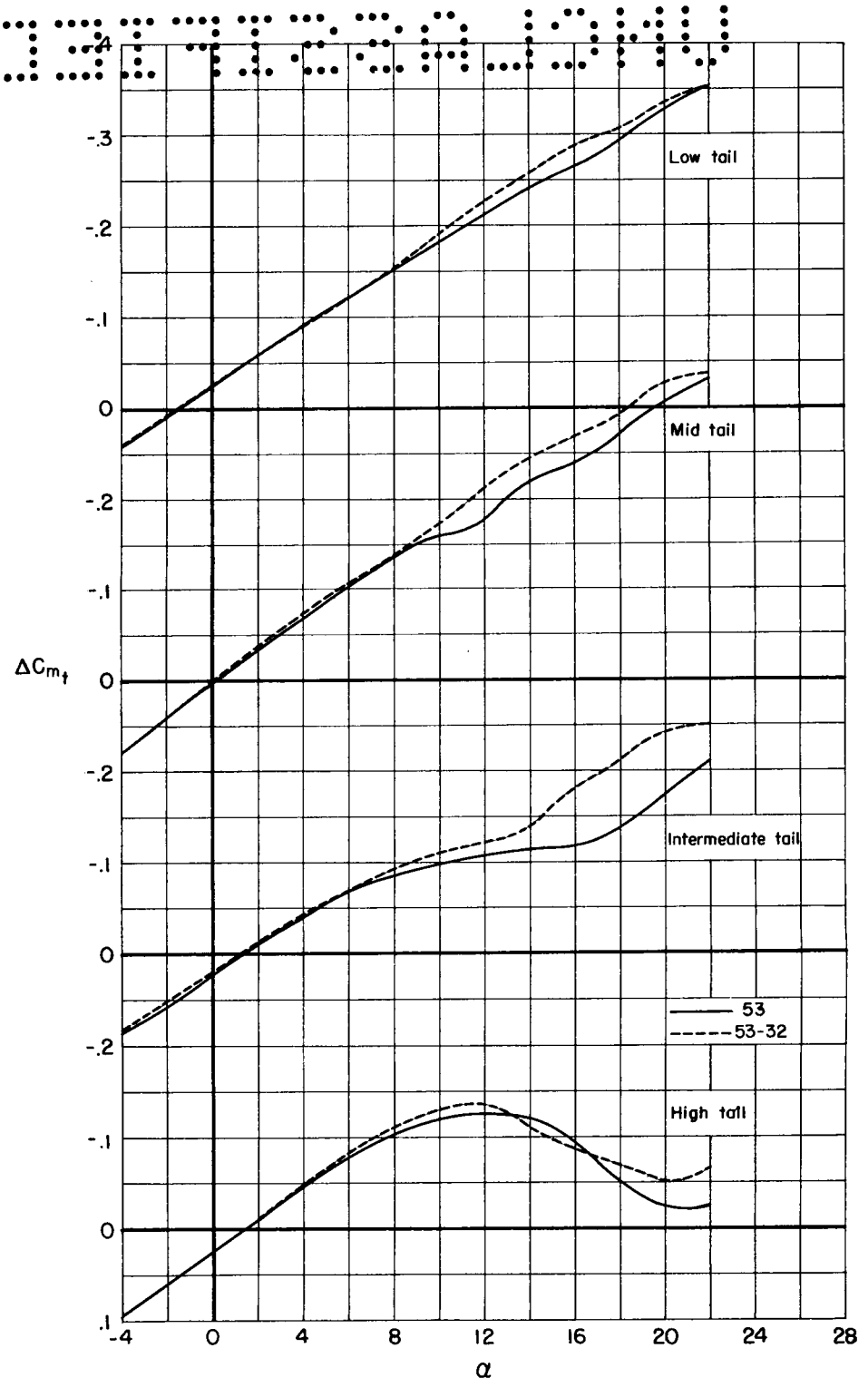

(i) M = 1.20

Figure 18.- Continued.

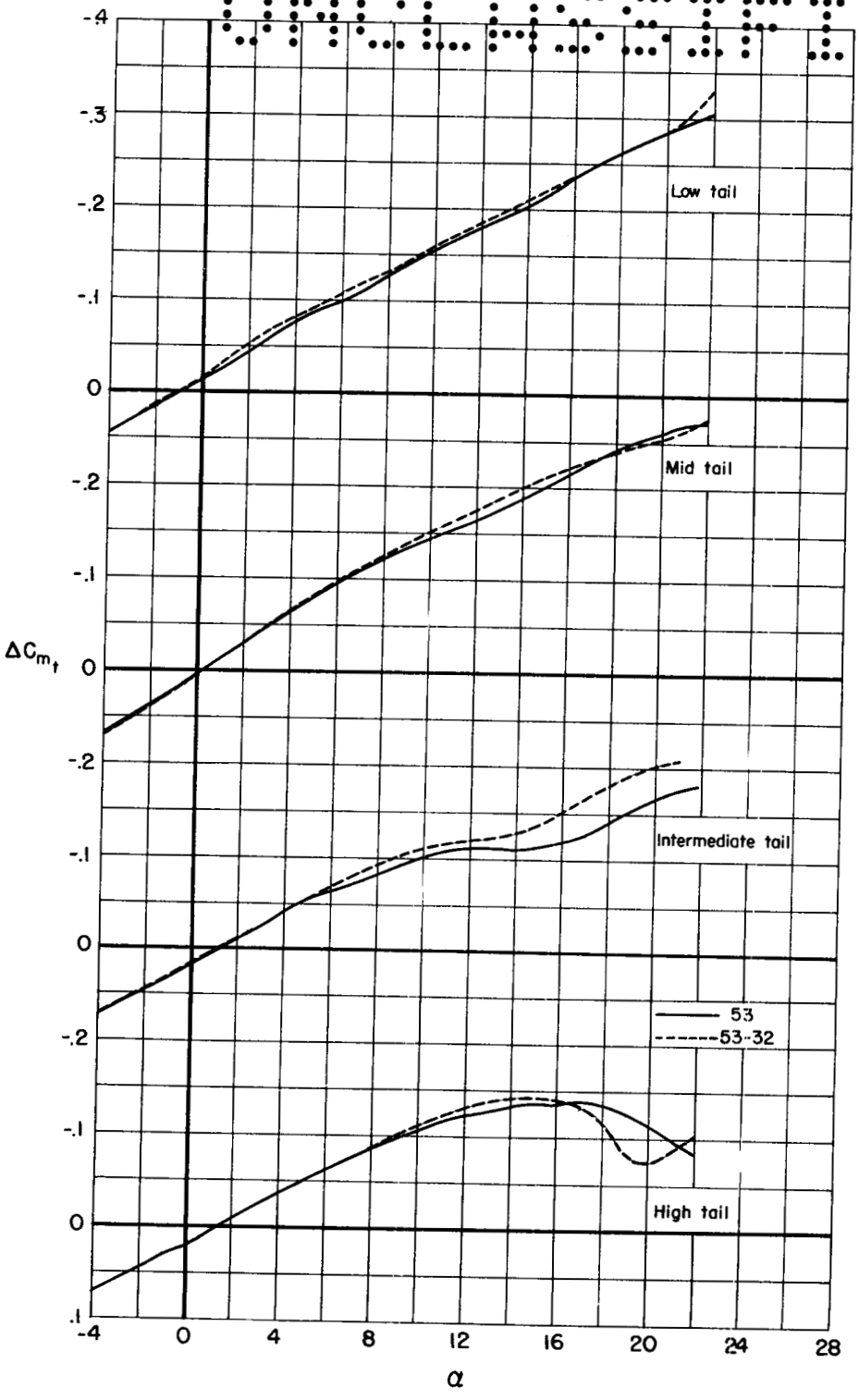

(j) M = 1.40

Figure 18.- Concluded.

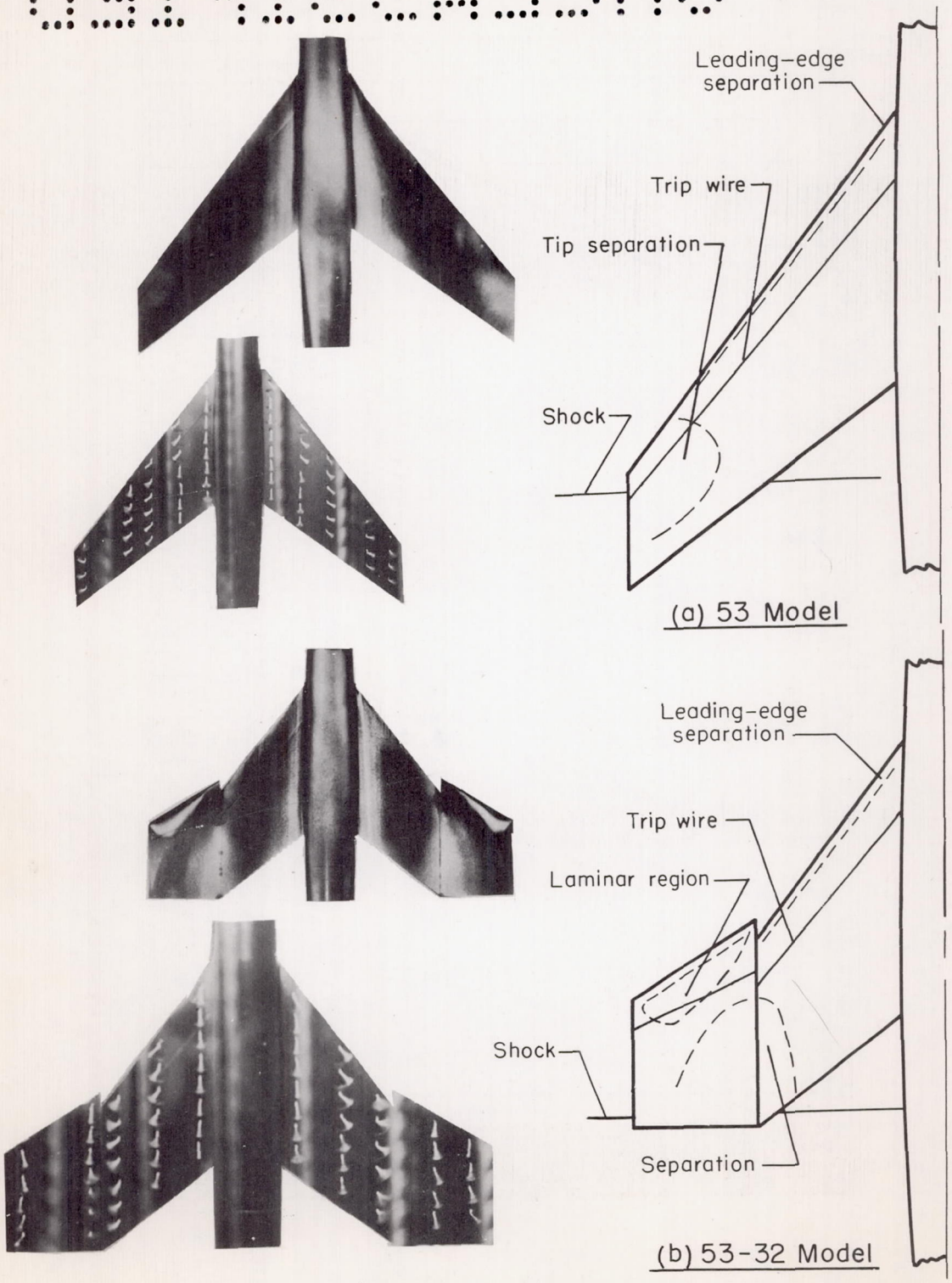

Figure 19.- Flow characteristics of wing-body models at M = 0.94 and α slightly above 9°.